INDUCED PN JUNCTIONS IN GERMANIUM: FUNDAMENTAL MECHANISMS AND APPLICATIONS AS LONG-WAVELENGTH PHOTODETECTORS

YEHKAI HSIEH

A thesis presented to the University of Manitoba
in partial fulfillment of the requirements for the degree of
DOCTOR OF PHILOSOPHY
in Electrical Engineering

WINNIPEG, MANITOBA, 1984

INDUCED PN JUNCTIONS IN GERMANIUM: FUNDAMENTAL MECHANISMS AND APPLICATION AS LONG-WAVELENGTH PHOTODETECTORS

BY

YEHKAI HSIEH

A thesis submitted to the Faculty of Graduate Studies of the University of Manitoba in partial fulfillment of the requirements of the degree of

DOCTOR OF PHILOSOPHY

© 1984

Permission has been granted to the LIBRARY OF THE UNIVERSITY OF MANITOBA to lend or sell copies of this thesis. to the NATIONAL LIBRARY OF CANADA to microfilm this thesis and to lend or sell copies of the film, and UNIVERSITY MICROFILMS to publish an abstract of this thesis.

The author reserves other publication rights, and neither the thesis nor extensive extracts from it may be printed or otherwise reproduced without the author's written permission.

ABSTRACT

Metal-semiconductor (gold contacts to moderately-doped n-type germanium) photodetectors with a P^+N junction, which is induced by the inversion layer beneath the metal electrode, have been fabricated. Experimental studies provide evidence that the dark currents in these devices are due predominantly to minority carrier transport in both forward and reverse bias. The devices are formally equivalent to conventional germanium P^+N junction photodetectors (the latter prepared with diffused or ion-implanted junctions) but avoid defects due to high-temperature fabrication processes, and do not require high dopant concentrations in the surface region. This unique structure has been found to be advantageous for the investigation of the recombination mechanisms responsible for the minority carrier lifetime. This parameter also impacts the performance of photodetectors for fiberoptic communications.

Measurements of open-circuit voltage decay following the application of both a dark forward current pulse and a photocurrent pulse have been made on these induced pn junction devices. Minority-carrier lifetime has been measured over a wide temperature range, as well as over a wide range of injection level. All of the results (dark current pulse) are accurately explained by the SRH model with a single acceptorlike trap level at an energy 0.128 ± 0.008 ev below the conduction band edge, i.e. above the equilibrium Fermi level in the n-type material. The dependence of the hole capture cross section on temperature is further quantitatively explained by the theory for Coulombic capture of Rose, without adjustable parameters. Other dependences on intensity of illumination and wavelength have also been measured by

photo excitation and the results are qualitatively consistent with theory with complications in the decay process and multidimensional surface recombination.

The limitations of Shockley-Read-Hall (SRH) statistics have been further identified by adding the optical emission rate through the defect centers to the excess carrier recombination arising from the optical excitation. In spite of the smaller photo-ionization cross section as compared to the thermal cross sections, the incident intensity plays the major role in deciding the applicability of the traditional SRH model. This consideration also focuses attention on the photon energy, for a threshold value is found in order to avoid hot electron effects and increase the photo-ionization energy, temperature, total volume concentration of centers and the energy location in the energy gap of the semiconductor.

ACKNOWLEDGEMENT

I would like to express my sincere and great appreciation to Professor Howard C. Card for his excellent guidance, endurable motivation, consistent and generous support throughout the investigation of this splendid work. I am also indebted to Professors K.C. Kao, A. Jakobschuk and J.L. Charlton for their constant help and cordial advice which has provided me deep confidence and full independence in this research.

I also wish to thank my wife, Gloria Rongleh Hsieh and my twin sons, Kenneth C. Hsieh and Benjamin C. Hsieh for their understanding and encouragement during the writing of my thesis.

The financial support of the Natural Science and Engineeirng Research Council of Canada (NSERC) under operating grant A1330 is gratefully acknowledged.

Finally, I would like to extend my gratitude to Mrs. M. Morrison for her tireless effort and constant patience in the typing of this manuscript.

TABLE OF CONTENTS

Page

CHAPTER

1 INTRODUCTION 1
1.1 Historical Outline 1
1.2 Research Objectives 4
1.3 Outline of the Present Study 6
References 7

2 GERMANIUM PHOTODETECTORS WITH INDUCED PN JUNCTIONS-PHYSICAL FABRICATION AND EXPERIMENTAL CHARACTERIZATION 9
2.1 Historical Introduction 10
2.2 Current Mechanisms in Metal-Semiconductor Contacts 11
2.3 Device Fabriation and Experimental Results 14
2.4 Discussion 16
References 31

3 INFLUENCE OF MINORITY CARRIER LIFETIME ON PERFORMANCE OF PHOTODETECTORS 32
3.1 Physical Background 32
3.2 Consequences of Lifetime for Photodetector Performance 34
3.2.1 Noise 35
3.2.2 Quantum Efficiency 37
3.2.3 Photoresponse Time 39
3.2.4 Gain 40
References 43

4 MINORITY CARRIER RECOMBINATION IN GERMANIUM-PHYSICAL MECHANISMS AND EXPERIMENTAL CHARACTERIZATION 46
4.1 Forward Current Induced Voltage Decay (FCVD) Method 46
4.1.1 Physical Background 46
4.1.2 Experimental Details 48
4.1.3 Experimental Results 49
4.1.4 Discussion 50
4.2 Photo-Induced Open-Circuit Voltage Decay (POVD) Method 64
4.2.1 Physical Background 64
4.2.2 Experimental Set-Up 66
4.2.3 Experimental Data and Discussion 67
References 81

5 LIMITATIONS TO SHOCKLEY-READ-HALL (SRH) GENERATION/RECOMBINATION MODEL 85
5.1 Historical Introduction 86
5.2 Theoretical Development 88
5.3 Discussion 98
References 109

Page

		Page
6	CONCLUSIONS	113
	6.1 On Germanium Photodetectors with Induced PN Junctions	113
	6.2 On Influence of Minority Carrier Lifetime	114
	6.3 On Minority Carrier Recombination in Germanium	114
	6.4 On Limitations to SRH Generation/Recombination Model	115
	6.5 Suggestions for Further Research	116

CHAPTER 1

INTRODUCTION

1.1 Historical Outline

At the beginning of the last two decades of our century, we find ourselves in a state of rapid flux in technological innovations. The adventure of technology is usually the result of incremental developments that move the existing state of the art forward in relatively small steps. Major breakthroughs and new ideas offer the preferred way of doing things and provide a basis for qualitatively new products to serve society's needs. Often they are the result of scientific discoveries that open the way to previously unforeseen applications. Following the advent of the laser in 1960, there has not only been astounding progress in the understanding of optical phenomena, but there has also been the creation of many new useful tools in a variety of areas. Among these complex and multidimensional applications, optoelectronics technology for communications, especially fiber optic communications, stands out.

Communications using light began a century ago; Alexander Graham Bell was the first to send speech over visible light beams and his photophone was capable of transmitting speech information over distances of several hundred meters. Later on, in the middle of the 19th century, such well-known scientists as James Clark Maxwell, Michael Faraday, Heinrich Hertz and Guglielmo Marconi subsequently discovered the applications to signal transmission of electromagnetic theory and developed much of the necessary equipment. Despite the discovery of microwave communications, the necessity for higher fre-

quencies approaching the optical region were not seriously developed until the laser was invented. Since then, an intense research effort has been launched concerned with the discovery and development of new laser devices, light-emitting diodes, and nonlinear optical materials. This effort provided the basis for the new optoelectronic technology and brought lightwave communications within reach.

The theoretical development of an effective optical transmission medium and the prediction of acceptable losses were first made in 1966 by Kao.[1] The practical realization of low-loss in glass fibers was not achieved until 1970 and the record of losses at that time was 20 dB/km.[2] Within the next couple of years, new production schemes for fibers led to losses of 1 dB/km and below.[3] In the same time, the achievement of semiconductor lasers also brought with it the reality of high-speed, high-bandwidth and low attenuation information transmission systems-optical fiber communications. Laboratory tests have now demonstrated the feasibility of operating single-mode systems at data rates in excess of 1 GHZ over distances greater than 100 km without repeaters.[4] Improvements in fabrication,[5-6] system design[7] and measurement techniques[8] have allowed researchers to observe and classify key optical properties such as loss mechanisms and bandwidth-controlling parameters. These advances, coupled with the installation and implementation of automated process-control systems, now make it possible to consistently produce high performance fibers.[9]

The general trend in the evolution of optical fiber systems has been towards long wavelength operation. By operating at longer wavelengths, one can take advantage of the inherent low losses associ-

ated with Rayleigh scattering in optical fibers, and high bandwidth which arises from low dispersion. The specific operating wavelengths for second-generation optical fibers are 1.3 and 1.5 μm where the losses can reach 0.2 dB/km.[10] The possibility of producing ultrahigh bandwidth single-mode fibers has been recognized since the beginning of optical fiber research. By operating the fiber at the region of zero-chromatic-dispersion, bandwidths of several hundred GHZ-km are theoretically[4] possible and this wavelength typically occurs in the 1300 to 1600 nm wavelength region. The investigation of durable (at room temperature) semiconductor lasers has been successfully developed for the requirement of long-wavelength communications.[11-12] Although the Si photodetector has existed for a long time, its cut-off wavelength at 1.1 μm has prohibited this device from being a potential candidate for long wavelength communications.

At present, the most promising materials for long wavelength photodectors are from the InGaAsP[13] alloy system, which is epitaxially grown from the constituent elements of In, Ga, As and P on bulk InP substrates. The atomic fractions are varied to control the bandgaps that range continuously from 1.35 ev (InP) to 0.73 ev ($In_{0.53}$ $Ga_{0.47}$ As). The InGaAsP alloy system is advantageous for three main reasons. First, a broad spectral sensititivity is obtainable from the wide choice of alloys. Second, the optically-absorbing alloy may be grown on InP substrates of relatively high quality with lattice-matched compositions for near-perfect epitaxial growth. This will reduce the crystalline imperfections that are introduced by mismatches in spacing between atoms in the epitaxial layers and in the substrate. Third, the InP substrates are transparent to long wavelength radiation, absorbing

at wavelengths below 0.95 μm. This will minimize losses from surface recombination of photo-generated carriers. Nevertheless, the disadvantages of this alloy system are lack of cost-effectiveness and reproducibility in commercial production.

On the contrary, Ge photodetectors(14-16) have long been available with a reliable and mature technology. In Japan, the Ge avalanche photodetector (APD) has undergone considerable development in spite of its disadvantages associated with high dark current, relatively low quantum efficiency and large avalanche excess noise. Commercial Ge devices usually employ a diffused or ion-implanted p-n junction structure; metal contact (Schottky Barrier) Ge photodetectors have also been found to be potentially useful. A novel photodetector device fabricated from gold contacts to moderately doped n type germanium will be introduced in this study with its attractive characteristics for long-wavelength photodetectors in optical fiber communication systems.

1.2 Research Objectives

Due to low fiber loss obtained in the 1.3-1.6 μm wavelength region, long-wavelength photodetectors(14-16) have been extensively studied recently in order to continue the evolutionary improvement of optical fiber transmission systems. Conventionally, the p-n junction structure has been adopted for reasons of fabrication ease in an established technology. The optoelectronic properties of metal-germanium induced-junction photodetectors have been found in the present study to be not only comparable to p-n junctions (diffused or ion-implanted) but with the added advantages of the absence of high impurity (acceptor) concentrations in the surface region and the elimination of high-

temperature fabrication processes with reduced defect concentrations. In addition, the transport mechanism is dominated by minority carrier injection, which has been recognized to be one of the most important factors governing device operation. Therefore, the purpose of this research has been the development of a photodetector device with minimal defect introduction which reduces dark currents controlled by minority carrier lifetime.

This has been substantiated by experimental evidence obtained on gold (Au) contacts to moderately-doped n-type germanium which we show exhibits an exception to the conventional pattern of thermionic-emission transport in Schottky barriers. The results show that minority carrier transport is dominant in either forward-bias or reverse-bias due to the extreme band bending associated with the large barrier height ($\geqslant$ 0.60 ev). Our further investigations concentrate on the fundamental (optoelectronic) properties of this device in order to develop a theoretical model of importance in noise reduction caused by the dark saturation current. This has been achieved by characterizing experimentally the physical mechanisms for recombination of minority carriers in germanium. The results show that quantitative agreement with SRH recombination statistics for electrical excitation (dark current) and qualitative agreement for optical excitation (photocurrent). We then focus attention on the limitations of the SRH model which are usually ignored in conventional treatments. These factors are together addressed in view of the ultimate goal-contributing towards the understanding and development of a low-noise, high-speed long-wavelength photodetector.

1.3 Outline of the Present Study

The state-of-the-art in optical fiber communication and the historical development of long-wavelength photodetectors comprise the introduction of this study in the first chapter. In order to experimentally address the object of this research, a novel device with an induced p-n junction has been fabriated and its distinctive transport mechanisms have been corroborated by the experimental characterization. This device is covered in the second chapter.

A review of the impact of carrier lifetime on the performance of photodetectors is discussed in the third chapter, serving as a bridge for the consideration of the mechanisms of minority carrier lifetime as the key to the functioning of this device. In Chapter 4 we present the investigation of carrier lifetime by two methods: Forward Current Induced Voltage Decay (FCVD) and Photo-Induced Open-Circuit Voltage Decay (POVD) for the induced junction device. The lifetime, which depends on the intensity of the optical illumination, the forward current density, the operating wavelength and the temperature has been characterized experimentally. The acknowledged inconsistency between these two methods has been found to be attributable to their distinctive excitation techniques and the resultant compelxity of the optical decay curves. The FCVD method is shown to provide reliable results. Further investigations of the limitations of the SRH recombination model are discussed in Chapter 5. Conclusions and suggestions from the various chapters complete this thesis.

References

1. K.C. Kao and G.A. Hockham, "Dielectric-fibre Surface Waveguide for Optical Frequency", Proc. IEE, vol. 113, no. 7, pp. 1151-1158, July 1966.
2. A.D. Pearson, W.G. French, and E.G. Rawson, "Preparation of a Light Focusing Glass Rod by Ion-Exchange Techniques", Appl. Phys. Lett., vol. 15, no. 2, pp. 76-78, February 1969.
3. T. Li, "Structure, Parameters, and Transmission Properties of Optical Fibers", Proc. IEEE, vol. 68,no. 10, pp. 1175-1180, October 1980.
4. I.D. Aggarwal, "Recent Developments in Optical Fibers", Laser Focus, pp. 115-117, November 1982.
5. J.B. MacChesney, "Materials and Processes for Preform Fabrication-Modified Chemical Vapor Deposition and Plasma Chemical Vapor Deposition", Proc. IEEE, vol. 68, no. 10, pp. 1181-1184, October 1980.
6. R.M. Atkins, J.W. Fleming, P.B. O'Connor, and V.R. Raju, "Plasma Fireball Process Speeds Lightguide Fiber Production", AT&T Bell Laboratories Record, pp. 4-11, February 1984.
7. W.E. Herold and H. Ohnsorge, "Optical-Fiber System with Distributed Access", Proc. IEEE, vol. 68, no. 10, pp. 1309-1315, October 1980.
8. Dietrich Marcuse, <u>Principles of Optical Fiber Measurements</u>, Academic Press, New York, 1981, Chap. 4-7.
9. J.R. Simpson and J.B. MacChesney, "Alternate Dopant for Silicate Waveguides", Topical Meeting on Optical Fiber Communication, Phoenix, Ariz., 1982.

10. T. Miya, Y. Terunuma, T. Hosaka, and T. Miyashita, "Ultimate Low-Loss Single-Mode Fibre at 1.55 μm", Electron. Lett., vol. 15, pp. 106-108, February 1979.

11. T. Yamamoto, K. Sakai, S. Akiba, and Y. Suematsu, "$In_{1-x}Ga_xAs_yP_{1-y}$/InP DH Lasers Fabricated on InP (100) Substrates", IEEE J. Quantum Electron., QE-14, no. 2, pp. 95-98, February 1978.

12. T.P. Lee and A.G. Dentai, "Power and Modulation Bandwidth of GaAs-AlGaAs High Radiance LED's for Optical Communication Systems", IEEE J. Quantum Electron, QE-14, no. 3, pp. 150-159, March 1978.

13. S.R. Forrest, "Photodiodes for Long-Wavelength Communication Systems", Laser Focus, pp. 81-90, December 1982.

14. T. Mikawa, S. Kagawa and T. Kaneda, "Germanium Avalanche Photodiodes for Optical Communication Systems", FUJITSU Scientific and Technical J., pp. 95-117, June 1980.

15. T. Mikawa, S. Kagawa, T. Kaneda, T. Sakurai, H. Ando, and O. Mikami, "A Low-Noise N^+NP Germanium Avalanche Photodiode", IEEE J. Quantum Electron., vol. QE-17, no. 2, pp. 210-215, February 1981.

16. M.C. Brain, "Characterization and Estimated Performance of Commercial N^+ - P Ge APDs for Long-Wavelength Optical Receivers", Optical and Quantum Electron., vol. 13, pp. 353-367, 1981.

CHAPTER 2

GERMANIUM PHOTODETECTORS WITH INDUCED PN JUNCTIONS - PHYSICAL FABRICATION AND EXPERIMENTAL CHARACTERIZATION*

An experimental investigation has been made of optoelectronic carrier transport processes in Au-Ge contacts, and their dependence on temperature, which shows that these devices behave as 'induced' P^+N junctions rather than as Schottky barriers. The dark currents are due predominantly to minority carrier injection in forward bias, and to generation in the quasi-neutral region in reverse bias. The devices are formally equivalent to germanium P^+N junction photodetectors with diffused or ion-implanted junctions, but require neither high temperature fabrication processes nor high dopant concentrations in the surface region.

This unique characteristic provides further impetus to investigate the potential of this device as a long-wavelength photodetector for fiberoptic applications (Chapter 3) due to the low attendant values of dark current, which reduces the noise of the photodetector and increases its ultimate sensitivity. Furthermore, the validity of the SRH recombination model has been examined by means of this device (Chapter4) over a wide range of carrier injection level and operating temperature.

---

*The contents of this chapter have been published as Y.K. Hsieh and H.C. Card, "Germanium Photodetectors with Induced p-n Junctions", IEEE Trnas. on Electron Devices, vol. ED-29, no. 9, pp. 1414-1420, September 1982.

2.1 Historical Introduction

Germanium photodetectors are of interest in fiberoptic communication systems operating at long wavelengths (1.3 μm to 1.7 μm), beyond the cutoff imposed by the optical absorption edge in silicon. In this region, they are an alternative to photodetectors based upon the quaternary alloy semiconductors lnGaAsP. In previous publications(1-4), they have reported on the optoelectronic properties of metal-germanium Schottky barrier photodetectors using a variety of metals. For the most part the characteristics of these devices conform to the thermionic emission theory of Schottky barriers(5).

We have recently discovered that gold (Au) contacts to moderately-doped N-type germanium exhibits an exception to this pattern. The Schottky barrier height is in this case sufficiently large (> 0.6 eV) that the thermionic emission of electrons provides a negligible contribution to the total current in either forward or reverse bias. Instead, the forward-bias current is due primarily to the injection of holes into the semiconductor, and the reverse-bias current to the generation of holes which are collected by the metal. This device therefore behaves as a P^+N junction, with a strongly inverted (P^+) region which is 'induced' by the extreme band bending associated with the large barrier height. The evidence for the PN junction mode of behaviour is presented in this paper. A preliminary theoretical analysis of these structures has been presented earlier(6). It is suggested that the performance of the present device as a photodetector may exceed that of a diffused or ion-implanted germanium PN junction in some cases, due to the absence of the high impurity (acceptor) concentrations in the surface region.

2.2 Current Mechanisms in Metal Semiconductor Contacts

Fig. 2.1 shows the energy band diagrams of a rectifying metal- semiconductor contact under dark conditions, for applied bias voltages of $V = 0$, $V > 0$ and $V < 0$ (V refers to voltage of metal with respect to semiconductor). An N-type semiconductor of moderate doping concentration is assumed. The mechanism corresponding to arrow 1 is thermionic emission of electrons from the semiconductor conduction band into the metal (forward bias, $V > 0$) or from the metal into the semiconductor (reverse bias, $V < 0$) . These currents usually dominate the characteristics of metal-semiconductor contacts, including the case of most metals on germanium(1,2,7). Mechanism 1 gives

$$J_1 \simeq A^* T^2 \exp(-\phi_b/V_T)\lfloor \exp(V/V_T) - 1 \rfloor \qquad (1)$$

where J_1 is current density (Acm^{-2}) , A^* is the modified Richardson constant(5), ϕ_b is the 'Schottky' barrier height (Fig. 1), V the applied voltage and $V_T = kT/q$.

Also shown in Fig. 2.1 is a component of the dark current due to recombination ($V > 0$) or generation ($V < 0$) of electrons and holes in the space-charge region. (process 2). This mechanism is generally well approximated by(5)

$$J_2 \simeq \frac{qn_i W}{\tau} \lfloor \exp(V/2V_T) - 1 \rfloor \qquad (2)$$

which again applies for either forward bias $(V > 0)$ or reverse bias $(V < 0)$. W is the width of the space-charge region, and τ is the carrier lifetime (recombination lifetime, $V > 0$, or generation lifetime, $V < 0$) in this region. n_i is the intrinsic carrier concentration which may be written in the form

$$n_i = 2\left(\frac{2\pi k}{h^2}\right)^{3/2} T^{3/2} (m_e^* m_h^*)^{3/4} \exp(-E_g/2kT) \quad (3)$$

with m_e^*, m_h^* the density of states effective masses for the conduction, valence bands, respectively. The energy gap E_g refers to the minimum (indirect) gap in semiconductors such as germanium, and may be approximated by[8]

$$E_g(T) = E_g(0) - \frac{aT^2}{T+b} \quad (4)$$

for a temperature T (°K). a and b are constants (see Table 2-1).

In general the factor 2 in the exponent of Eqn. (2) may be replaced by a parameter n_2 with $1 < n_2 < 2$ dependent upon the energy distribution of recombination and generation centers in the space-charge region[9], but $n_2 \simeq 2$ in most cases conforms closely to previous studies of this mechanism[10].

The third mechanism in Fig. 2.1 (process 3) arises from recombination $(V > 0)$ or generation $(V < 0)$ of holes in the quasi-neutral region of the semiconductor. This is the dominant component of current in ideal P^+N junctions, and is given by[8]

$$J_3 \simeq \frac{n_i^2}{N_d} \left(\frac{qkT \mu_p}{\tau_p}\right)^{1/2} \left[\exp(V/V_T) - 1\right] \quad (5)$$

where μ_p is the mobility of holes and τ_p is their lifetime in the quasi-neutral region and N_d is the doping concentration (assumed uniform) of the N-type semiconductor.

This component J_3 is always present in rectifying metal-semiconductor contacts, but is usually negligible as compared to J_1. We will argue however that in the devices under study J_3 is the dominant component of dark current with secondary contributions from component J_2. This arises because of the large value of ϕ_b in Eqn (1) and the relatively large n_i associated with the small E_g in germanium.

The mobility of holes in N type germanium has been observed to exhibit a dependence on temperature given by the empirical expression[11]

$$\mu_p = 9.1 \times 10^8 \, T^{-2.3} \quad (6)$$

with μ_p expressed in units of $cm^2 V^{-1} s^{-1}$.

Under illumination with photons having energy in excess of E_g, photogeneration in the semiconductor gives rise to an additional component of current in the direction of the reverse current (not shown in Fig. 2.1). This component we may call J_4. For $V = 0$, in the absence of large series resistances, the total current density $J = J_4$, since Eqns (1) to (3) reduce to zero in this case. If on the other

hand we examine the conditions for zero total current, the voltage $V = V_{oc}$, the open-circuit voltage. That is

$$J = \sum_{i=1}^{4} J_i(V) = 0 \quad \text{for} \quad V = V_{oc}$$

or

$$\sum_{i=1}^{4} J_i(V_{oc}) = 0 \tag{7}$$

Provided the photons are absorbed sufficiently close to the semiconductor surface, the optical absorption coefficient considerably exceeds the inverse of the hole diffusion length $L_p = (kT\mu_p\tau_p/q)^{1/2}$, and the component J_4 representing the photocurrent will be independent of voltage. Provided also that the currents J_1 to J_3 are not appreciably modified by the illumination, the total current is simply the sum of the dark current and the short-circuit current J_4. This is sometimes referred to as the superposition theorem for photodetectors(12).

2.3 Device Fabrication and Experimental Results

The germanium wafers used in these studies were (111) oriented N-type polished wafers obtained from General Diode Co., with doping concentration $N_d = 2.08 \times 10^{15} cm^{-3}$, as determined from high-frequency capacitance-voltage characteristics. The Au electrodes were deposited by thermal evaporation at a base pressure of 10^{-6} torr in an oil diffusion pumped vacuum chamber. Contact areas were $2 \times 10^{-2} cm^2$ and Au thicknesses were ≈ 250Å.

Measurements of current-voltage characteristics were performed in a liquid-nitrogen cooled cryostat with a resistive heating element which maintained the temperature within $\pm 2°K$ over the range $100°K$ to $340°K$ during the measurement. Optical illumination was provided by a GTE ELH Tungsten-Halogen lamp.

In Fig. 2.2 we show an example of the dependence of dark current upon voltage under both forward and reverse bias conditions for several values of temperature.

In Fig. 2.3 we give a typical example of the current-voltage characteristics on a linear scale for various intensities of optical illumination. Figs. 2.4 and 2.5 show the dependence of current upon temperature for particular values of forward and reverse bias voltages, respectively. The theoretical characteristics in these figures are discussed in the following section. Figs. 2.6 and 2.7 show the observed dependence of open-circuit voltage and short-circuit current upon temperature for three values of optical illumination intensity. Finally, in Fig. 2.8 is shown the dependence of short-circuit current upon open- circuit voltage for three values of temperature. For a given temperature, these curves have been obtained by varying the optical illumination intensity.

The data presented in Figs. 2.2 to 2.8 is representative of that obtained in a variety of similar Au-N-type Ge structures. The characteristics were observed to be stable against aging effects or degradation over the period of several weeks during which measurements were being taken. The errors coming from each experimental point have been measured and the standard deviation found to be less than 1%. No accelerated life tests have yet been performed at elevated temperatures.

2.4 Discussion

The results of Fig. 2.2 have been interpreted both on the basis of the Schottky barrier theory and P^+N junction theory. The parameters used in the theoretical calculations are listed in Table 2-1. In the case of Schottky barrier theory, Eqn. (1) is assumed to describe the device behaviour, i.e. J_1 is assumed to be the dominant current. The adjustable parameter in the calculations in this case is ϕ_b, the Schottky barrier height. While the experimental results such as Fig. 2.2 can be made approximately consistent with Eqn. (1) for a single temperature, the predictions of J_1 at other temperatures do not agree with experiment. The thermal activation energy over the temperature range of study predicted by Eqn. (1) is $q(\phi_b - V)$, since $J_1 \sim \exp[-q(\phi_b - V)/kT]$ except at extremely high temperatures where the T^2 term enters in. Experimentally the activation energy is considerably larger than this, as indicated in Table 2-2.

On the other hand, in interpreting results such as those of Fig. 2.2 on the basis of P^+N junction theory, Eqn. (5) is assumed to apply. That is, in this case J_3 is assumed to be the dominant component of current. Here all parameters are known with reasonable accuracy except for the hole lifetime τ_p, which is treated as an adjustable parameter. For this interpretation, the activation energy from Eqn. (5) is approximately $(E_g - qV)$, with the E_g in the $J_3 \sim \exp\lfloor -(E_g - qV) \rfloor$ dependence arising from the n_i^2 term in accordance with Eqn. (3). Eqn. (5) is found to be in close agreement with experiment as demonstrated in the comparison of activation energies in Table 2-2. The correspondence of the data with the P^+N junction theory of Eqn. (5) is evident in Fig. 2.4. The predictions of Schottky barrier

theory, Eqn. (1), do not agree with experiment, since the magnitude of the slope in Fig. 2.4 is in this case too low. The vertical displacement in Fig. 2.4 between the predictions for the Schottky barrier theory and the experimental results is a consequence of determining ϕ_b at a low temperature (200°K). The two curves will cross at a current magnitude which is well below those shown on this figure.

Agreement between the P^+N junction theory and experiment is preserved for the bias voltage dependence of the current and the activation energy, provided a contribution to the total current from space-charge recombination is included. Since this component J_2, described by Eqn. (2), has a weaker voltage dependence than J_1, ($\exp(V/2V_T)$ as opposed to $\exp(V/V_T)$), its contribution under forward bias is important only at low voltages. Rhoderick[5] has shown that the sum of $\exp(V/V_T)$ and $\exp(V/2V_T)$ components can be approximated over an extensive range of current by an $\exp(V/nV_T)$ dependence with $1 < n < 2$. The value of n depends upon the ratio of the pre-exponential factors in Eqns. (1) and (2). For a given forward bias voltage V, the relative importance of J_1 and J_2 also depends upon temperature since the activation energy for J_1 is $(E_g - qV)$ whereas that for J_2 is $(\frac{E_g - qV}{2})$ since $J_2 \sim n_i$ and not n_i^2.

Considering the case of reverse bias, one can clearly identify two activation energies in Fig. 2.5. At high temperatures $E_a \sim E_g$ whereas at low temperatures $E_a \sim E_g/2$. This indicates that J_3 is dominant in reverse bias for high temperatures ($T \geqslant 250$°K in Fig. 2.5) and J_2 is dominant at lower temperatures. The transition temperature is not strongly dependent on the applied voltage since the $(\exp(V/V_T)-1)$ and $(\exp(V/2V_T)-1)$ dependences reduce to -1 for $V \ll 0$.

There will be a weak dependence on V because of the term $W \sim V^{1/2}$ in the pre-exponential factor of Eqn. (2).[8]

Under optical illumination a photocurrent (J_4) is produced which gives rise to characteristics such as those of Fig. 2.3. The temperature dependence of the short-circuit current density of Fig. 2.6 ($I_{sc}=AJ_4$ with A the device area) may be understood in terms of the reduction in the energy gap with increasing temperature expressed by Eqn. (4) and its attendant increase in the optical absorption coefficient at all wavelengths λ. According to the P+N junction theory, the photocurrent density J_4 gives rise to an open-circuit voltage determined by $J_3(V_{oc}) + J_4 = 0$, where J_1 and J_2 have been assumed to be negligible in Eqn. (7). Substitution of Eqn. (5) for J_3 leads to

$$V_{oc} \simeq V_T \ \ln\left[\frac{J_4 N_d}{n_i^2}\left(\frac{\tau_p}{qkT\mu_p}\right)^{1/2}\right]$$

$$= \frac{kT}{q} \ln\left[\frac{J_4 N_d}{N_c N_v}\left(\frac{\tau_p}{qkT\mu_p}\right)^{1/2}\right] + \frac{E_g}{q} \qquad (8)$$

At sufficiently high temperatures, $V_{oc} \approx \frac{E_g(T)}{q} - CT$ with C a positive quantity which is only weakly dependent upon temperature. The experimental results of Fig 2.6 show that the extrapolation of this region to $T = 0°K$ gives an intercept of $E_g(0)/q$, in excellent agreement with the known value for the 0°K gap in germanium[8] of 0.74 eV. This provides additional verification for the treatment of these devices as induced P+N junctions, with currents obeying Eqn. (5). If the results of Fig. 2.6 were interpreted on the basis of the Schottky barrier theory, Eqn.

(1) rather than Eqn. (5) would be used in arriving at the expression for V_{oc}. In this case the 0°K intercept should be equal to ϕ_b, which is clearly not the case.

The dependence of open-circuit voltage upon short-circuit current observed in Fig. 2.8 is also consistent with Eqn. (8), with $I_{sc} = AJ_4$ and $\tau_p \simeq 10^{-7}$ sec in agreement with the value obtained from the dark data. The slope of $\ell n\ J_{sc}$ vs V_{oc} in Fig. 2.8 is approximately 1.09, somewhat smaller than those of Fig. 2.2. This indicates some influence of series resistance effects in Fig. 2.2.

All of the data of Figs. 2.2 to 2.8 substantiate our claim that these Au-N type Ge structures are in fact induced P^+N junctions. To attempt to interpret their behaviour in terms of the conventional Schottky barrier model of thermionic emission of electrons leads to several inconsistencies with experiment and to an underestimate of the true 'Schottky' barrier height. The metal Fermi energy must lie considerably more than 0.6 eV below the germanium conduction band edge at the surface.

It is expected that the induced P^+N germanium devices of this study will exhibit some advantages over conventional diffused or ion-implanted P^+N junctions in germanium in their applications as photodetectors. The absence in our structures of the large acceptor (P^+) impurity concentrations of conventional devices will improve the carrier lifetime in the surface region and will enhance the quantum efficiency of strongly absorbed radiation ($\lambda \leqslant 1.5\ \mu m$). It may also result in a reduction of excess noise introduced by defects associated with the large doping concentrations. Finally, one may speculate that the absence of large doping concentrations may give rise to less energy

gap narrowing because in these induced P+N junction diodes only the effects of electrostatic interaction[13] will influence E_g in the P+ region.

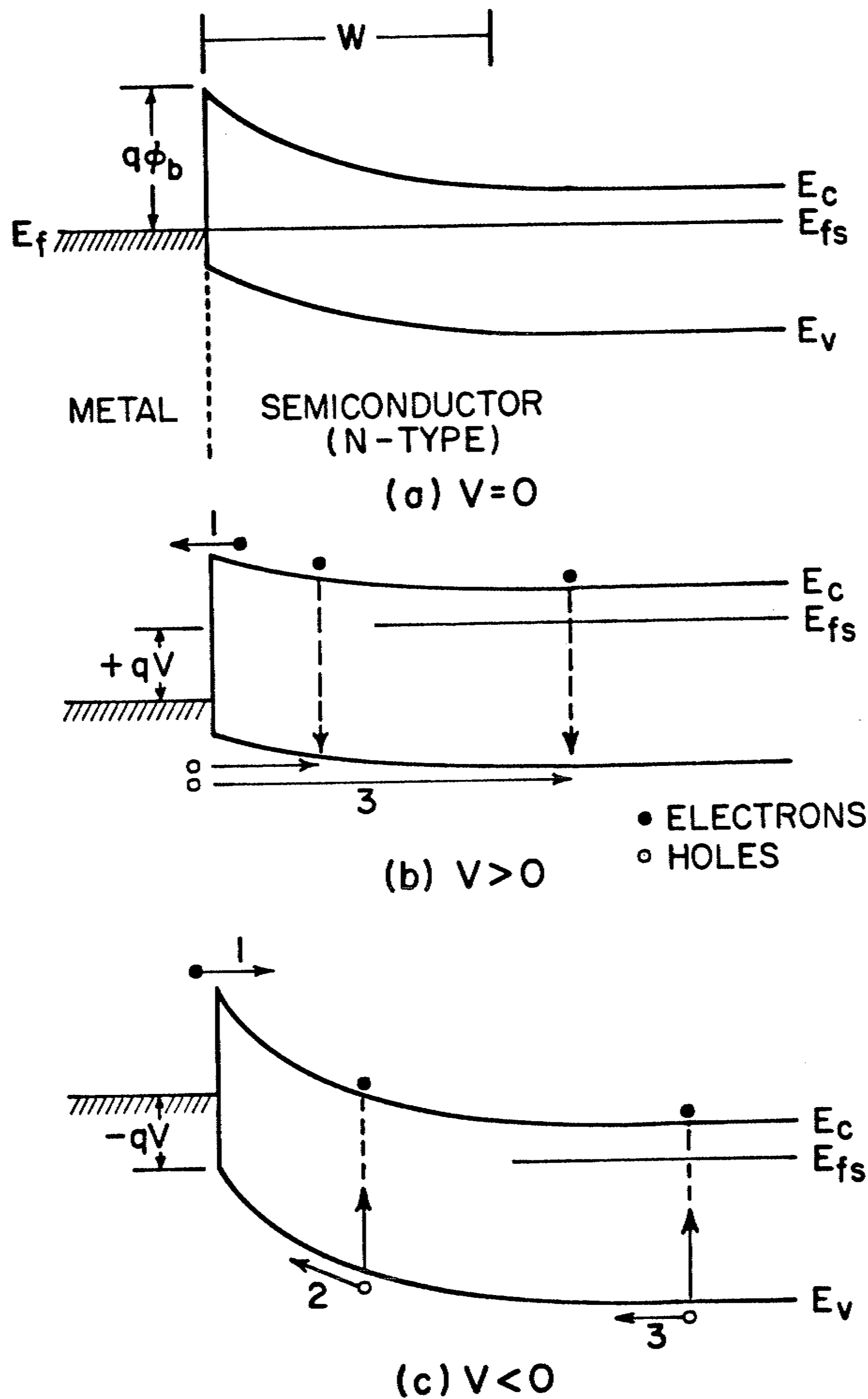

FIG. 2.1 Electron energy-band diagrams for rectifying metal-semiconductor contacts (a) in equilibrium, (b) under forward bias, and (c) under reverse bias. Dark conditions are assumed and V is the voltage of the metal with respect to the semiconductor.

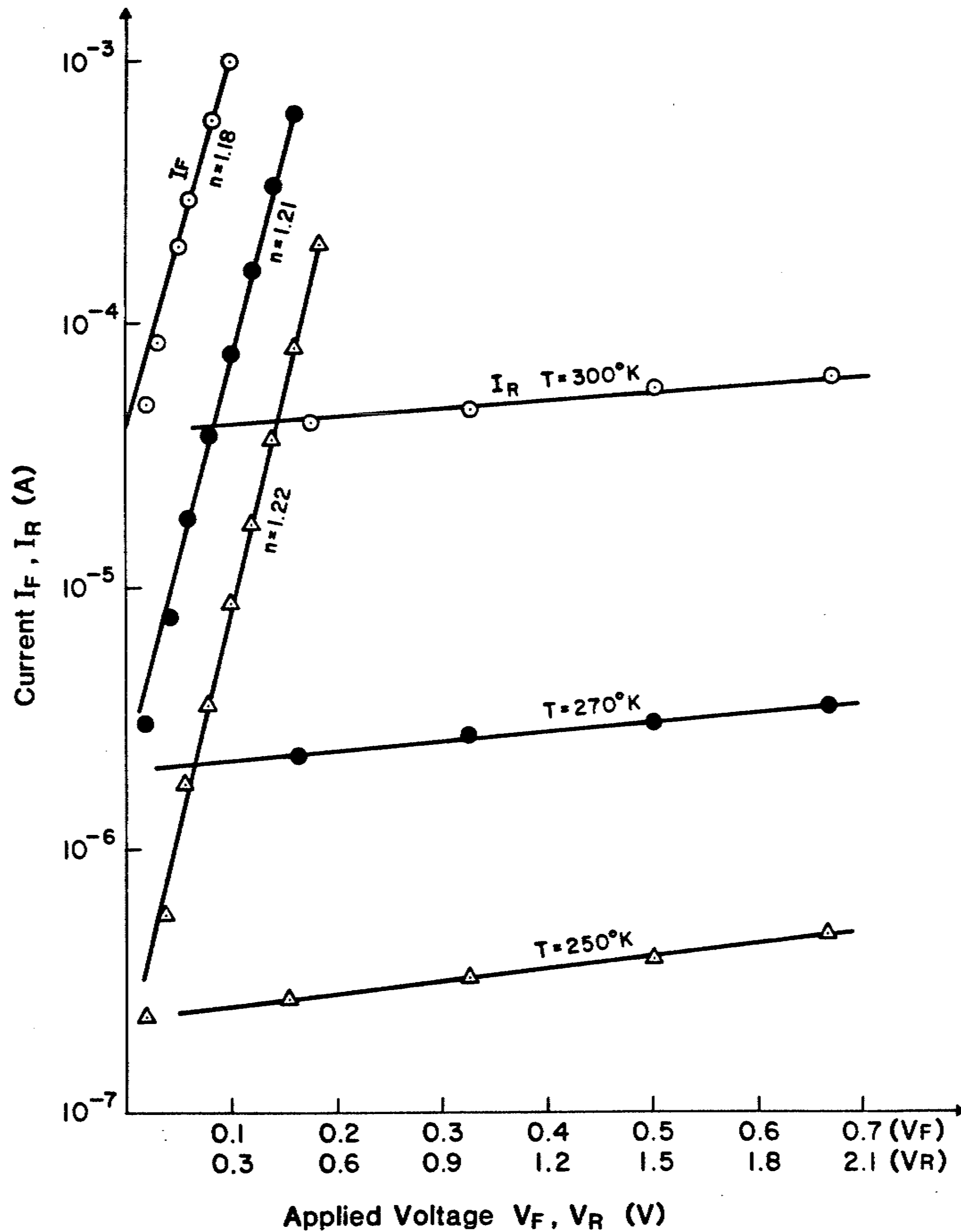

FIG. 2.2 Semilogarithmic current-voltage characteristics obtained experimentally for Au-N type Ge structures under dark conditions. Three measurement temperatures are indicated.

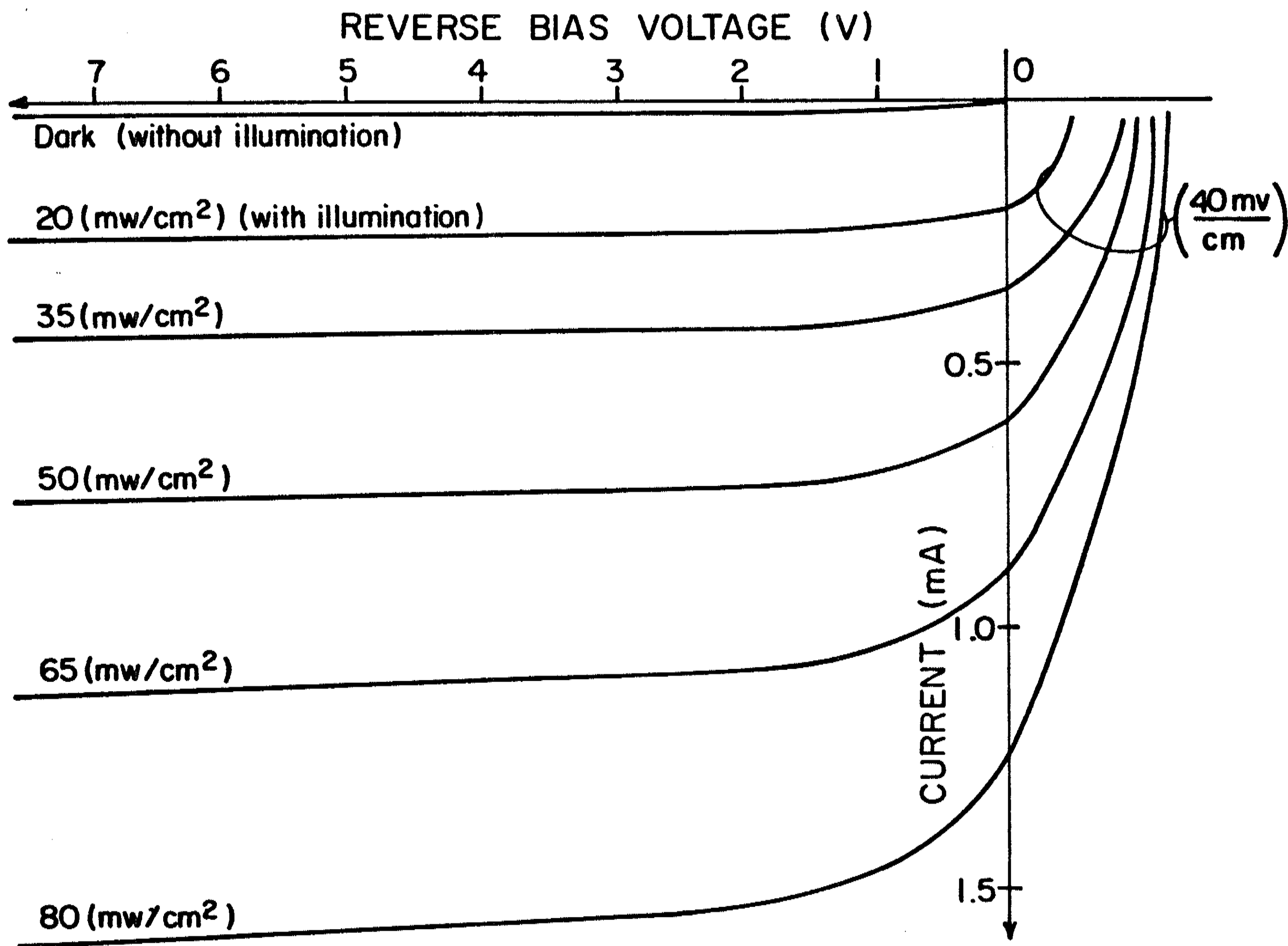

FIG. 2.3 Linear current-voltage characteristics of Au-N type Ge structures with optical illumination intensit-y as a parameter.
NOTE: expansion in scale from 1V/division to 40 mV/division in forward bias.

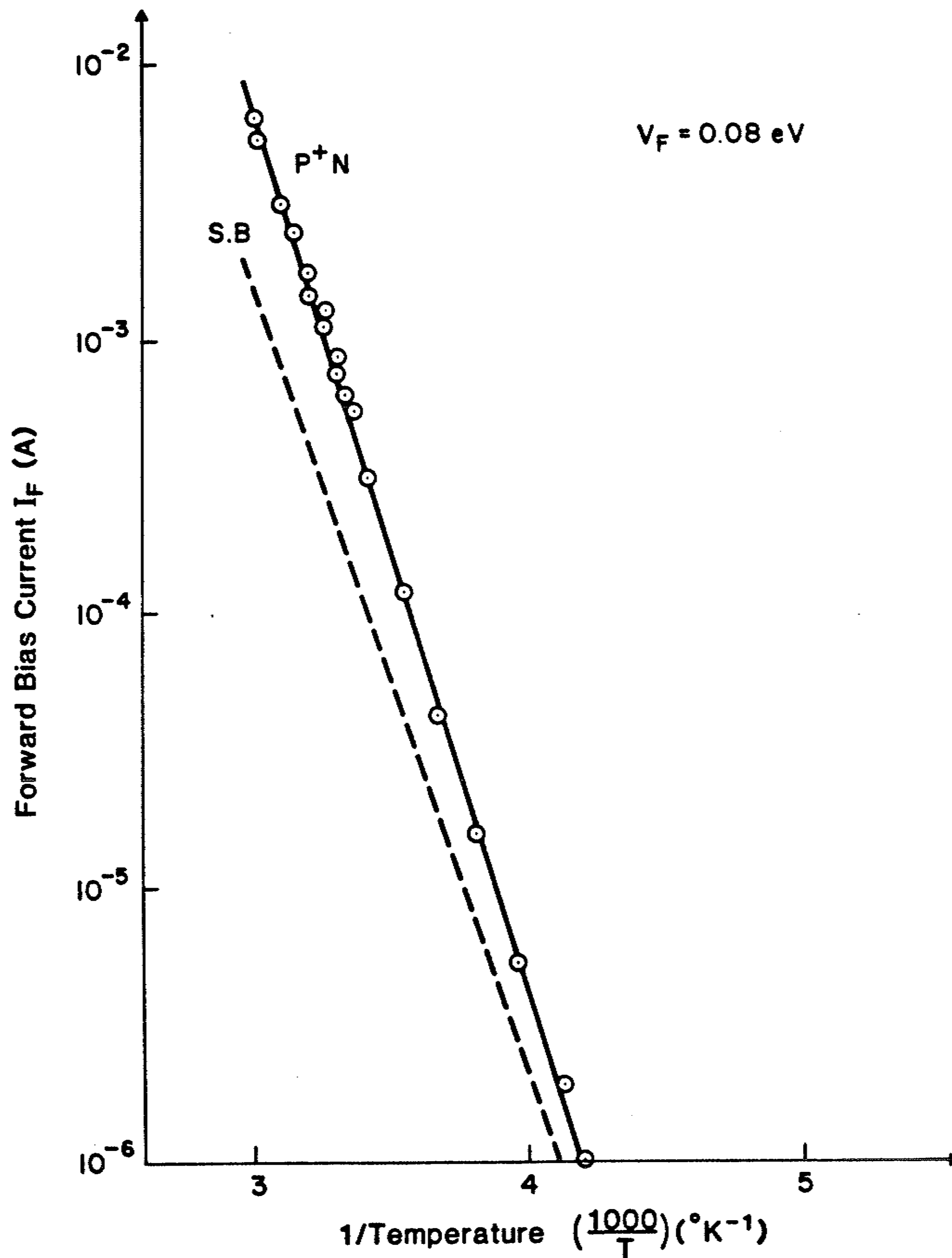

FIG. 2.4 Dependence of dark current upon temperature for Au-N type Ge structures under forward bias voltage V = 0.08V in the form logI vs 1/T . Dashed and solid lines show Schottky barrier theory (Eqn. (1)) and P^+N junction theory (Eqn. (5)) respectively. Circles indicate experimental data points.

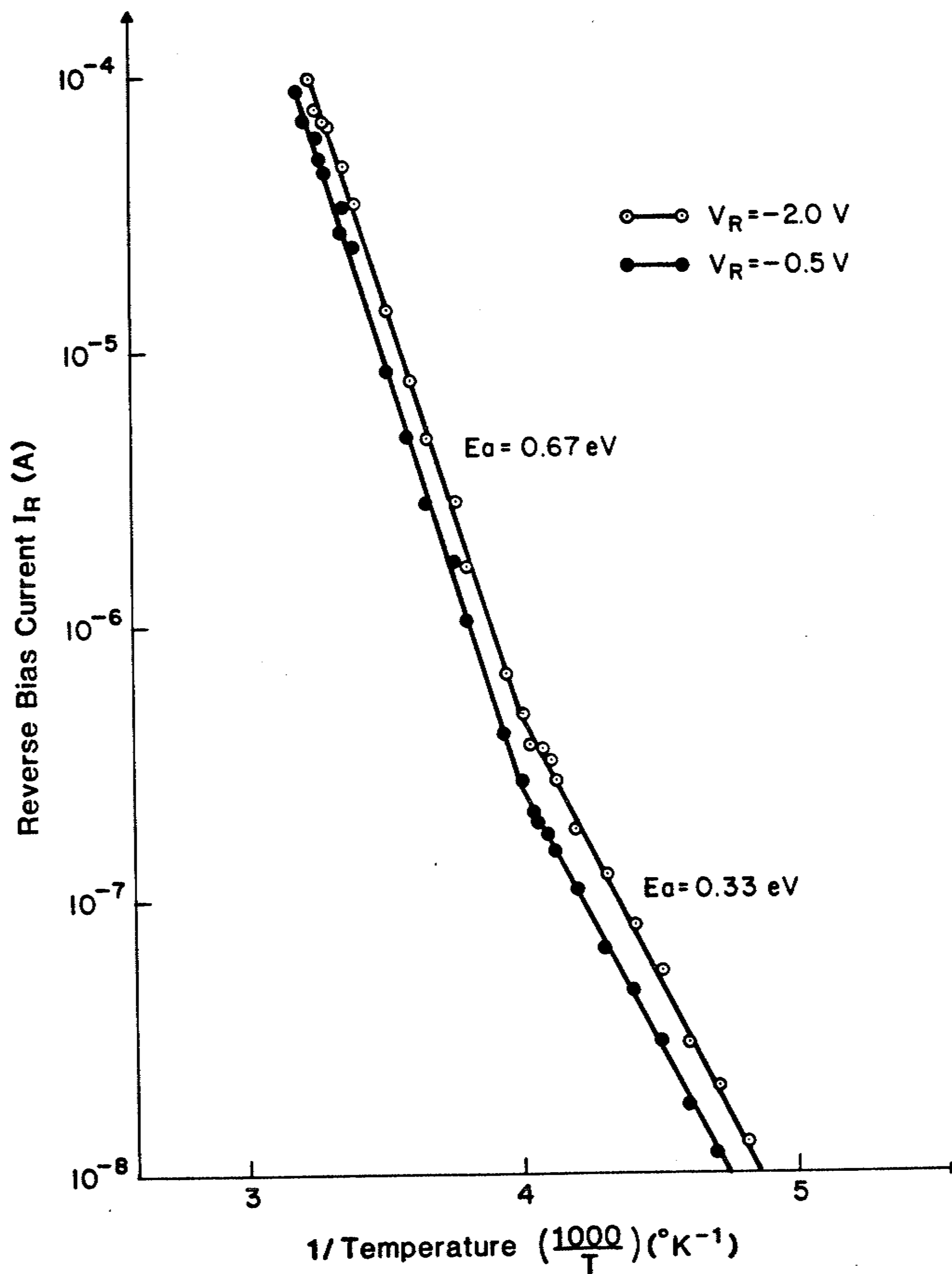

FIG. 2.5 Experimental dependence of dark current upon temperature for Au-Ntype Ge structures under reverse bias voltages V = -0.5V and V = -2.0V. Also shown are thermal activation energies determined from slope in the two regions.

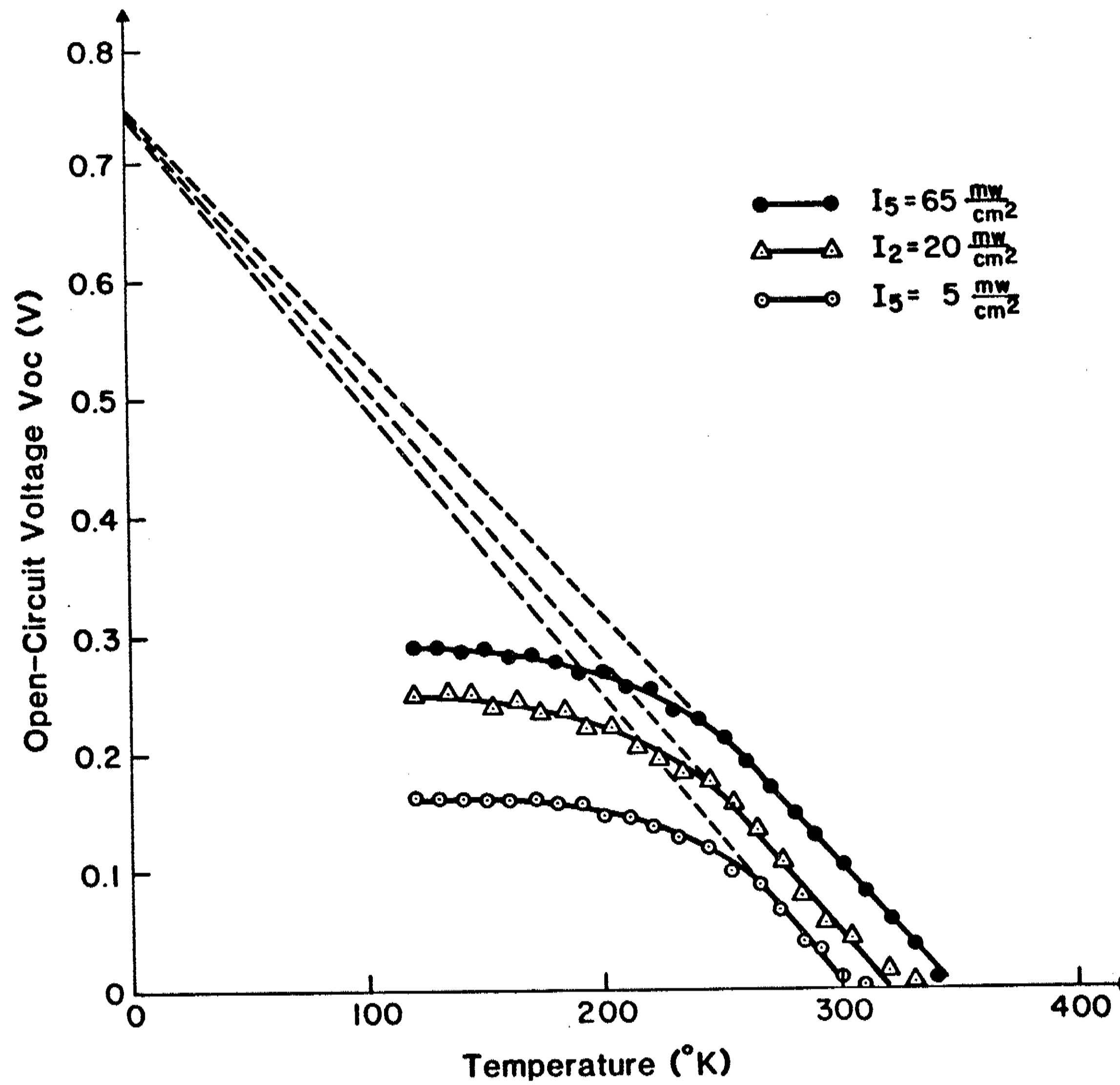

FIG. 2.6 Experimental dependence of short circuit current upon temperature for Au-Ntype Ge structures, for three optical illumination intensities.

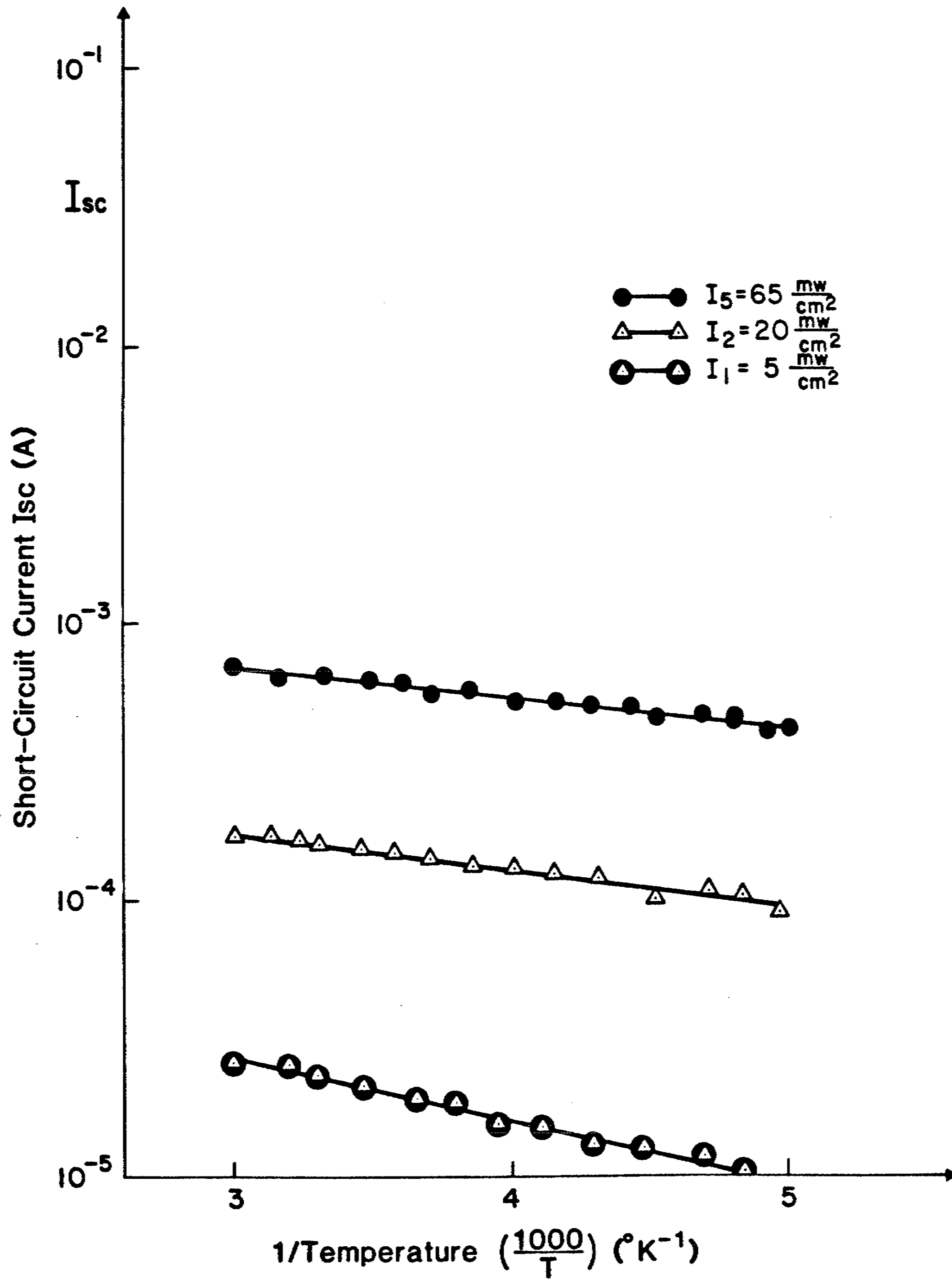

FIG. 2.7 Experimental dependence of open circuit voltage upon temperature for Au-Ntype Ge structures, for three optical illumination intensities.

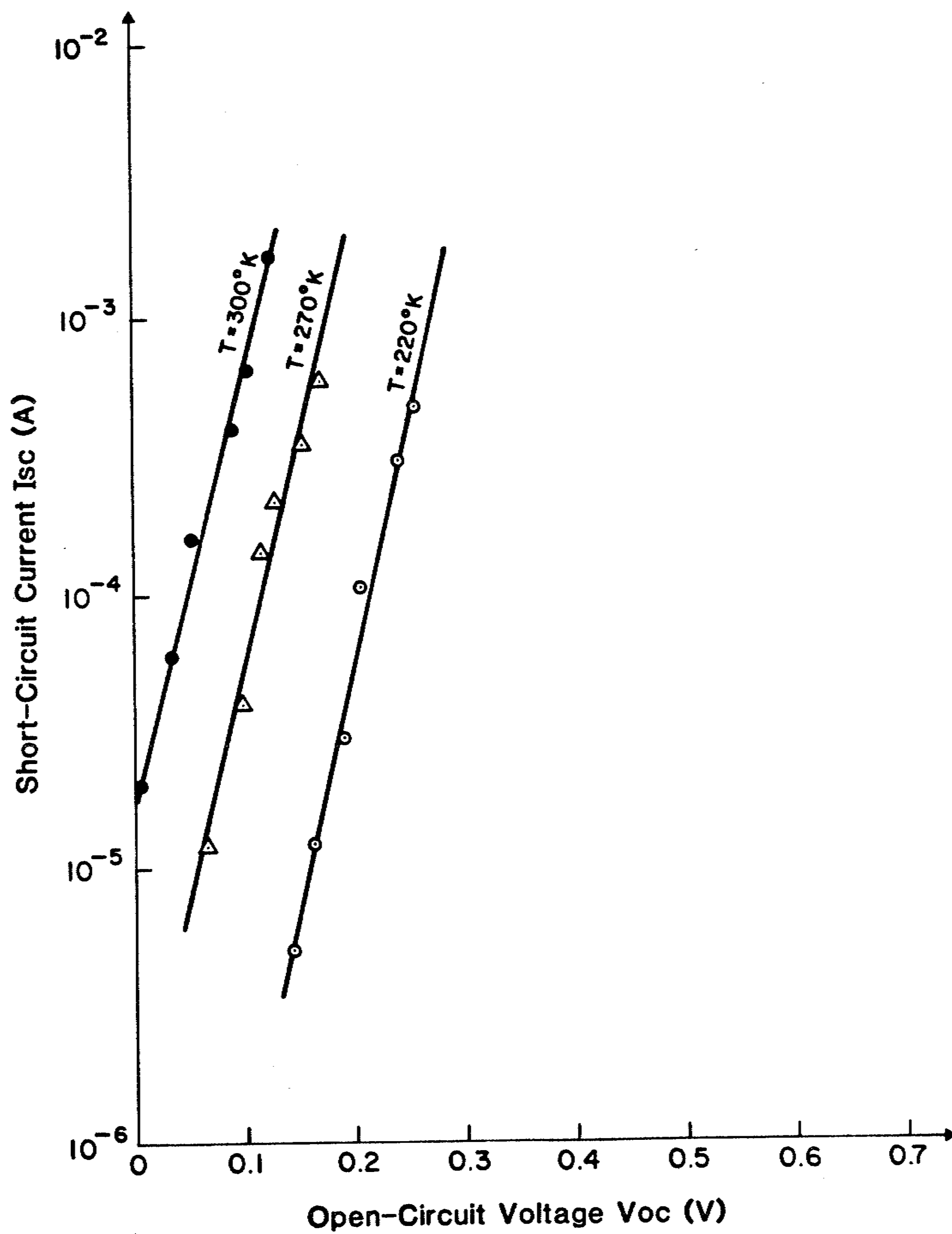

FIG. 2.8 Dependence of short-circuit current on open-circuit voltage for Au-Ntype Ge structures.

TABLE 2-1 Parameters used in Theoretical Calculations

NOTATION		VALUES
A	device area	2×10^{-2} cm^2
A^*	modified Richardson constant	50 Acm^{-2}K^{-2}
a	constants in Eqn (4) for energy gap	4.56×10^{-4}
b		210°K
$E_g(0)$	Energy gap at 0°K	0.7412 eV
h	Planck constant	6.63×10^{-34} J-sec
k	Boltzmann constant	8.62×10^{-5} eV/°K
m_e^*	density of states effective mass of electrons	$0.55m_o = 5.0105 \times 10^{-31}$ Kg
m_h^*	density of states effective mass of holes	$0.37m_o = 3.3707 \times 10^{-31}$ Kg
N_d	donor doping concentration	2.08×10^{15} cm^{-3}
D_p	diffusion coefficient for holes	47.238 cm^{2}S^{-1} at 300°K
μ_p	mobility for holes	1826.68 cm^{-2}V^{-1}S^{-1} at 300°K
τ_p	lifetime for holes	10^{-7}s obtained by fitting to experimental results for $V > 0$ (recombination lifetime).

TABLE 2-2 Activation Energies

	P^+N Theory	SB Theory	These experiments
Ea_1(eV) (Ref. Fig. 2.5)	0.67	0.60	0.66
Ea_2(eV) (Ref. Fig. 2.4)	0.64	0.57	0.63
Ea_3(eV) (Ref. Fig. 2.6)	0.021 0.026 0.041	0.151 0.146 0.091	0.019 0.026 0.038
$E_g(0)$(eV) (Ref. Fig. 2.7)	0.7412	0.60	0.744 0.743 0.742

E_{a1}: Activation energy calculated from I-1/T at reverse bias voltage -2.0V

E_{a2}: Activation energy calculated from I-1/T at forward bias voltage 0.08V

E_{a3}: Activation energy calcualted from I_{sc} - 1/T at three different optical intensities.

$E_g(0)$: Energy gap for 0°K determined at three different optical intensities from V_{oc} vs T .

References

1. E.Y. Chan and H.C. Card, "Optoelectronic Properties of Metal-Germanium Schottky Barrier Quantum Detectors," IEEE Int. Electron Dev. Mtg., Washington, D.C., Digest of Tech. Papers, pp. 653-656, December 1978.
2. E.Y. Chan and H.C. Card, "Infrared Optoelectronic Properties of Metal-Germanium Schottky Barriers," IEEE Trans. on Electron Devices, vol. ED-27, pp. 78-83, January 1980.
3. E.Y. Chan, H.C. Card and M.C. Teich, "Internal Photoemission Mechanisms at Interfaces between Germanium and Thin Metal Films," IEEE J. Quantum. Electron., vol. QE-16, pp. 373-381, March 1980.
4. E.Y. Chan and H.C. Card, "Near IR Interband Transitions and Optical Parameters of Metal-Germanium Contacts," Appl. Opt., vol. 19, pp. 1309-1315, April 1980.
5. E.H. Rhoderick, Metal-Semiconductor Contacts, Clarendon Press: Oxford, 1978.
6. D.A. Buchanan and H.C. Card, "On the Dark Currents in Germanium Schottky Barrier Photodetectors," IEEE Trans. on Electron Devices, vol. ED-29, pp. 154-157, January 1982.
7. A. Thanailakis and D.C. Northrop, "Metal-Germanium Schottky Barriers," Solid St. Electron., vol. 16, pp. 1383-1389, 1973.
8. S.M. Sze, Physics of Semiconductor Devices, 2nd Edition, John Wiley and Sons: New York, 1981.
9. A Nussbaum, "Generation-Recombination Characteristic Behaviour of Silicon Diodes," Phys. Stat. Sol. (a), vol. 19, pp. 441-450, 1973.
10. P. Panayotatos and H.C. Card, "Recombination in the Space-Charge Region of Schottky Barrier Solar Cells," Solid-State Electronics, vol. 23, pp. 41-47, 1980.
11. M.B. Prince, "Drift Mobilities in Semiconductors: I. Germanium," Phys. Rev., vol. 92, pp. 681-687, November 1953.
12. F.A. Lindholm, J.G. Fossum and E.L. Burgess, "Application of the Superposition Principle to Solar Cell Analysis," IEEE Trans. on Electron Devices, vol. ED-26, pp. 165-171, March 1979.
13. F.J. Morin and J.P. Maita, "Conductivity and Hall Effect in the Intrinsic Range of Germanium," Phys. Rev., vol. 94, pp. 1525-1529, June 1954.

CHAPTER 3

INFLUENCE OF MINORITY CARRIER LIFETIME ON PERFORMANCE OF PHOTODETECTORS

The unique transport mechanism in a Au-n type germanium induced-junction device under dark conditions has been introduced in the previous chapter. This characteristic of the device has also been cited as responsible for its potential as a long-wavelength photodetector, in addition to its inexpensive and nondestructive fabrication processes which contrast with those of the quaternary compound semiconductor devices, for example.

A review of the effects of the minority carrier lifetime on the performance of existing photodetectors will be presented in this chapter. This will serve to underline its importance as a long-wavelength photodetector in recently developed optical-fiber communication systems, and will provide motivation for the fundamental studies of Chapters 4 and 5.

3.1 Physical Background

During the early years of semiconductor science, the physical processes of charge carrier generation and recombination received a great deal of attention because of their importance in the understanding and characterization of semiconductor materials and devices. Although much of the research direction has since shifted to other areas due to the improvement of material quality, the demands on device performance and wafer quality are still increasing. Furthermore, characteristic microdefects associated with a variety of semiconductor

devices have been attributed to various production processes associated mainly with the heating and doping steps in fabrication. This inherent limitation has brought about renewed efforts in basic research on material defects and increased attention to the subject of carrier recombination lifetime.

The usual definition of carrier recombination lifetime is the time required for the excess (nonequilibrium) charge carriers to decay to a factor 1/e of its initial value[1], after the external stimulus is removed. The physical defects which are inherent to devices provide the major paths for charge decay or recombination, with the excess energy being converted either to phonons or photons; these are referred to as nonradiative and radiative recombination respectively. Depending upon the regions (space-charge region or quasi-neutral region) where the recombination occurs, the measured values of carrier lifetime in widely-known semiconductor devices varies from 10^{-12} to 10^{5} sec.[2] While these defects can be reasonably controlled and largely eliminated by using modern process technology, their effects on the electrical parameters of the devices and their performance cannot generally be neglected. We focus here on the understanding of the impact of carrier lifetime on optoelectronic devices, especially photodetectors of the induced-junction type, in which the dark current is due to minority carriers as shown in the previous chapter. Discussion of the physical mechanisms of carrier recombination and the characterization of carrier lifetime will be deferred until the next chapter.

It is well-known that the recombination lifetime of the excess charge carriers has a major impact on the characteristics of most semiconductor devices. Depending on the applications, a variety

of devices, such as solar cells, photoconductors and injection laser diodes have been satisfactorily modelled by employing the appropriate recombination statistics. It may be expected that the active layer in these devices is in most cases sufficiently large that the diffusion length (determined by lifetime) is of central importance, otherwise (for narrow active regions) surface or interface recombination becomes dominant. Details of these considerations can be readily found in various textbooks.[3-5] In this chapter, we explore some effects of excess charge carrier lifetime which are directly related to the behaviour of avalanche or PIN photodetectors. Although a compromise must be made between the speed of response and the gain of these devices, it is assumed that the thickness of the active layer (region of high electrical field) in photodetectors is in excess of the diffusion length, with which the significant effects of (volume) carrier lifetime are concerned. Since these photodetectors operate under reverse bias voltages, the excess carriers are created primarily from the incident illumination intensity according to the form of the optical pulses. If we neglect the effects on carrier lifetime of the high electric field and the pulses are assumed to be of sufficient duration, we may discuss the consequences for performance of the carrier lifetime. This chapter therefore reviews the existing theory of recombination lifetime and applies these considerations to the understanding of the behaviour of photodetectors.

3.2 Consequences of Lifetime for Photodetector Performance

The operation of photodetectors is based on the photoelectric effect.[6] The performance of photodetectors will be determined by the

following factors: (1) noise, (2) quantum efficiency, (3) photoresponse time, and (4) gain. Each factor has its own distinguishing characteristics which may be directly or indirectly related to the carrier lifetime. Based on the geometrical structure of avalanche and PIN photodetectors. We now address these factors in turn.

3.2.1 Noise

Semiconductor detectors are limited by the minimum radiant power which they can detect due to the presence of noise. The noise may arise in the detector itself, in the radiant energy to which the detector responds, or in the electronic system following the detector. Here, we are interested in the noise internal to the detector. The remainder of the noise sources are not treated here; see Motchenbacher and Fitchan(7), Van Vliet(8) for details.

In addition to the thermal (Johnson) noise, there are three bias-dependent excess noise mechanisms in most semiconductor devices. These are generation-recombination noise, shot noise and flicker noise. Regarding the PN junctions and Schottky barrier photodetectors, we focus on shot noise, which arises from randomness in the diffusion and drift of carriers due to the reverse bias voltage. This is usually the dominant noise source in these devices. Multiplication noise arising from impact ionization in avalanche photodiodes will also be discussed below.

(1) Shot Noise

In general the rms shot noise current is given by(9)

$$I_N = \left[(2qI + 4qI_o)B \right]^{1/2} \quad (1)$$

where B is the measurement bandwidth, I is diode current, I_o is the reverse bias saturation current and q is electron charge. Under sufficient reverse bias, $I = -I_o$ and Eqn. (1) becomes

$$I_N = (2qI_oB)^{1/2} \qquad (2)$$

As mentioned in a previous chapter, the saturation current I_o is related to carrier lifetime by

$$I_o = \frac{qN_iW}{\tau_p} \quad \text{in the space-charge region} \qquad (3)$$

or

$$I_o = \frac{n_i^2(qkT\ \mu_p)^{1/2}}{N_d\ \ \tau_p} \quad \text{in the neutral region} \qquad (4)$$

where N_i is intrinsic carrier concentration, W is the width of the depletion region, q is electronic charge, N_d is the impurity doping concentration, τ_p is the minority carrier lifetime (for holes) and μ_p is the hole mobility. (Refer to Chapter 2)

Similar results in PN junction diodes which show the reverse saturation current to be carrier lifetime-dependent can be found in the paper by Pell.[(10)] Obviously, the noise current is inversely proportional to (a fractional power of) the carrier lifetime. The signal-to-noise power ratio (SNR) is directly proportional to the carrier lifetime. Usually at high temperature, the thermal noise is dominant; nevertheless, the carrier lifetime plays a role in the noise current since it also depends upon the temperature. This is discussed below.

(2) Multiplication Noise

Multiplication noise arises from the mechanism of impact ionization in the space-charge region of avalanche photodiodes under the high electric field. Usually the transit times for the carriers through the avalanche region are so short (typically 10^{-11} sec) that it is reasonable to neglect recombination (carrier lifetime typically is larger than 10^{-8} sec). Thus, there seems to be no direct effect of carrier lifetime on multiplication noise regardless of the excitation frequency ($f > 10$ MHZ) considered.[11-13]

3.2.2 Quantum Efficiency

In photodetectors, the quantum efficiency is defined as the number of electron-hole pairs generated by an incident photon:[14]

$$\eta = (\frac{I_p}{q})(\frac{P_p}{h\nu}) \qquad (5)$$

where I_p is the photogenerated current due to the absorption of incident optical power P_p at a wavelength λ, which corresponds to a photon energy $h\nu = h\frac{C}{\lambda}$. Due to the reflectivity of the surface of the photodetector, the quantum efficiency is below 100%; anti-reflection coatings appreciably reduce this loss of the incident power. Therefore, the photogenerated current I_p is the factor which determines the quantum efficiency.

In the PIN photodiode, under steady-state conditions, the total current density J_{tot} (i.e. photogenerated current density) through the reverse-biased depletion layer is given by[14]

$$J_{tot} = J_{drift} + J_{diff} \qquad (6)$$

in which

$$J_{drift} = -q\int_0^W G(x)dx = -q\int_0^W \phi_o\ \alpha\ e^{-\alpha x}\ dx$$

$$= q\ \phi_o(1 - e^{-\alpha W}) \qquad (7)$$

where G(x) is the electron-hole photo generation rate, α is the optical absorption coefficient and is a function of wavelength, W is the width of the depletion layer and ϕ_o is the incident photon flux density. Also,(14)

$$J_{diff} = -q\ D_\pi\left(\frac{\partial P_n}{\partial x}\right)_{x=W}$$

$$= q\ \phi_o\left(\frac{\alpha\ L_p}{1+\alpha\ L_p}\right)e^{-\alpha W} + q\ P_{no}\left(\frac{D_p}{L_p}\right) \qquad (18)$$

where $L_p = \sqrt{\tau_p D_p}$ is the diffusion length for minority carriers (holes) through the bulk n-region. D_p is the diffusion coefficient for holes and P_{no} is the equilibrium hole density. Thus,

$$J_{tot} = q\ \phi_o\left(1 - \frac{e^{-\alpha W}}{1+\alpha L_p}\right) + q\ P_{no}\left(\frac{D_p}{L_p}\right) \qquad (9)$$

The quantum efficiency can be obtained from Eqns. (9) and (5) under the assumption of a negligible P_{no}

$$\eta = 1 - \frac{e^{-\alpha W}}{1+\alpha\ L_p} = 1 - \frac{e^{-\alpha W}}{1+\alpha\sqrt{D_p\tau_p}} \qquad (10)$$

For high quantum efficiency, a large minority carrier lifetime is desirable for a fixed incident wavelength; however the minority carrier lifetime makes no significant contribution to the quantum efficiency as long as $\alpha W >> 1$. For example, for our Ge photodetectors with α (300°K) $= 4 \times 10^4 cm^{-1}$ at a wavelength $\lambda = 15.5$ μm, $D_p = 47.24 cm^2 sec^{-1}$ with $\tau_p = 2.5 \times 10^{-6}$ sec (see Chapter 4) and $\alpha W = 10$, $\eta = 1$, neglecting reflection losses. The same result can easily apply to a Si PIN photodiode. Therefore in this case the minority carrier lifetime has little influence on the quantum efficiency provided optimized conditions have been reached between the transit time and the depletion width.

3.2.3 Photoresponse Time

The photoresponse time is defined as the time spent by the minority carrier within the active region of the photodetector before being collected. This determines the bandwidth for the photodiode. Obviously the response time depends on the carrier saturation velocity under high reverse bias. It can be shown that[(15-16)]

$$f_{3dB} \simeq 0.44/t_d \quad \text{for PIN photodiodes} \quad (11)$$

$$f_{3db} \simeq 0.59/t_d \quad \text{for avalanche photodiodes} \quad (12)$$

where f_{3dB} is the 3dB cut-off frequency (i.e. $|FR| = 1/\sqrt{2}$, FR = Frequency Response) and t_d = drift time.

The above two equations were obtained by solving the transport equations assuming the following two conditions:[(15)] (1) no trapping effects, (2) the transit time of the carriers across a junction is much shorter than the bulk recombination lifetime. For the latter case, under an appropriate reverse-bias voltage and assuming modern technology in device processing, these conditions are usually satisfied. For the former case, the mathematics are quite complicated. It

is not clear whether the minority carrier lifetime provides any significant contribution to the photoresponse time in general. The details of these results will be presented for further investigation.

3.2.4 Gain

For broadband optical signal detection, avalanche photodiodes with a built-in gain mechanism are useful in overcoming the thermal noise. This gain can be obtained by multplying the optically generated carriers via impact ionization. Since this process is random, additional noise is introduced and this multiplication noise has been previously discussed.[13] As far as the gain is concerned, the multiplication factor M will be considered as the principal factor in determining the gain. Also, the multiplication factor M is dependant on the impact ionization coefficients for electrons and holes in the high-field region.

The mechanism of impact ionization can be simply regarded as arising from a chain-reaction due to the accelerated primary carriers which multiply to create secondary electron-hole pairs in the high electric field region. The number of ionizing collisions per unit length is termed the ionization coefficient α .

This coefficient is an averaged vlaue because of the random nature of the process. Basically, α_n and α_p can be measured from the experimental data and have been found to be dependent on the applied field,[17] crystal orientation,[18] temperature[19] and the doping profile[20] of the depletion region. The latter factor is actually interrelated to the electric field via the doping distribution. Both α_n and α_p can be approximated by[21-23]

$$\alpha_n = \alpha_{n\infty} \exp(-A_n/|F|)^d \quad (13)$$

$$\alpha_p = \alpha_{p\infty} \exp(-A_p/|F|)^d \quad (14)$$

where $\alpha_{n\infty}$, $\alpha_{p\infty}$, A_n, A_p and d are obtained by fitting to experimental data. They are dependent on the material and d is approximately unity for most photodetectors.[15] F is the electric field and usually is in the range of 10^4 - 10^7 volt/cm. It is obvious that the ionization coefficients will increase for increasing electric field. Regarding the temperature-dependence, Grant[24] has found that the constants A_n and A_p are linearly proportional to temperature with the result that the ionization coefficients decrease when the temperature is increased.

It has been recently reported that the thermal emission (ionization) rate will be enhanced in the high-field region regardless of whether the center is Coulombic[25] or neutral.[26] This is called the Poole-Frankel effect and has been used to interpret the detrapping of trapped carriers arising from tilted energy bands due to the electric field (> 10^4 volt/cm). For example, the thermal emission rate for electrons[27] is

$$e_n^{PF} = e_n^0 \exp(-\frac{E_i - \Delta E_i}{kT}) \quad (15)$$

and

$$\Delta E_i = q(\frac{eF}{\varepsilon^* \varepsilon_o})^{1/2} \quad (16)$$

In this model the correction ΔE_i depends only on the long-range portion

of the center potential. q is the electronic charge, F is the electric field and ε^* and ε_o are the dielectric constants for the semiconductor and the Vacuum respectively. The increasing emission rate reduces the net recombination rate which increases the effective lifetime. This positive effect on the carrier lifetime is opposite to the negative effects due to increasing ionization coefficients. Thus, these are independent mechanisms which react indirectly to the electric field. Therefore, there is no direct effect of carrier lifetime on the ionization coefficient.

References

1. J.S. Blakemore, Semiconductor Statistics, International Series of Monographs on Semiconductors, Edited by H.K. Henisch, vol. 3, Pergamon Press; New York 1962.

2. A. Milnes, Deep Impurities in Semiconductors, Wiley; New York, 1973, Chap. 1.

3. B.O. Seraphin, Editor, Solar Energy Conversion, Topics in Applied Physics, vol. 31, Springer-Verlag, Berlin Heidelberg, N.Y. 1979, Chap. 5.

4. C.P. Sandbank, Editor, Optical Fibre Communication Systems, John Wiley & Sons Ltd., 1980, Chap. 7 and 8.

5. M.K. Barnoski, Editor, Fundamentals of Optical Fiber Communications, 2nd Edition, Academic Press, 1981, Chap. 4 and 5.

6. R.J. Keyes, Editor, Optical and Infrared Detectors, Topics in Applied Physics, vol. 19, Springer-Verlag, 1977, Chap. 2.

7. C.D. Motchenbacher, F.C. Fitchen, Low Noise Electronic Design, Wiley-Interscience, New York, 1973.

8. K.M. Van Vliet, "Noise Limitations in Solid State Photodetectors", Appl. Opt., vol. 6, no. 7, pp. 1145-1169, July 1967.

9. A. Van Der Ziel, Noise in Measurements, John Wiley & Sons; New York, 1976, Chap. 10.

10. E.M. Pell, "Reverse Current and Carrier Lifetime as a Function of Temperature in Germanium Junction Diodes", J. of Appl. Phys., vol. 26, no. 6, pp. 658-665, June 1955.

11. R.B. Emmons and G. Lucovsky, "The Frequency Response of Avalanching Photodiodes", IEEE Trans. on Electron Devices, vol. ED-13, pp. 297-305, March 1966.

12. R. Kuvas and C.A. Lee, "Quasistatic Approximation for Semiconductor Avalanches", J. of Appl. Phys., vol. 41, pp. 1743-1755, March 1970.

13. I.M. Naqui, "Effects of Time Dependence of Multiplication Process on Avalanche Noise", Solid-State Electronics, vol. 16, pp. 19-28, 1973.

14. S.M. Sze, Physics of Semiconductor Devices, 2nd edition, Wiley-Interscience, New York, 1981, Chap. 13.

15. J. Muller, "Photodiodes for Optical Communiation", From Advances in Electronics and Electron Physics, Edited by L. Marton and C. Marton, vol. 55, Academic Press, Inc., New york, 1981.

16. D.E. Sawyer and R.H. Rediker, "Narrow Bae Germanium Photodiodes", Proc. of IRE, vol. 46, pp. 1122-1130, June 1957.

17. P.A. Wolff, "Theory of Electron Multiplication in Silicon and Germanium", Phys. Rev., vol. 95, no. 6, pp. 1415-1420, Sept. 1954.

18. T.P. Pearsall, R.E. Nahory and J.R. Chelikowsky, "Orientation Dependence of Free-Carrier Impact Ionization in Semiconductors: GaAs", Phys. Rev. Lett., vol. 39, no. 5, pp. 295-298, Aug. 1977.

19. C.R. Crowell and S.M. Sze, "Temperature Dependence of Avalanche Multiplication in Semiconductors", Appl. Phys. Lett., vol. 9, no. 6, pp. 242-244, Sept. 1966.

20. C.A. Baraff, "Distribution Functins and Ionization Rates for Hot Electrons in Semiconductors", Phys. Rev., vol. 128, no. 6, pp. 2507-2517, Dec. 1962.

21. C.A. Lee, R.A. Logan, R.L. Batdorf, J.J. Kleimack and W. Wiegmann, "Ionization Rates of Holes and Electrons in Silicon", Phys. REv., vol. 134, no. 3A, pp. 761-773, March 1964.

22. T.P. Persall, R.E. Nahory and M.A. Pollack, "Impact Ionization Coefficients for Electrons and Holes in $In_{0.14}Ga_{0.86}As$", Appl. Phys. Lett., vol. 27, no. 6, pp. 330-332, Sept. 1975.

23. H.D. Law, K. Nakano, L.R. Tomasetta and J.S. Harris, "Ionization Coefficients of $Ga_{0.27}Al_{0.28}Sb$ Avalanche Photodetectors", Appl. Phys. Lett., vol. 33, pp. 948-950, 1978.

24. W.N. Grant, "Electron and Hole Ionization Rates in Epitaxial Silicon at High Electric Fields", Solid-State Electronics, vol. 16, no. 7, pp. 1189-1203, 1973.

25. G. Vincent, A. Chantre and D. Bois, "Electric Field Effect on the Thermal Emission of Traps in Semiconductor Junctions", J. of Appl. Phys., vol. 50, no. 8, pp. 5484-5487, Aug. 1979.

26. P.A. Martin, B.G. Streetman and K. Hess, "Electric Feild Enhanced Emission From Non-Coulombic Traps in Semiconductors", J. of Appl. Phys., vol. 52, no. 12, pp. 7409-7415, Dec. 1981.

27. M. Jaros, Deep Levels in Semiconductors, Adam Hilger Ltd., Bristol, 1982, Chap. 8, p. 177.

CHAPTER 4

MINORITY CARRIER RECOMBINATION IN GERMANIUM - PHYSICAL MECHANISMS AND EXPERIMENTAL CHARACTERIZATION*

The induced-junction device introduced in the previous chapter (Chap. 2) is a unique structure for the investigation of the recombination mechanisms responsible for the minority carrier lifetime. We have already seen that this parameter and its dependence upon temperature, optical intensity and wavelength, etc. are of important in the optimization of photodetector structures.

In this chapter we take a fundamental look at the recombinaation process principally using an experimental method entitled forward-current induced voltage decay (FCVD). Further information is potentially available using another measurement method, photo-induced open-circuit voltage decay (POVD). We discuss the information obtained by these two methods, and the characterization of the germanium materials and devices which results. We further are able to make some academic judgements which concern the validity of existing recombination models. These judgements are of benefit to those research workers who wish to model photodetector devices and semiconductor materials.

4.1 Forward Current Induced Voltage Decay (FCVD) Method

4.1.1 Physical Background

The original phenomenological theory of Shockley and Read[1] and of Hall,[2] which is generally referred to as SRH statistics or the SRH model, has found wide application in semiconductor device characterization. The majority of the experimental work validating this

---

*Part of the contents of this chapter have been published as Y.K. Hsieh and H.C. Card, "Recombination in Germanium: Voltage Decay Experiments on Induced-Junction Devices and Validity of SRH Model", Solid-State Electronics, in press for 1984.

model is restricted to a single measurement temperature, or to low-level injection conditions, or both. Various authors have speculated that the original assumptions in the SRH treatment are expected to fail under extreme conditions, such as high-level injection (see, for example, Refs. 3-5).

A proven technique for unambiguous carrier lifetime measurements is the forward-current induced voltage-decay (FCVD) experiment.[6-8] This method requires an injecting pn junction in order to readily establish the distribution of excess minority carriers in the material. The fabrication procedures for creation of the pn junction may however interfere with the intrinsic material properties one is attempting to measure, for example by introducing unwanted impurities, dislocations, or other defects as a conseqeunce of the elevated processing temperatures and the heavily-doped regions.

We have introduced a germanium device in the previous chapter for application as a photodetector in fiberoptic systems, which provides for the same minority-carrier injection in forward bias as a pn junction without the need for the doped p-type region. This device is referred to as an induced pn junction; the surface region of moderately-doped n-type germanium is inverted to p-type by the presence of a thin (optically-transparent) layer of Au as a consequence of its large work function. The electronic and optical properties of this device have been described previously, along with a definitive experimental proof of the pn junction-like behaviour.[9] The induced pn-junction is not a new idea in photodetector technology; it was employed for example with PbTe and InAs much earlier.[10]

The purpose of this investigation is to understand the recombination mechanisms in high-quality germanium material, such as that employed in the fabrication of photodetectors, by FCVD measurements on these devices. The practical importance of this work is that for infrared photodetectors in germanium, the carrier lifetime intrinsic to the material must be known as a function of both the temperature and the injection level in order to optimize the device and system design. One may be interested in the behaviour of cooled detectors in order to reduce detector noise. Even in germanium detectors not of the induced-junction type, the intrinsic recombination processes define a maximum carrier lifetime. The scientific importance of this work is that the present results provide a comprehensive examination of the validity of the SRH recombination model. The wide range of temperatures and injection levels investigated in the experiments, and the self-consistency of the data with cross-sections supported by quantitative theoretical arguments, inspires considerable confidence in the SRH model, at least for these germanium samples, over a wide range of conditions.

4.1.2 Experimental Details

The devices employed in this study were fabricated by the evaporation at 10^{-6} torr of gold thin films onto moderately-doped n-type germanium single-crystal wafers. The Au contact areas were in the range 1-3 x 10^{-2} cm^2 (circular electrodes) and the Au thicknesses were ≃ 250 Å . The germanium wafers were (111) oriented n-type material, obtained from General Diode Corporation, Sb-doped, with a specified dislocation density of 3000 cm^{-2}, and were 350 ± 10 μm in thickness. The germanium surfaces were chemically-prepared, and the doping concentration was N_d = 2.08 x 10^{15} cm^{-3} as determined from high-

frequency capacitance-voltage measurements. Near-ideal current-voltage behaviour was observed. The 'Schottky' barrier heights at the Au-Ge interface were in excess of 0.6 eV; the germanium surface region was hence strongly-inverted and the conduction in forward bias was dominantly hole injection as in a p+n junction. We refer to these devices as induced-junction diodes; their d.c. properties have been reported and discussed in considerable detail elsewhere.[9]

The open-circuit voltage decay, following the termination of an applied (dark) forward current density J_F , was monitored during the return to equilibrium. This technique is termed the forward current-induced voltage decay (FCVD) method. Details of the apparatus have been described by many authors, for example by Lederhandler and Giacoletto.[6] Our experiments followed their method closely.

Approximately 50 samples have been fabricated and the behaviour of the majority of these devices were very similar. The results presented below are typical of these 50 devices. The characteristics were stable with time; provided the surfaces were cleaned in methanol prior to the deposition of gold no appreciable ageing effects were observed.

4.1.3 Experimental Results

An example of the raw data for the dependence of the open-circuit voltage V_{oc} on time for the devices in this study is given in Fig. 4.1. The particular results of Fig. 4.1 were obtained at a temperature T of 300 K. The experimentally-observed decay of the open-circuit voltage following the termination of the current pulse is described, for $t \leq 3$ μs, by

$$V_{oc} = V_o - \frac{kT}{q}\frac{t}{\tau_p} \qquad (1)$$

with an error of $\leq$ 5%. This is predicted by the simple theory for FCVD[6-7] and leads to the determination of the recombination lifetime for holes, τ_p , in the n-type germanium.

The dependence of the hole lifetime on the forward current density (or injection level) J_F , which was applied to establish the initial value of V_{oc} , is shown by the data points in Fig. 4.2, for T = 300 K. In Fig. 4.3 we show the dependence of τ upon temperature for a particular injection level (J_F = 1.2 mA cm^{-2}) in the form log τ_p vs 1/T . This corresponds to a low injection level according to Fig. 4.2, as explained in the next section. Finally, Fig. 4.4 illustrates the dependence of τ_p upon the excess carrier concentrations at the edge of the space-charge region, which has been determined from measurements of τ_p vs J_F at three measurement temperatures.

4.1.4 Discussion

In the interpretation of the experimental results presented above, we employ the statistical SRH recombination model which predicts a net recombination rate of[1,2]

$$U = \frac{pn - n_i^2}{\tau_{po}(n+n_1) + \tau_{no}(p+p_1)} \qquad (2)$$

where $\tau_{po} = (\sigma_p V_{th} N_t)^{-1}$ and $\tau_{no} = (\sigma_n V_{th} N_t)^{-1}$, with N_t the volume concentration of recombination centers, σ_p and σ_n the capture cross sections of these centers for holes and electrons respectively, and V_{th} the thermal velocity of free holes and electrons, assumed to be equal. p and n are the hole and electron concentrations, n_i is the intrinsic carrier concentration, and

$$n_1 = n_i \exp\left(\frac{E_t - E_i}{kT}\right) \qquad (3)$$

$$p_1 = n_i \exp\left(\frac{E_i - E_t}{kT}\right) \qquad (4)$$

where E_t is the energy level of the recombination centers and E_i is the intrinsic level (near midgap).

The recombination lifetime for holes is given by

$$\tau_p = \frac{p - p_o}{U} \qquad (5)$$

where p_o is the equilibrium concentration of holes. In terms of the excess concentrations of holes and electrons Δp and Δn respectively, we have that $p = p_o + \Delta p$ and $n = n_o + \Delta n$, where outside the space-charge region in the semiconductor, $n_o \simeq N_d$, the doping concentration of the n-type germanium, and $p_o \simeq n_i^2/N_d$ for the temperature range studied in this paper. Also $\Delta n = \Delta p$ in this region as a consequence of space-charge neutrality.[11]

We assume, on the basis of our observations, that a single trap state or recombination center dominates the recombination process in our devices. The energy E_t of this state is assumed to produce the inequalities

$$n_1 > n_0 \gg p_o > p_1 \qquad (6)$$

In other words E_t is assumed to lie well above the equilibrium Fermi level in energy.

Combining Eqns. (2) to (6) leads to

$$\tau_p \simeq \frac{\tau_{po}\,(n+n_1) + \tau_{no}\,(p+p_1)}{n}$$

$$\simeq \tau_{po}(1 + \frac{n_1}{n}) + \tau_{no}(\frac{p}{n}) \quad (7)$$

In low-level injection ($p \ll n$) this reduces to

$$\tau_p \simeq \tau_{po}\,(1 + \frac{n_1}{n}) \quad (8)$$

and for high-level injection ($p \simeq n \gg n_1$) to

$$\tau_p \simeq \tau_{po} + \tau_{no} \quad (9)$$

For intermediate injection levels, the full expression of Eqn. (6) is required.

Under conditions of low-level injection, Eqn. (8) may also be expressed as

$$\tau_p \simeq \tau_{po}\,\left[1 + \exp\left(\frac{E_t - E_{fn}}{kT}\right)\right]$$

$$\simeq \tau_{po}\,\left[1 + \exp\left(\frac{E_t - E_c}{kT}\right)\exp\left(\frac{E_c - E_{fn}}{kT}\right)\right]$$

$$\simeq \tau_{po}\,\left[1 + \exp\left(\frac{E_t - E_c}{kT}\right)\left(\frac{N_c}{N_d}\right)\right] \quad (10)$$

where we have used the result for low-level injection conditions and assuming complete ionization of donors, that $E_c - E_{fn} = kT\,\ln(N_c/N_d)$.

In these expressions N_c is the effective density of states in the conduction band given by

$$N_c = 2\left(\frac{2\pi\, m_n^* kT}{h^2}\right)^{3/2}$$

$$= 1.04 \times 10^{19} \left(\frac{T}{300}\right)^{3/2} \text{cm}^{-3} \qquad (11)$$

for germanium.(12)

The experimental activation energy in Fig. 4.5 based on Eqn. (10) and the data of Fig. 4.3 for τ_p vs. T , leads to the conclusion that the recombination proceeds through a single trapping level with an energy $E_t = E_c - 0.128 \pm 0.008$ eV. In obtaining this result, adjustments to the data points in Fig. 4.5 were made to take account of the (weak) temperature dependence of τ_{po} , discussed below. Note that this recombination is presumed to occur primarily in the quasi-neutral region of the semiconductor. There is an initial phase after the termination of the applied current pulse which is very rapid on the time scale of these experiments during which excess carriers in the space-charge region are removed from this region, both by the high electric fields and by space-charge recombination.(13) We are not concerned with this phase in the present paper.

We now employ the Shockley approximation(11,12) to evaluate the excess carrier concentration at the edge of the space-charge region. We therefore have that

$$\Delta p = \Delta n = \frac{L_p J_f}{q D_p} \qquad (12)$$

where $L_p = (D_p \tau_p)^{1/2}$ and L_p , D_p are the diffusion length, diffusion coefficient, respectively. On the basis of Eqn. (12) one can therefore plot the dependence of τ_p upon $\Delta p = \Delta n$, and this has also been shown in Fig. 4.2. The diffusion coefficient $D_p = (kT/q)\mu_p$ where the 300°K hole mobility has been taken to be 1900 $cm^2 V^{-1} s^{-1}$ for our doping concentration, in the calculation of Fig. 4.2. Since the hole lifetime τ_p is dependent upon the injection level according to Eqn. (7), the correspondence between Δp and J_F was based upon a particular injection level; this is indicated by the arrow in Fig. 4.2. Since τ_p varies by less than a factor of 2 from this value, the magnitudes of $\Delta p = \Delta n$ in Fig. 4.2 are accurate to a factor of approximately $\sqrt{2}$, according to Eqn. (12). Comparison is made with Eqn. (7) for the value of E_t (and hence n_1) given above; the result is the dashed line referred to as theory in Fig. 4.2.

From the results of Fig. 4.2 and Eqns. (7) to (9) we also deduce that $\tau_{no} = 1.70 \pm 0.02 \times 10^{-6}$s and $\tau_{po} = 2.98 \pm 0.02 \times 10^{-7}$s at T = 300K. The calculation of Eqn. (7) with these parameters at T = 125K and 200K (together with the 300K result) are shown by the solid lines in Fig. 4.4, which compare very favourably with the experimental points.

We have also examined the temperture dependence of τ_p in the low-temperature region under low-level injection conditions, for which case $n_1 \ll n$ and $\tau_p \simeq \tau_{po}$. These results are shown in Fig. 4.6. From this figure, we have extracted an activation energy for the hole cap ture cross-section of $\Delta E = 0.029 \pm 0.003$ eV, where we have used $\tau_{po} = (N_t \sigma_p V_{th})^{-1}$, and have assumed N_t to be independent of temperature, and V_{th} to obey the relation $\frac{m_p^* V_{th}^2}{2} = 3/2\ kT$. Here, m_p^* is the effec

tive mass of holes which can be taken to be 0.37 m_o ; $V_{th} \approx 1.2 \times 10^7$ cm/s at T = 125K.[12]

Rose[14] has shown that for capture by a Coulombic attractive center, the cross section is described by

$$\sigma_p = \frac{\pi q^4}{(4\pi\varepsilon)^2 \, 4(kT)^2} \qquad (13)$$

Substitution of $\varepsilon = 16$ for germanium gives the results shown by the data points in Fig. 4.7. These results may be approximated, over the range of T in Fig. 4.7, by the first-order approximation

$$\sigma_p \simeq \sigma_{po} \exp\left(\frac{\Delta E}{kT}\right) \qquad (14)$$

where $\sigma_{po} = 9.4 \times 10^{-14}$ cm^2 and $\Delta E = 0.023 \pm 0.001$ eV. This activation energy agrees very favourably with the value obtained above on the basis of the experimental results of Fig. 4.6. The concentration of recombination centers is obtained from $N_t = (\sigma_p V_{th} \tau_{po})^{-1}$ to be $N_t \simeq 1.06 \times 10^{12}$ cm^{-3} . One reason for the success of the simple treatment of Rose is the large value of the cross section which implies capture over a larger volume than that associated with the particular microscopic potential of the defect.

On the basis of these results we conclude that recombination occurs primarily via isolated point defects that are acceptorlike and hence exhibit Coulombic capture for holes. In capturing electrons these centers will be neutral which accounts for the much smaller cross sections for electron capture. $\sigma_n \simeq \sigma_p (\tau_{no}/\tau_{po}) = 1.66 \times 10^{-14}$ cm^2 .

The origin of the particular defect has not been determined. We may speculate that it is structural in nature, as the parameters identified above do not conform to those of known impurities in germanium.[15]

Note that in the present validation of the SRH treatment of recombination in germanium, we have not seen evidence of trap saturation under high-injection conditions or other possible limitations to this model which have been argued to arise in the extremes of injection level or temperature.

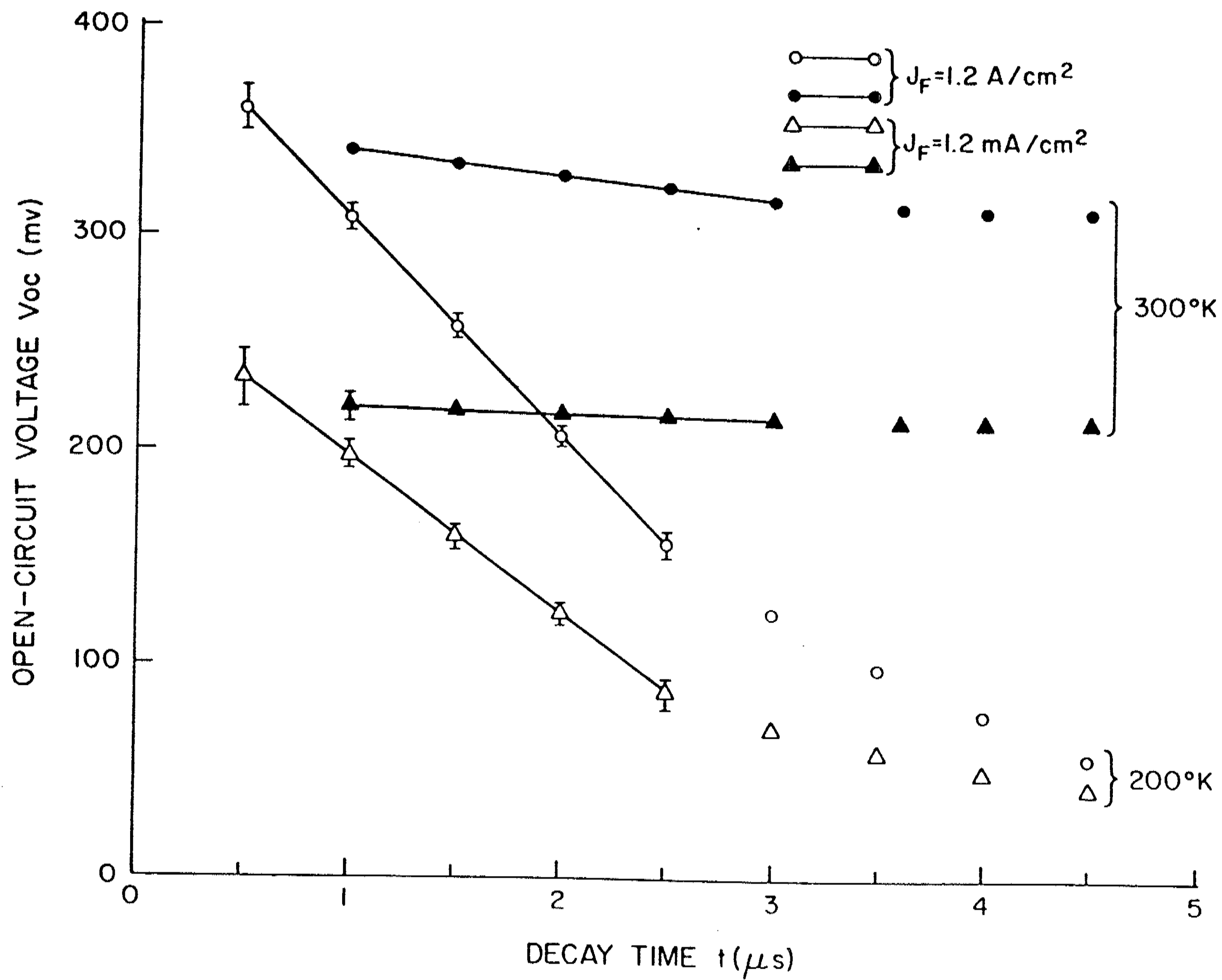

FIG. 4.1 Typical example of open-circuit voltage decay following the termination of an applied current pulse.

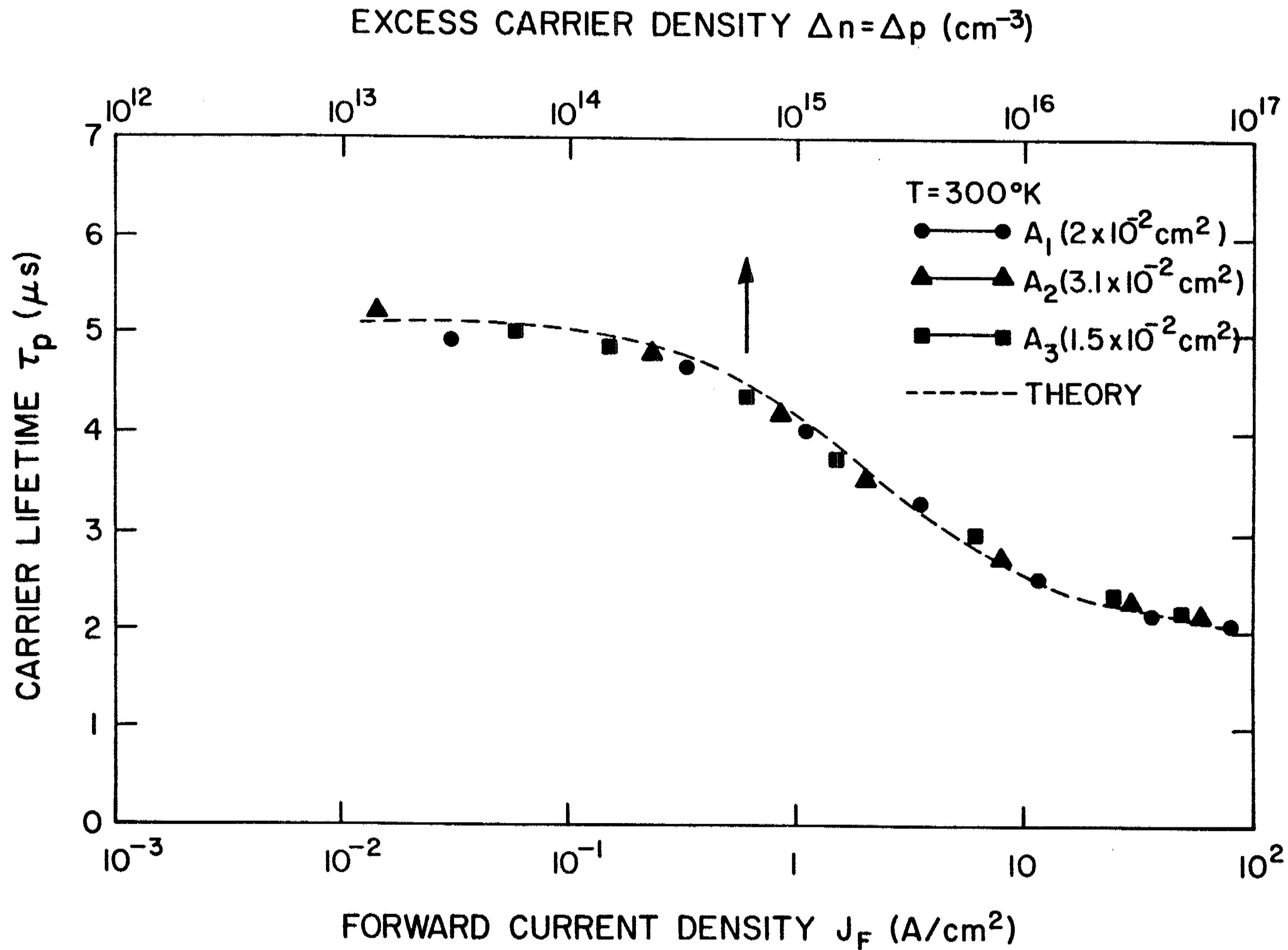

FIG. 4.2 Dependence of minority carrier (hole) lifetime of germanium upon current density applied, J_F , and upon excess carrier concentration at edge of space-charge region, $\Delta n = \Delta p$, for t = 300K. ▲ ● experimental points, ---- theory of Sec. 4.

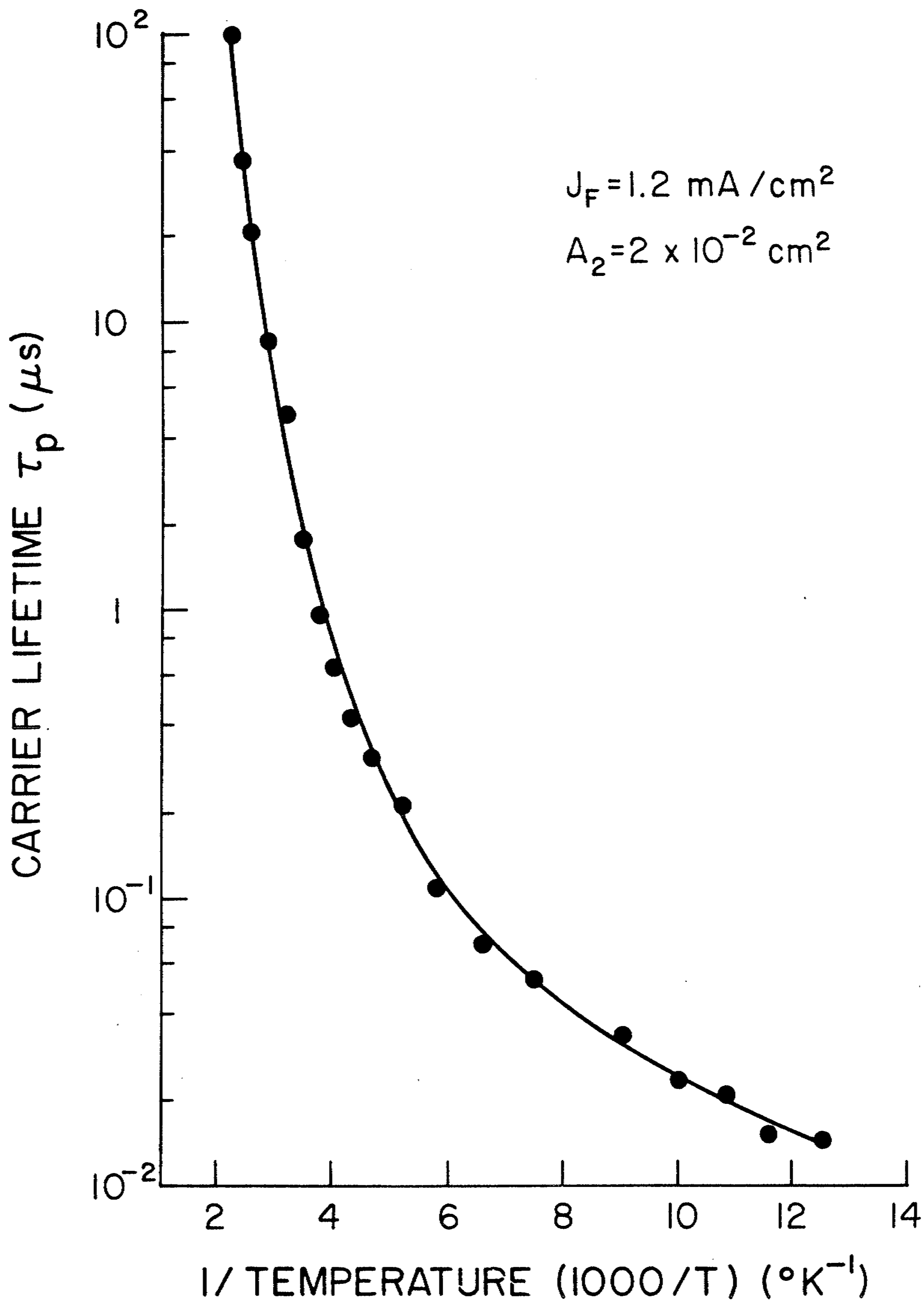

FIG. 4.3 Dependence of minority carrier lifetime upon temperature for low injection conditions (J_F = 1.2 mA cm $^{-2}$).

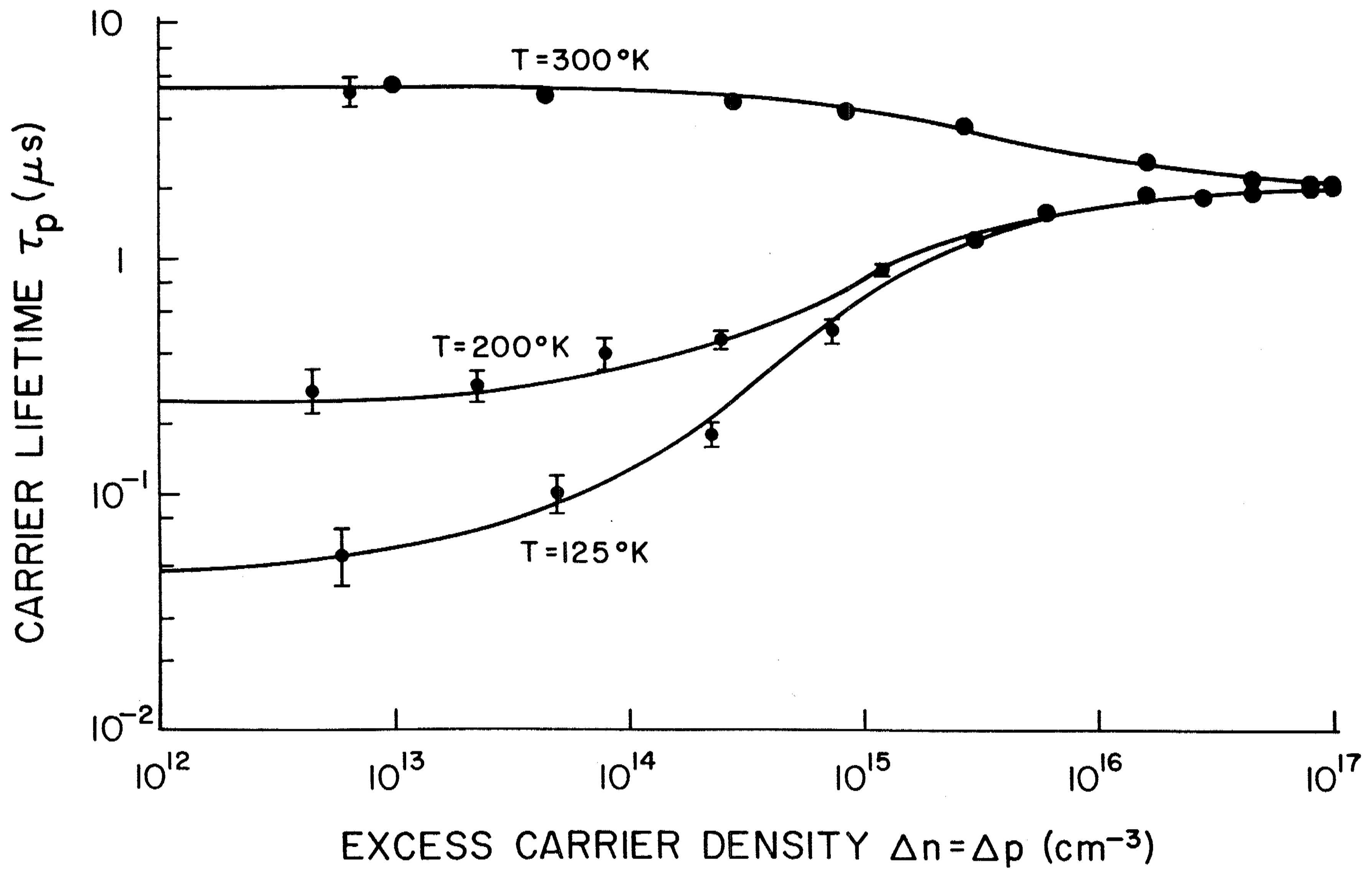

FIG. 4.4 Dependence of minority carrier lifetime upon excess carrier density at edge of space-charge region experimental data points, _____ SRH model.

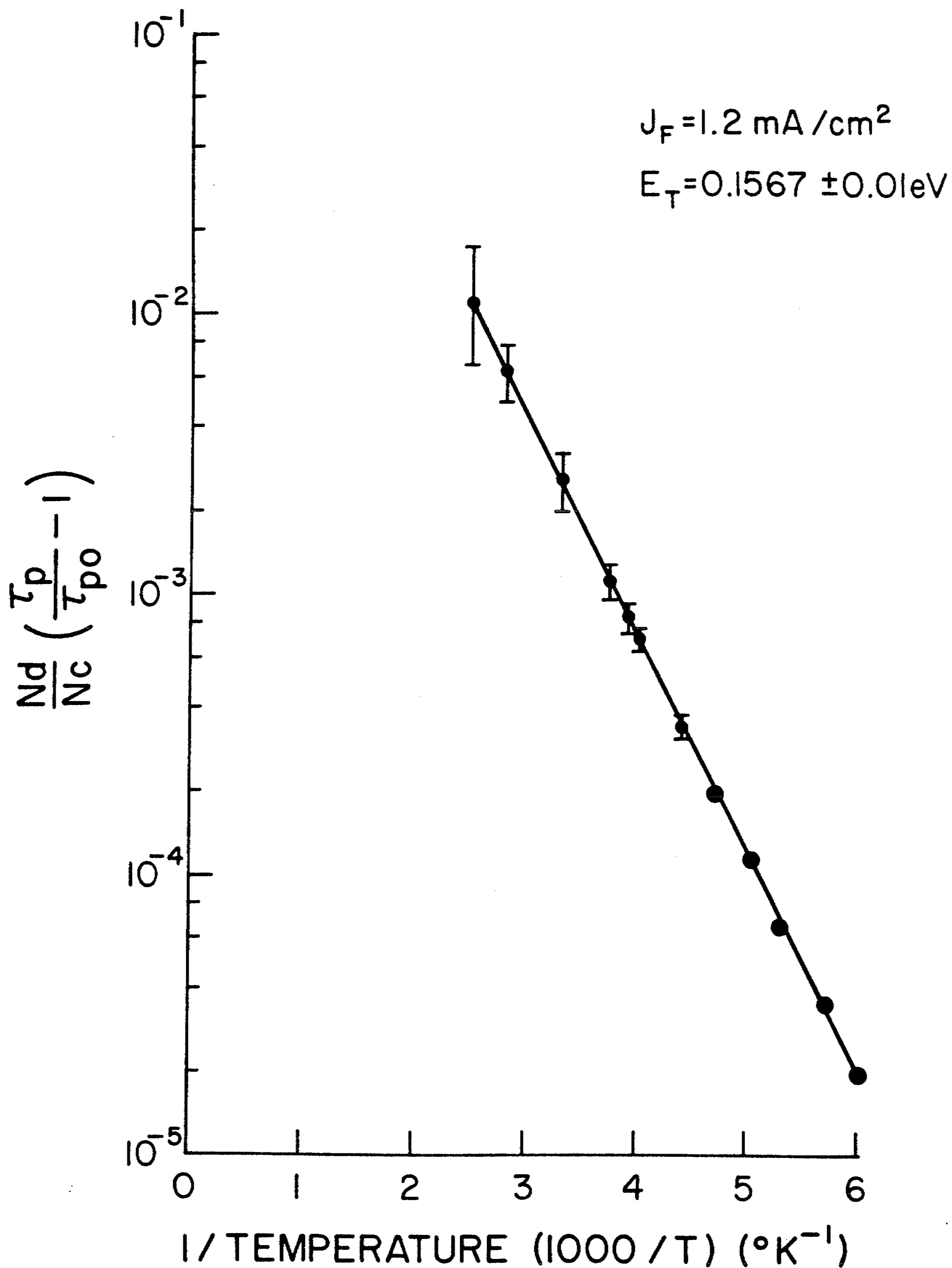

FIG. 4.5 Determination of activation energy (E_c - E_t) in Eqn. (10) from the experimental data of Fig. 4.3 for τ_p vs T in low-injection conditions. Corrections for minor temperature dependence of τ_{po}(see Fig. 4.6) have been made.

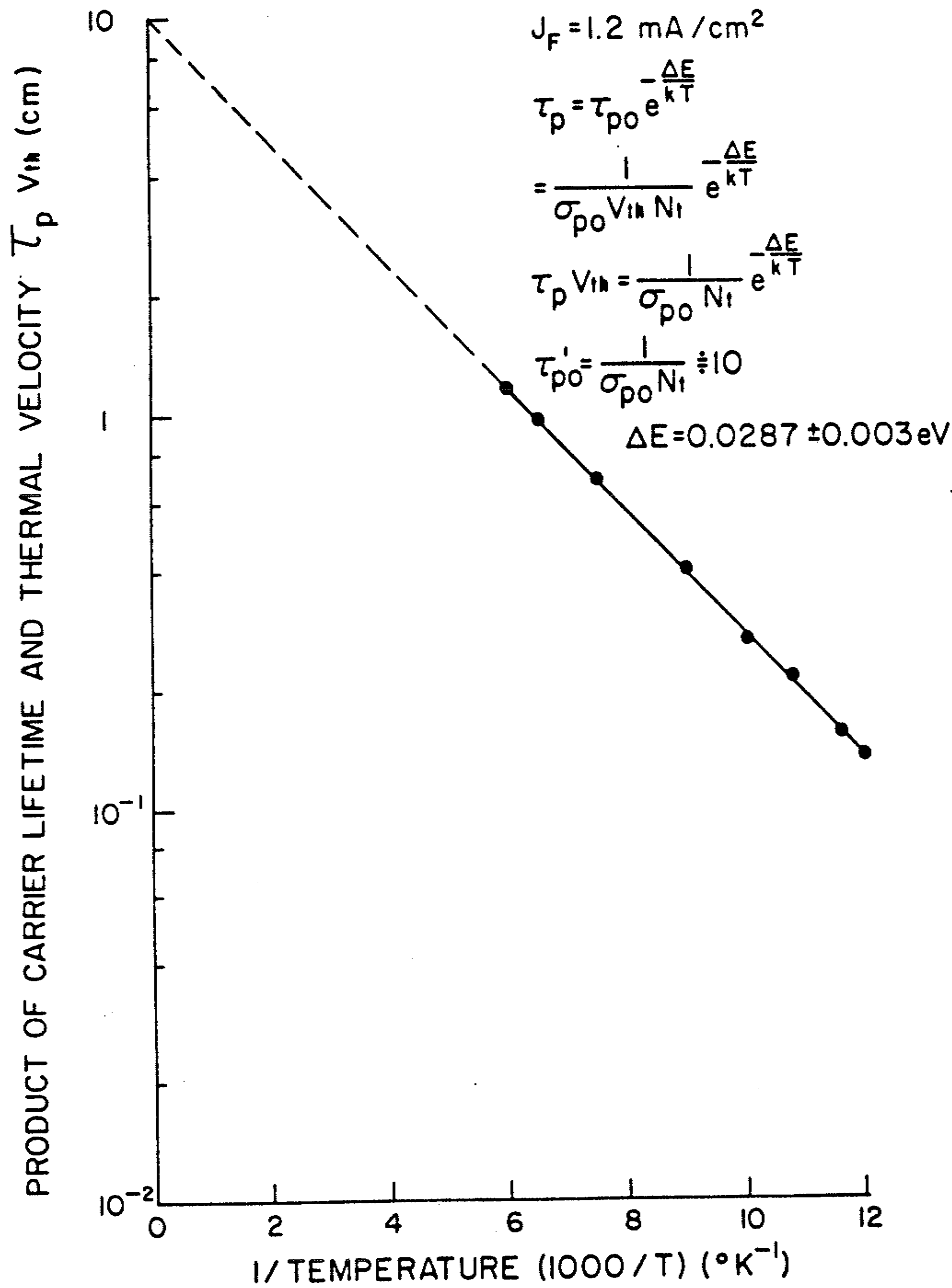

FIG. 4.6 Temperature dependence of τ_{po} is obtained from data for τ_p in low injection and low temperature region, where Eqn. (7) becomes $\tau_p \simeq \tau_{po}$. Correction made for temperature dependence of V_{th} .

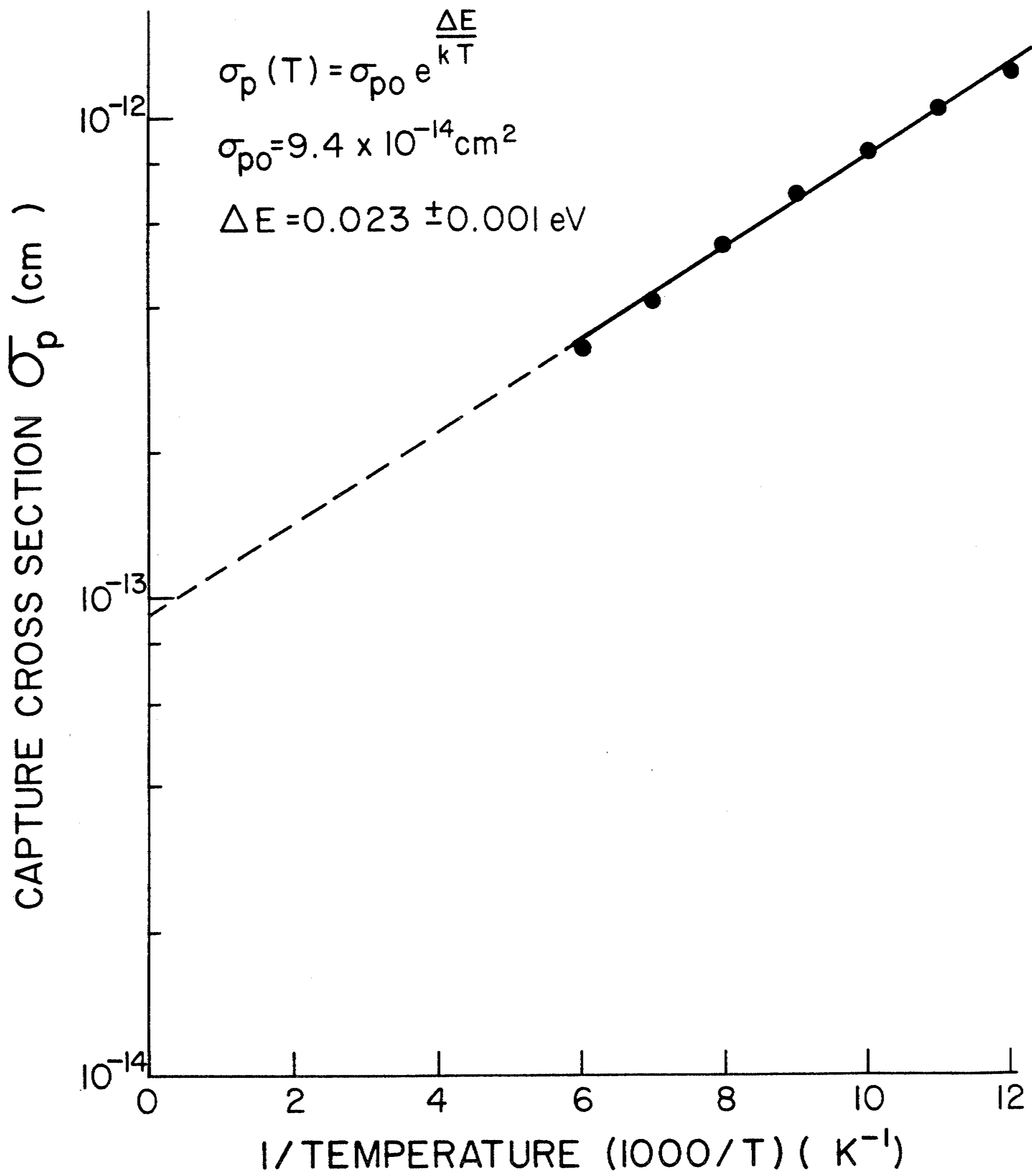

FIG. 4.7 Prediction of Rose for dependence of capture cross-section upon temperature for Coulombic capture. Activation energy compares favourably with experimental observations in Fig. 4.6.

4.2 Photo-Induced Open-Circuit Voltage Decay (POVD) Method

4.2.1 Physical Background

Since 1955, the measurement of excess carrier decay induced by electrical (dark-current) or optical (photo-current) excitation has been widely used to determine the average recombination time within the quasi-neutral base region of a variety of semiconductor devices. So far, more than nine methods[8] to measure the carrier lifetime have been developed for semiconductor characterization. Each available method has its own applicability which depends on the physical structures (pn-junction, Schottky barrier, MOS, MIS devices, etc.) and inherent parameters (energy gap, absorption spectrum, etc.) of devices. Most important, it is the theoretical derivation (formulation and assumption) which distinguish these methods if the limitations and errors of experimental apparatus are negligible. In so far as accuracy and convenience is concerned, there has not been sufficient proof that any two of these methods give the same results.

An investigation of recombination centers through the measurement of minority carrier lifetime in induced-junction devices has been presented in the previous section. The parameters of the recombination centers, such as their volume concentration, energy level and temperature-dependent capture cross-sections have been presented quantitatively based on the SRH recombination model. In 1979, a convenient experimental technique for determining the excess carrier lifetime within the neutral region of P-N junction solar cells was proposed by J.E. Mahan et al.[16] This method is based upon the observation of the decay of the open-circuit voltage following the termination of an applied optical signal and is termed the photo-

induced open-circuit voltage decay (POVD) technique. Since then, both theoretical and experimental investigation on the application of this method to the characterization of photovoltaic devices has been discussed and further extended.[17-22] Although this method has been declared to be successful in determining the minority carrier lifetime under certain restrictions, it has not been widely accepted as a standard method for measuring the carrier lifetime for the following reasons: (1) the decay curves (open-circuit voltage decay) are much more complicated than expected on the basis of the simple theory, i.e. the expected linear decay is not easy to obtain, in contradiction to the theoretical prediction; (2) external circuit components such as parasitic capacitances, shunting resistances and inherent response time of oscillioscopes have been found to interfere substantially with the measurements; (3) controversial results[4] have arisen from devices of small base thickness (in comparison with the diffusion length).

We have applied this POVD method under the most favourable experimental conditions to the characterization of our devices in order to further investigate the minority carrier recombination process. Also, due to the unique characteristic (current transport dominated by minority carriers) of these devices, we expect to cast additional light on the photo-induced voltage decay method.

After describing the experimental apparatus, the experimental results will be given in view of the precautions discussed above. At the same time the discussion of the resultant data analysis will be provided.

4.2.2 Experimental Set-Up

The experimental apparatus for the POVD measurements can be seen in Fig. 4.8(a). Unlike Mahan's[16] case, a flashing light source with spectral content from 400-1000 nm and pulse duration of 3 μs has been required to uniformly illuminate the device. This is accomplished by placing a monochrometer and filter after the electronic stroboscope. The purpose of this addition is to investigate the variation of lifetime with wavelength and also to provide for the compensation of second harmonic effects when the longer wavelengths are employed. A typical open-circuit voltage decay after the illumination with external triggering has also been shown in Fig. 4.8(b). The experimental conditions are also included for reference. The determination of lifetime was made according to the following equation[23]

$$\tau_p = \left(\frac{q}{kT}\right)\left(\frac{d\,t}{d\,V_{oc}}\right) \qquad (15)$$

A region of linear decay was obtained after the plateau (see Fig. 4.8(b)).

The same device structure as described in the previous section 4.1.2 has been used. In Fig. 4.9, the variations of photon flux density and optical absorption coefficient α with wavelength ϕ_o have been measured by means of a photometer and an absorption spectrometer. The spectrum of the xenon-gas filled electronic stroboscope (STROBOTAC, Type 1538A) was found to be very similar to the manufacturer's specification. Also, the absorption coefficients α are close to those measured for germanium by W.C. Dash, et al.[24] It can be seen that the same value (9.0×10^{17} photons/cm^{2}sec) of photon flux density ϕ_o can be

found at λ = 633 and 1000 nm. This is convenient because the same amount of photons should be considered for comparison as far as the excess carriers decay is concerned. Here, of course we have to assume that the quantum efficiency of the device is also the same for those two wavelengths. To support this assumption, it is important to note that the creation of electron-hole pairs by radiation of those two wavelengths is completely restricted to the depletion-layer (~ 0.5 - 0.6 um), as can be seen from the absorption coefficient curves.

4.2.3 Experimental Data and Discussions

At room temperature, with illumination of wavelength λ = 633 nm, the measurements of lifetime τ_p vs incident intensity ϕ_o are given in Fig. 4.11. Two groups of samples have been used for this measurement; one group was the normal device (see Chap. 2) and the other was further processed by thermal annealing (300-500°C) and subsequent quenching (-20°C). We expect that the lifetime for the second class of device should be reduced due to the creation of further defects. Also, we can observe the decreasing lifetime with increasing photon flux density for the normal induced pn junction device. This decay is consistent with the SRH recombination theory as we have described in the previous section (Refer to Fig. 4.2). More precisely, it can be interpreted by solving the one-dimensional time-dependent minority-carrier diffusion equation which is discussed in the following paragraphs.

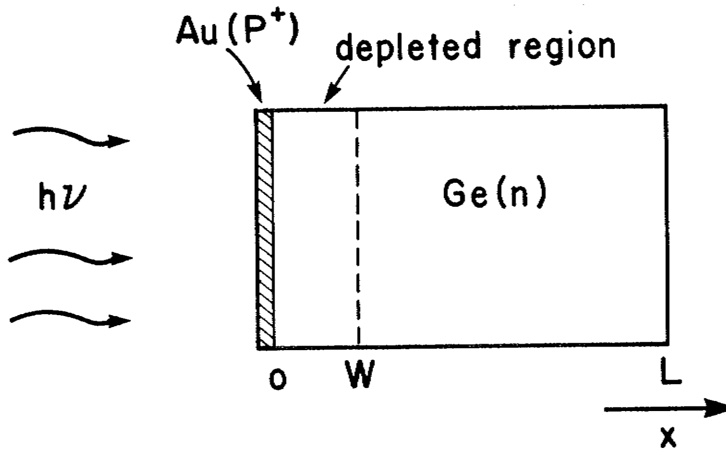

FIG. 4.10 Schematic diagram for induced p-n junctions under uniform illumination

Referring to Fig. 4.10, the continuity and transport equation (1-D) for the excess minority carrier (hole) concentration P(x,t) in the neutral region of an n-type Ge Schottky barrier device (with an induced p^+n junction) can be written as

$$D_p \frac{\partial^2 P}{\partial X^2} - \frac{P - P_o}{\tau_p} + G = \frac{\partial P}{\partial t} \tag{16}$$

$$G(x, t) = \phi_o(t)\ \alpha \exp(-\alpha x)(1-R) \tag{17}$$

here, $D_p = \frac{kT}{q}\mu_p$ is the diffusion coefficient, P_o is the concentration of holes in thermal equilibrium, τ_p is the hole lifetime, α is the absorption coefficient (with its accompanying wavelength-dependence) and R is the reflection coefficient of the sample surface. Also assuming the steady-state condition.

$$\frac{\partial P}{\partial t} = 0 \tag{18}$$

Under the open-circuit condition, the following boundary conditions apply

$$\left.\frac{\partial P}{\partial t}\right|_{X=0} = 0 \tag{19}$$

$$P(x,t)\Big|_{x=\infty} = 0 \tag{20}$$

Several authors[17][25] have solved this equation with these boundary conditions. The solution is

$$\frac{P(x)}{F} = \frac{1}{A-1}\left[Ae^{-x'} - e^{-Ax'}\right] \tag{21}$$

where

$$F = \frac{\alpha\ \phi_o (1-R)\tau_p}{1+A} \tag{22}$$

$$X' = \frac{X}{L_p} = \frac{X}{\sqrt{D_p \tau_p}} \tag{23}$$

$$A = \alpha\ L_p = \alpha\ \sqrt{D_p \tau_p} \tag{24}$$

here, ϕ_o is illuminating intensity of light source. For convenience, we choose p at x = 0. Thus

$$\tau_p = \frac{P(0)}{\phi_o (1-R)} \left(L_p + \frac{1}{\alpha}\right) \tag{25}$$

Solving for τ_p from this eqn. (25) under the assumption of $4\phi_o(1-R) \ll P(0)D_p\ \alpha$, we have

$$\sqrt{\tau_p} = \frac{2P(0)\sqrt{D_p}}{\phi_o(1-R)} + \frac{4}{\sqrt{D_p}\,\alpha} \qquad (26)$$

Note that this can account qualitatively for the decay of lifetime with increasing intensity in Fig. 4.11.

In Fig. 4.12, the spectrum of lifetime vs wavelength at the same optical intensity is given for the two classes of processed devices. We may expect that the lifetime will increase linearly with increasing wavelength λ according to eqn. (26) since α decreases with λ. Although the square root of lifetime was derived from the theoretical relations, the absorption coefficient α is also an inverse function of the square root of wavelength.(26) Therefore the dashed line may be drawn in Fig. 4.12 under the assumptions that: (1) the reflection coefficient R is not comparable to absorption coefficient in its dependence on wavelength; and (2) the initial hole concentration at $x = 0$, i.e. P(0) is also weakly wavelength-dependent. The former restriction will explain why the lifetime is comparatively lower than expected in the upper region of wavelength. The latter assumption is responsible for the scatter in the values of lifetime at the lower wavelengths. The damaged device behaves as expected from the viewpoint of a higher defect concentration (lower lifetime) than the normal device.

The variation of carrier lifetime with intensity over a wide range (10^{15}-10^{18} photons/cm^2 sec) has been given in Fig. 4.13. Similar results have also been found in Si solar cells.(27) The lifetime begins rising in the low-intensity region and subsequently reaches a

plateau in the region for which the photogenerated carriers concentration becomes equivalent to the doping concentration $N_D (2.08 \times 10^{15}$ $cm^3)$.* For further increases in intensity, the lifetime decreases rapidly until it reaches a final saturation value which is $\tau_p = \tau_{po} + \tau_{no} \simeq 2$ μs. This is exactly what we obtained in the previous measurements (see 4.1).

Although two trapping levels in energy were suggested to account for similar results for silicon in the literature,[27] we cannot endorse this interpretation in view of the previous experiments (see 4.1) and their interpretation results. On the other hand, the uncertainty involved in the identification of the linear decay region could provide substantial error in the application of this method to its lower level of excitation as compared to FCVD and also due to possible recombination through the surface and depletion region at these levels. Therefore, we would expect the true lifetime to be the highest value as we express by dashed line in Fig. 4.13. Nevertheless, this discrepancy is still not clear and in fact we have pointed out already that a serious drawback of this POVD measurement is the complexity of the decay relations observed.

As we have seen in the Sec. 4.1 the measurement of the temperature-dependence of the lifetime is important and leads to the determination of physical parameters of the recombination centers, their capture cross-section. From these measurements which are shown

---

*This calculation is based on $J = q \int_o^w G(x)\, dx = q \int_o^{0.5} \phi\, \alpha(1-R) e^{-\alpha x} dt =$ $q\phi(1-R)(1-e^{-\alpha \cdot 0.5}) \simeq q\, \phi(1-R)$, given $\alpha = 7 \times 10^4 cm^{-1}$ at $\lambda = 633$ nm. Then we can figure out the excess carriers $\Delta n = \Delta p$ using eqn. (12).

in Fig. 4.14, the temperature-dependence of the lifetime is quite different from that observed in the dark case, especially in the low temperature region. Obviously, there are three distinctive regions in Fig. 4.14, in which the excess carriers are presumed to be controlled by different recombination mechanisms. τ_p starts to decay as the temperature decreases which is similar to the FCVD case. Subsequently, τ_p increases and eventually saturates at the lowest temperatures. This distinctive behaviour has also been observed in antimony-doped germanium following irradiation and annealing.[28]

It has been shown by several authors[29-30] that the decay of excess carriers excited by a transient optical pulse should be governed by the two simultaneous equations

$$-\frac{d(\Delta n)}{dt} = C_n(N_r^o + n_o + n_1)\Delta n - C_n(n_o + n_1)\Delta p \qquad (27)$$

$$-\frac{d(\Delta p)}{dt} = C_p(N_r^- + p_o + p_1)\Delta p - C_p(p_o + p_1)\Delta n \qquad (28)$$

where Δn and Δp are small changes from the thermal equilibrium concentrations n_o and p_o of electrons and holes respectively. C_n and C_p are trap capture coefficients for electrons and holes respectively. n_1 and p_1 are the density of electrons and holes in the conduction band and valence band respectively when the Fermi level coincides energetically with that of the recombination center. N_r^o and N_r^- are the concentrations of unoccupied and occupied centers. Also, $N_r^o + N_r^- = N_r$, the total concentration of the centers. The solution of these linear differential equatins can be written as

$$\Delta n = \Delta p = Ae^{-\frac{t}{\tau_A}} + Be^{-\frac{t}{\tau_B}} \tag{29}$$

$$\tau_A = \lfloor C_p(N_r^- + p_o + p_1) + C_n(N_r^o + n_o + n_1) \rfloor^{-1} \tag{30}$$

$$\tau_B = \frac{\tau_{no}(N_r^- + p_o + p_1) + \tau_{po}(N_r^o + n_o + n_1)}{n_o + p_o + \dfrac{N_r^o N_r^-}{N_r}} - \frac{1}{C_p(N_r^- + p_o + p_1) + C_n(N_r^o + n_o + n_1)} \tag{31}$$

here

$$\tau_{no} = (C_n N_r)^{-1} \tag{32}$$

$$\tau_{po} = (C_p N_r)^{-1} \tag{33}$$

$$\frac{N_r^o}{N_r^-} = \frac{n_1}{n_o} = \frac{p_o}{p_1} \tag{34}$$

Compared to τ_B, τ_A is much shorter and is defined as the adjustment time required before the electrons and holes begin to be captured at the same rate.(29) The final experimental decay constant should be given as τ_B . also, this time constant can be reduced to the SRH treatment under certain simplifying approximations.

We again consider n-type material with a single recombination level in the upper half of the energy gap. The following approximations can be made

$$n_1 > n_o \gg p_o > p_1 \tag{35}$$

and

$$N_r^- = \frac{n_o}{n_o + n_1} N_r \tag{36}$$

$$N_r^o = \frac{n_1}{n_o + n_1} N_r \tag{37}$$

Thus, Eq. (31) will give

$$\tau_p = \tau_B = \frac{1}{C_n n_1} + \frac{1}{C_p N_r} + \frac{1}{C_p N_r}\left(\frac{n_1}{n_o}\right) - \frac{1}{C_p N_r + C_n (n_o + n_1)} \tag{38}$$

$$\simeq \frac{1}{C_n n_1} + \tau_{po}\left(1 + \frac{n_1}{n_o}\right) \tag{39}$$

The last term in Eqn. (38) has been neglected due to its small value. Also, we can see the difference between Eqn. (39) and Eqn. (8) in the previous section. This also explains why the measured value of τ_p by POVD is higher than that by FCVD. A physical interpretation can also be made by considering that the exponential decay of excess carriers for both electrons and holes are equivalent in the transient case due to the simultaneous solution for both types of carriers. Therefore, the temperature-dependence of the lifetime is qualitatively consistent with Eqn. (39).

As temperature decreases further, the subsequent increase in lifetime can also be explained qualitatively if we assume the presence of a hole retrapping center close to the valence band. This suggestion has been developed in the literature,(31) which can be consulted for further details. We believe that the limitations discussed earlier to the POVD technique, preclude the application of this method to quantitative device diagnosis.

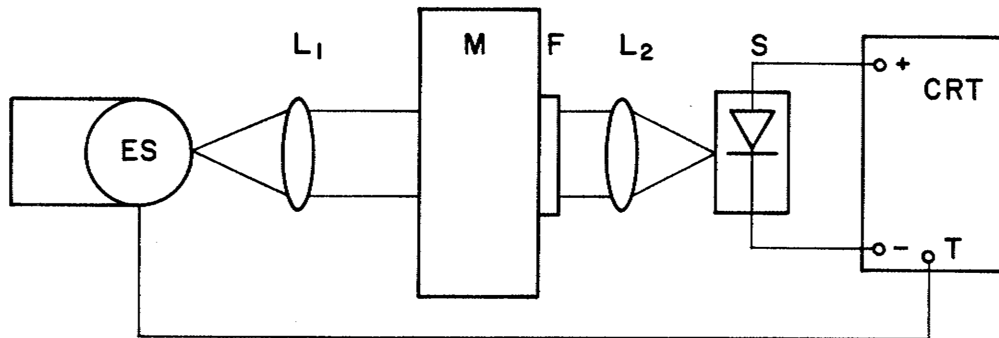

ES : Electronic Stroboscopes
L_1, L_2 : Focal Lens
M : Monochromator
F : Filter
T : Triggering
S : Device

FIG. 4.8(a) Experimental set-up for photo-induced open-circuit voltage decay (POVD) measurement.

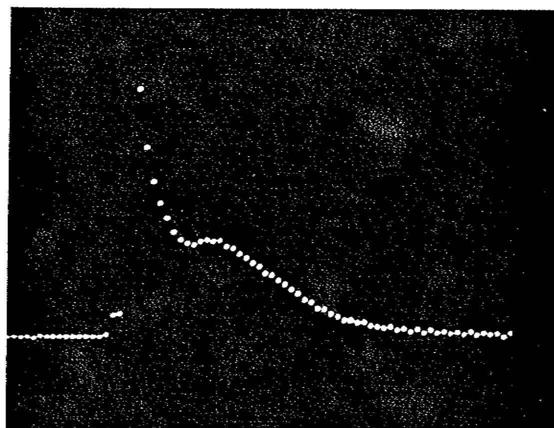

λ = 633 nm
V = 50 mV/cm
H = 5 μs/cm
T = 300°K
τ_p = 32 μs

FIG. 4.8(b) Typical open-circuit voltage decay curve on CRT.

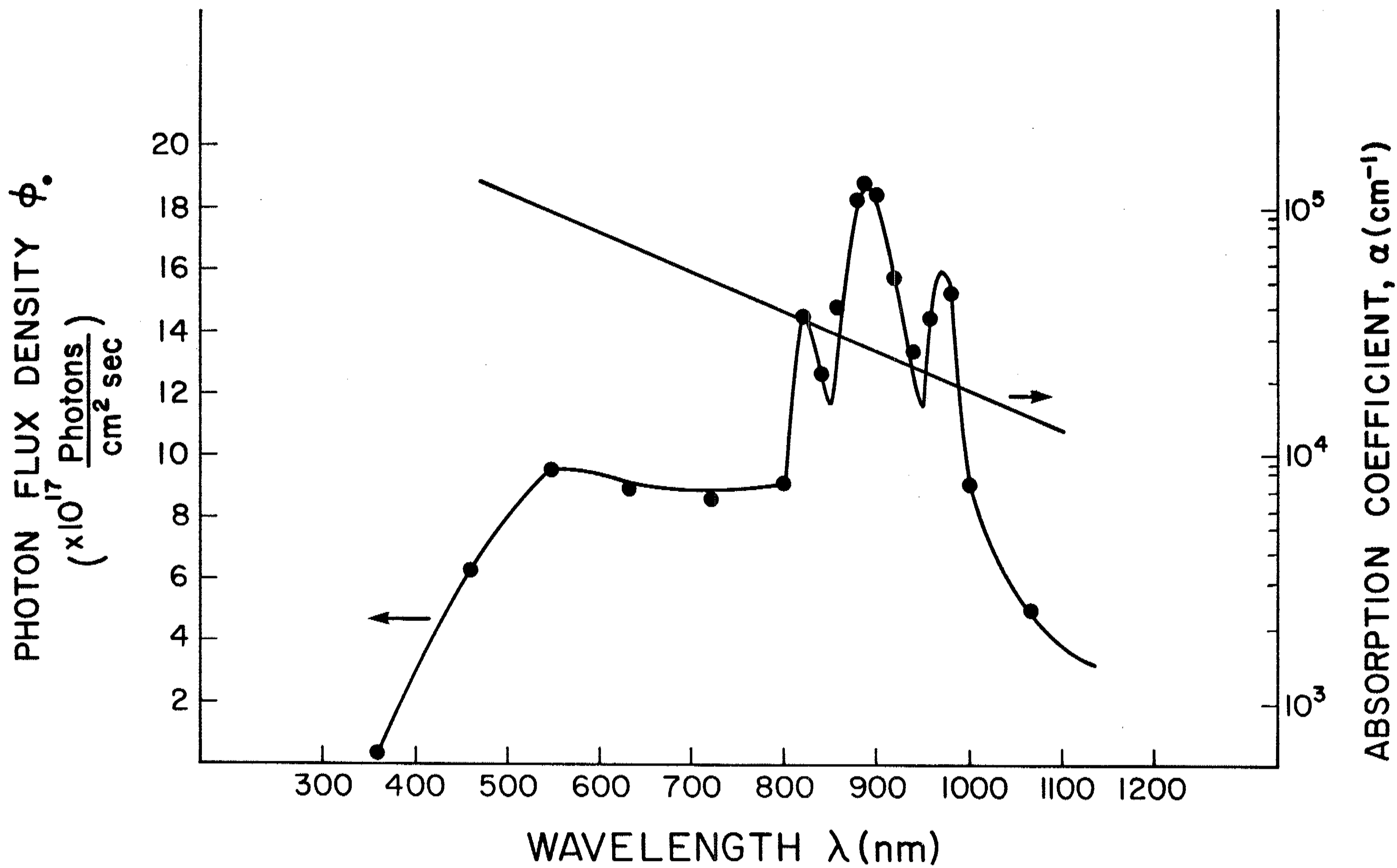

FIG. 4.9 Spectrum of stroboscope and optical absorption coefficient in germanium.

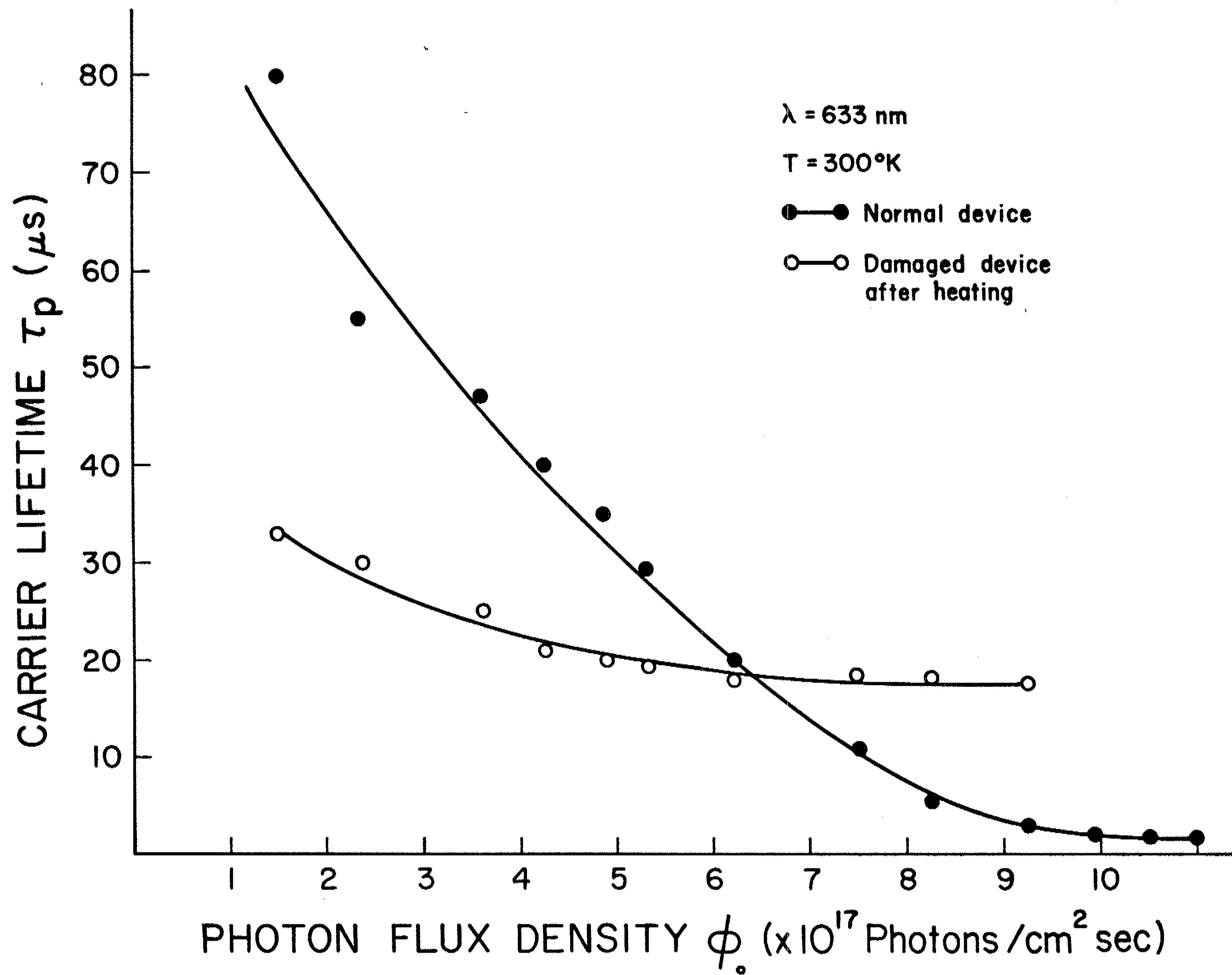

FIG. 4.11 Variation of lifetime with photon flux density for normal and damaged devices at T = 300 K and λ = 633 nm.

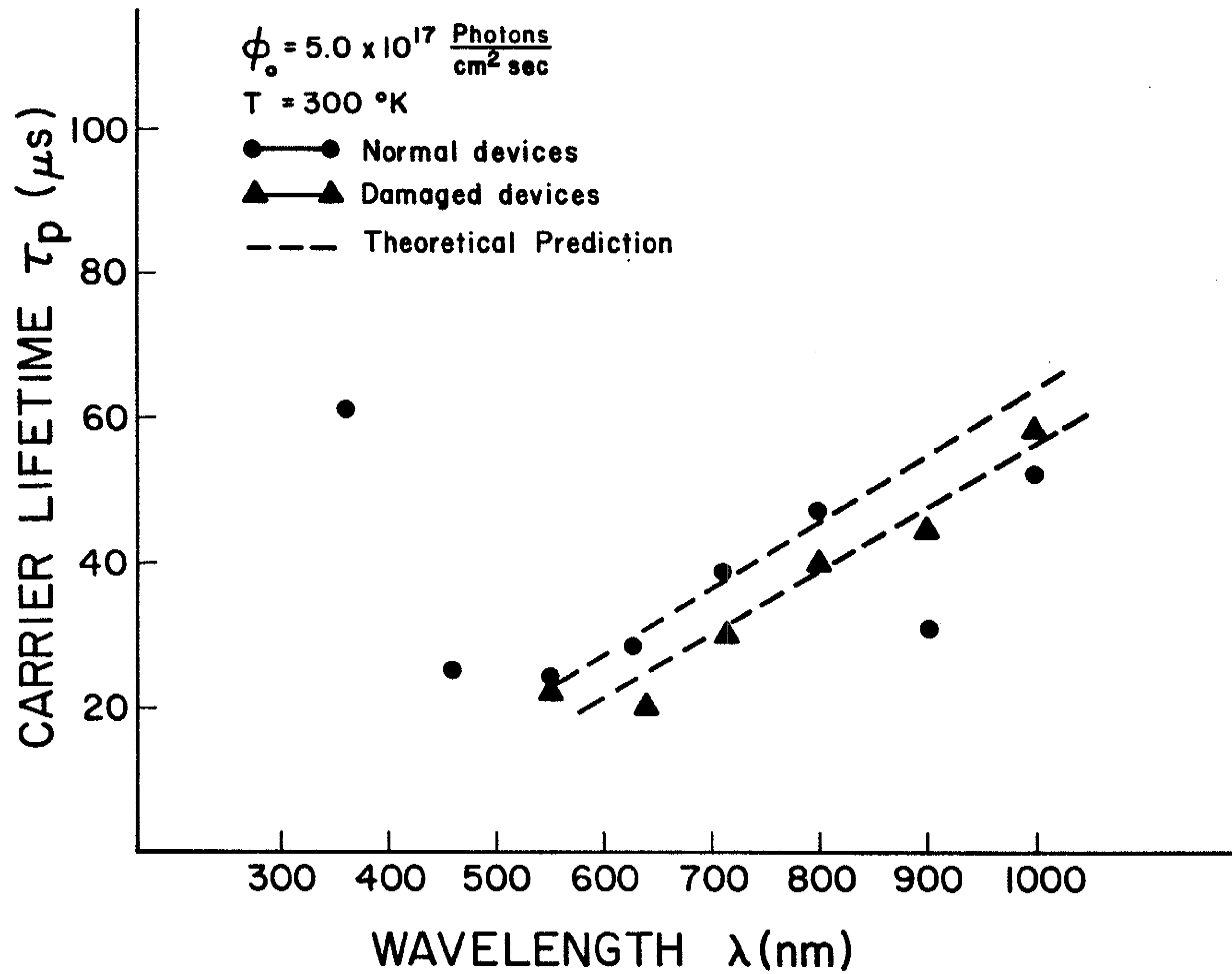

FIG. 4.12 Spectrum of lifetime with fixed intensity.

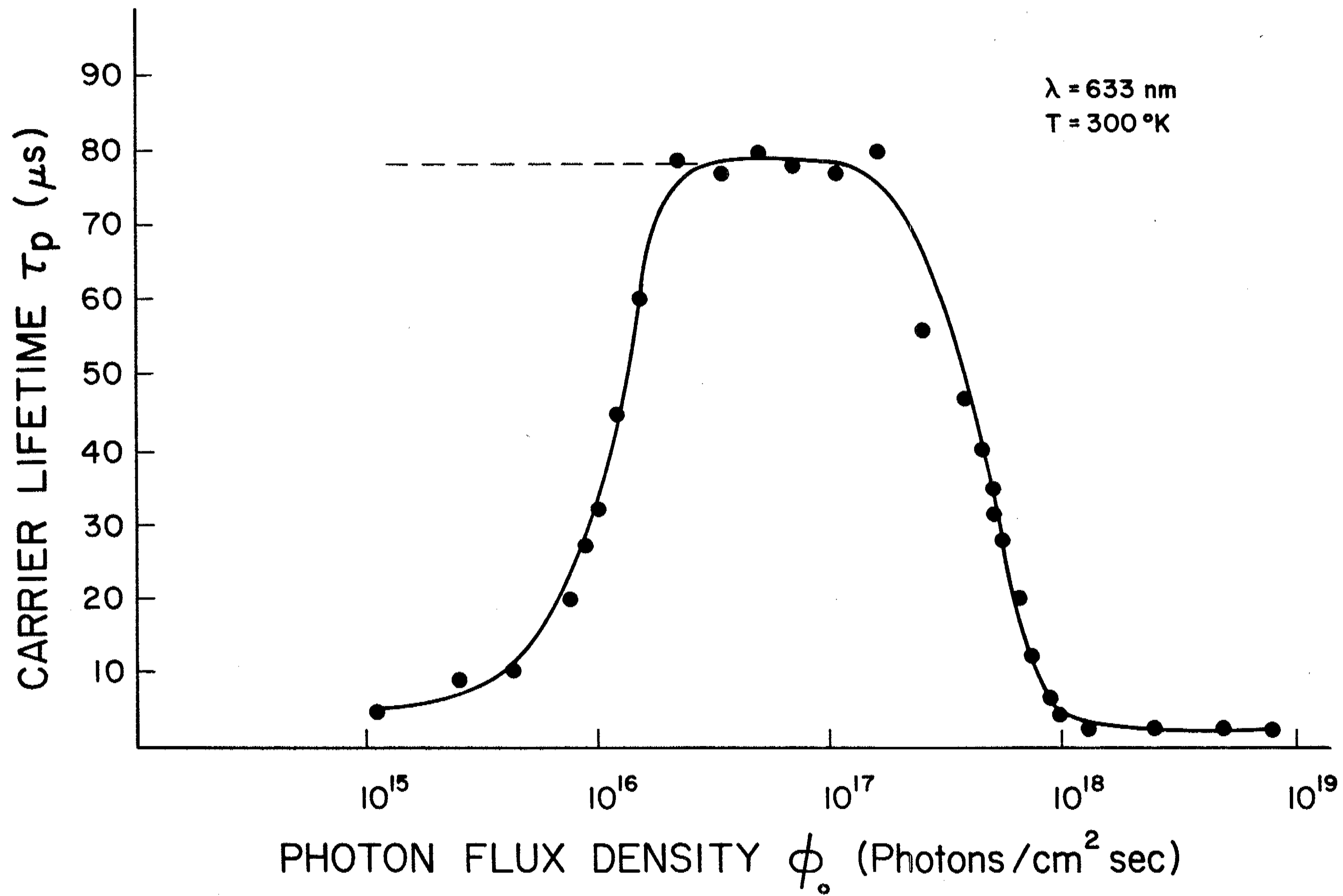

FIG. 4.13 Variation of lifetime with a wide range of photon flux density at T = 300 K and λ = 633 nm. The dashed line shows the expected value.

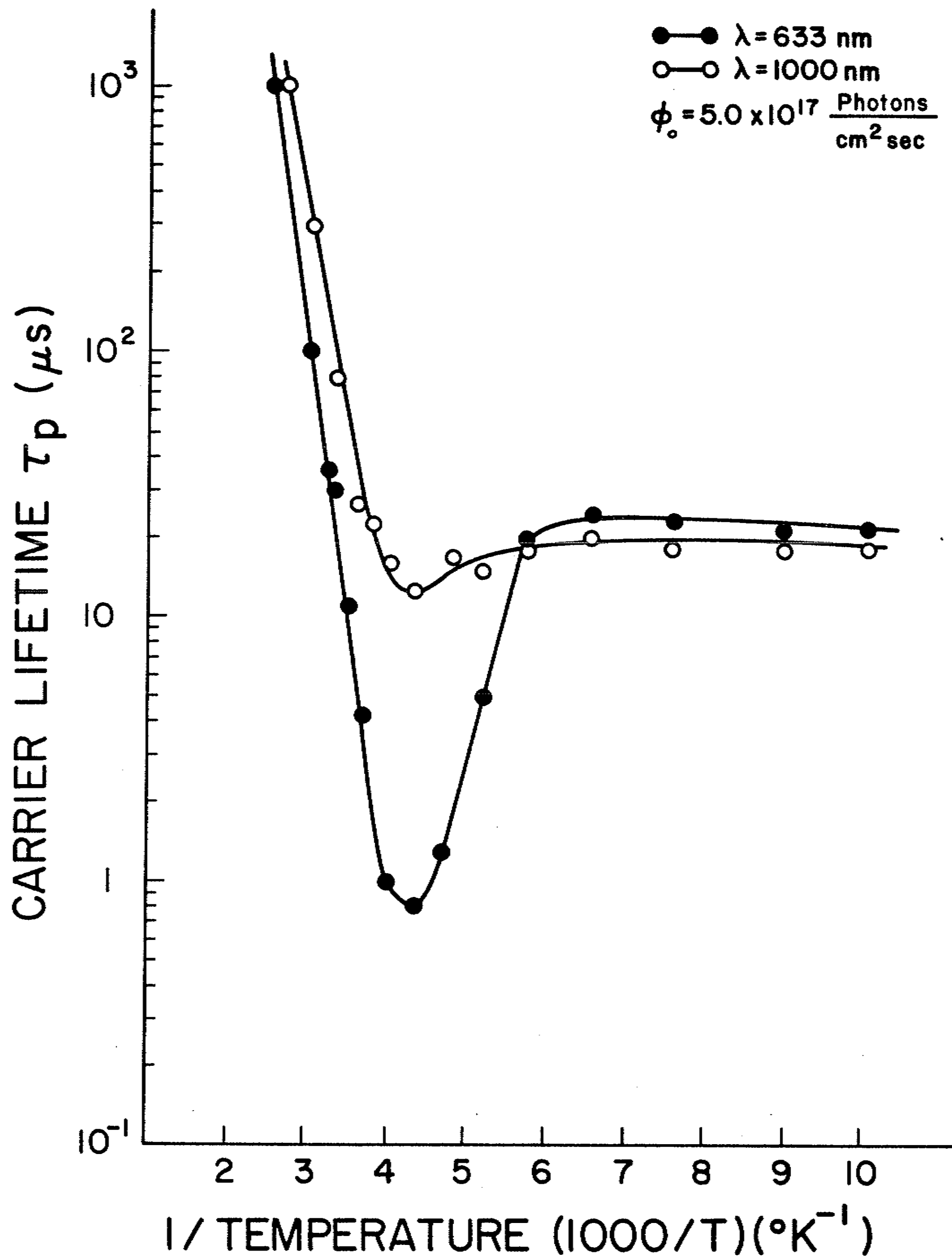

FIG. 4.14 Variation of lifetime with inverse temperature for two different wavelengths, at the same intensity of optical illumination (5.0×10^{17} photons/cm^2 sec).

References

1. W. Shockley and W.T. Read, Jr., "Statistics of the Recombination of Holes and Electrons", Phys. Rev., vol. 87, no. 5, pp. 835-842, September 1952.

2. R.N. Hall, "Electron-Hole Recombination in Germanium", Phys. Rev., vol. 87, p. 387, September 1952.

3. D.S. Dhariwal, L.S. Kothari and S.C. Jain, "On the Recombination of Electrons and Holes at Traps with Finite Relaxation Time", Solid-State Electronics, vol. 24, no. 8, pp. 749-752, 1981.

4. S.K. Agarwal, S.C. Jain, and S. Harsh, "Variation of Minority Carrier Lifetime with Level of Injection in p-n Junction Devices", Electronics Lett., vol. 18, no. 7, pp. 298-299, April 1982.

5. P.T. Landsberg and M.S. Abrahams, "Surface Recombination Statistics at Traps", Solid-State Electronics, vol. 26, no. 9, pp. 841-849, 1983.

6. S.R. Lederhandler and L.J. Giacoletto, "Measurement of Minority Carrier Lifetime and Surface Effects in Junction Devices", Proc. of IRE, vol. 43, pp. 477-483, 1955.

7. B.R. Gossick, "On the Transient Behaviour of Semiconductor Rectifiers", J. of Appl. Phys., vol. 26, no. 11, pp. 1356-1365, November 1955.

8. S.R. Dhariwal and N.K. Vasu, "A Generalized Approach to Lifetime Measurement in pn Junction Solar Cells", Solid-State Electronics, vol. 24, no. 10, pp. 915-927, 1981.

9. Y.K. Hsieh and H.C. Card, "Germanium Photodetectors with Induced pn Junctions", IEEE Trans. on Electron Devices, vol. ED-29, no. 9, pp. 1414-1420, September 1982.

10. J.N. Walpole and K.W. Nill, "Capacitance-Voltage Characteristics of Metal Barriers on P-PbTe and P-InAs: Effects of the Inversion Layer", J. of Appl. Phys., vol. 42, no. 13, pp. 5609-5617, December 1971.

11. W. Shockley, Electrons and Holes in Semiconductors, Van Nostrand: New York, p. 309, 1950.

12. S.M. Sze, Physics of Semiconductor Devices, 2nd Edition, Wiley: New York, 1981.

13. J.E. Mahan and D.L. Barnes, "Depletion Layer Effects in the Open-Circuit-Voltage-Decay Lifetime Measurement", Solid-State Electronics, vol. 24, no. 10 pp. 989-994, 1981.

14. A. Rose, Concepts in Photoconductivity and Allied Problems, Wiley: New York, 1963; see also K.C. Kao, and W. Hwang, Electrical Transport in Solids, Pergamon: New York, p. 237, 1981.

15. A. Milnes, Deep Impurities in Semiconductors, Wiley: New York, 1973, Chapter 2.

16. J.E. Mahan, T.W. Ekstedt, R.I. Frank and R. Kaplow, "Measurement of Minority Carrier Lifetime in Solar Cells from Photo-Induced Open-Circuit Voltage Decay", IEEE Trans. on Electron Devices, vol. ED-26, no. 5, pp. 733-739, 1979.

17. S.C. Jain, "Theory of Photo Induced Open Circuit Voltage Decay in a Solar Cell", Solid-State Electronics, vol. 24, no. 2, pp. 179-183, 1981.

18. S.R. Dhariwal and N.K. Vasu, "Mathematical Formulation for the Photo-Induced Open Circuit Voltage Decay Method for Measurement of Minority Carrier Lifetime in Solar Cells", IEEE Electronic Device Letters, vol. EDL-2, no. 2, February 1981.

19. S.C. Jain and R. Muralidharan, "Effect of Emitter Recombination on the Open Circuit Voltage Decay of a Junction Diode", Solid-State Electronics, vol. 24, no. 12, pp. 1147-1154, 1981.

20. Oldwig Von Raes, "Analysis of the Photo Voltage Decay (PVD) Method for Measuring Minority Carrier Lifetimes in p-n Junction Solar Cells", J. of Appl. Phys., vol. 52, no. 9, pp. 5833-5837, 1981.

21. D. Vijay Kumar and S.K. Sharma, "Theory of Open-Circuit Photo-Voltage in Degenerate Abrupt p-n Junctions", Solid State Electronics, vol. 25, no. 12. pp. 1161-1164, 1982.

22. S.C. Jain and U.C. Ray, "Photovoltage Decay in p-n Junction Solar Cells Including the Effects of Recombinations in the Emitter", J. of Appl. Phys., vol. 54, no. 4, pp. 2079-2085, April 1983.

23. R.J. Bassett, "Observations on a method to determining the Carrier Lifetime in p^{+}-v-n^{+} diodes", Solid-State Electronics, vol. 12, pp. 385-391, 1969.

24. W.C. Dash and R. Newman, "Intrinsic Optical Absorption in Single-Crystal Germanium and Silicon at 77°K and 300°K", Phys. Rev., vol. 99, no. 4, pp. 1151-1155, August 1955.

25. D.M. Bielle-Daspet and G.D. Gasset, "Bulk Carrier Lifetime Measurement From Transient Diffusion Photocurrent in Semiconductor Devices", Solid-State Electronics, vol. 21, no. 12, pp. 1219-1226, 1978.

26. J.I. Pankove, Optical Processes in Semiconductors, Prentice-Hall, Inc. New Jersey, 1971, Chapter 3.

27. V.L. Dalal and A.R. Moore, "Design Considerations for High-Intensity Solar Cells", J. of Appl. Physics, vol. 48, no. 3, pp. 1244-1251, March 1977.

28. B.G. Streetman, "Recombination and Trapping in ^{60}Co Gamma-Irradiated n-Type Germanium", J. of Appl. Phys., vol. 37, no. 8, pp. 3145-3152, July 1966.

29. D.J. Sandiford, "Carrier Lifetime in Semiconductors for Transient Conditions", Phys. Rev., vol. 105, no. 2, p. 524, January 1957.

30. G.K. Wertheim, "Transient Recombination of Excess Carriers in Semiconductors", Phys. Rev., vol. 109, no. 4, pp. 1086-1091, February 1958.

31. B.G. Streetman, "Carrier Recombination and Trapping Effects in Transient Photoconductive Decay Measurements", J. of Appl. Phys., vol. 37, no. 8, pp. 3137-3144, July 1966.

CHAPTER 5

LIMITATIONS TO SHOCKLEY-READ-HALL (SRH) GENERATION/RECOMBINATION MODEL

In Chapter 4 we have shown that the SRH model was able to account for the recombination processes in our germanium devices, following the injection of minority carriers associated with a dark current. The SRH statistics were very effective in explaining these phenomena, even under extreme conditions of temperature and injection level.

In optoelectronic and photovoltaic devices, however, the excess carriers are established by photogeneration, rather than injection. In these cases there are additional complications which may arise in the recombination processes. One of these complications is that direct photoionization of the trapping centers can affect the carrier concentrations, and energy distributions. This is normally not considered in those cases of photoconductive or photovoltaic devices when the photon energy exceeds the energy gap so that interband processes are possible. We address this issue in the present chapter and clearly define the restrictions on SRH statistics which arise from the neglect of direct photoionization of traps.

Other limitations to SRH statistics which are associated with hot-electron and trap saturation effects are mentioned briefly below but are not the primary subject matter of this chapter, as they have been addressed to a degree by previous researchers.

5.1 Historical Introduction

In the early stages of semiconductor technology, the overall behaviour of impurities, which are often referred to as shallow donors and acceptors, was understood quite adequately in terms of the hydrogenic model.[1] It was recognized that such an impurity may drastically modify the electrical and optical properties of the host material in a particular way. However, the recent emergence of sophisticated semiconductor devices has encouraged the use of new techniques[2-5] in order to investigate the localized electronic states lying energetically deep in the forbidden gap of the host crystal. These impurity systems which cannot be described by the Coulomb potential model are generally known as "deep-level impurities". These deep centers often control minority carrier lifetime and play a significant part in affecting the functioning of a variety of semiconductor devices. The characterization of defect centers, therefore, provides a substantial contribution to the development of new semiconductor devices. Among these achievements the gold impurity doping of silicon has become well-known as a means to control the minority carrier lifetime and to result in the improvement of switching diodes and power transistors.

In spite of much progress in the past decade, the understanding of carrier generation, recombination, trapping and transport in semiconductors remains dependent upon a better understanding of defects in semiconductor devices. Among these studies, there is a common foundation which is based on the SRH recombination theory.[6-7] The practical application of this theory and the verification of its validity when extended to high-level injection for dark current conditions[8] have been discussed in Chapter 4.

There are, nevertheless, a number of limitations to the strict application of SRH statistics to the modelling of nonequilibrium phenomena in most semiconductor devices. Among these common assumptions in using the SRH relation are:

(1) The traffic of electrons and holes through the recombination centers is governed by the thermal capture and emission rates which depend only upon the carrier concentrations within the conduction and valence bands. Under optical excitation with photon energy in excess of the energy gap, which establishes a nonequilibrium concentration of electrons and holes within the bands, the direct photoionization of the defect states (both electron and hole photoionization, the latter of which corresponds to the excitation of valence electrons into the defect states) are usually neglected.

(2) Under high levels of excitation (far from the equilibrium condition), the capture rate predicted by SRH statistics may be too large as a consequence of saturation of the traps. These traps cannot capture another electron during a "dead time" during which the first electron relaxes into the ground state of the defect. This problem has already been addressed so some extent theoretically.[9]

(3) The capture cross-sections may show strong dependences upon the electric field. One reason for this (which has been studied before[10-11]) is the modification by the field to the potential distribution around the defect - a popular way of dealing with this effect is the so-called Poole-Frenkel model. There should however be other dependences which result from the effects of the

field on the free carriers: for example, when these carriers become "hot" in the high field, their energy distributions in the bands are affected - becoming Maxwellian with large effective electron temperatures. Similarly, under optical excitation with photon energies that are well in excess of the energy gap, there will be a steady-state energy distribution for the electrons and holes in the bands which is determined by the balance between photoexcitation and scattering, which will not resemble the thermal distribution. This does not necessarily require high optical intensity, but rather a high photon energy.

In this chapter we address ourselves to the first limitation above which we believe may be of particular interest to researchers concerned with photovoltaic and photoconductive devices. The other limitations have been discussed elsewhere,[12-13] however the theoretical model has not been fully explored due to the absence of sufficient physical evidence. We begin with the basic derivation of non-equilibrium thermal and optical occupation statistics. Next, we will concentrate on the determination of the threshold photon energy for which the photo generated carriers through the interband absorption will be affected and modified from the conventional SRH theory. Finally, we will discuss the impact of this work on the modelling of some practical devices.

5.2 Theoretical Development

Figure 5.1 shows a diagram of energy states of a semiconductor with the assumption of a single-level defect, with energy level E_t within the energy gap. Both recombination and emission rates for elec-

trons and holes can be written as follows:

$$N_r = C_n n N_t (1 - f_t^n) \quad (1)$$

$$N_e^T = C_n n_1 N_t f_t^n \quad (2)$$

$$N_e^O = \phi_o \sigma_n^o N_t f_t^n \quad (3)$$

$$H_r = C_p P N_t f_t^n \quad (4)$$

$$H_e^T = C_p P_1 N_t f_t^p = C_p P_1 N_t (1 - f_t^n) \quad (5)$$

$$H_e^O = \phi_o \sigma_p^o N_t f_t^p = \phi_o \sigma_p^o N_t (1 - f_t^n) \quad (6)$$

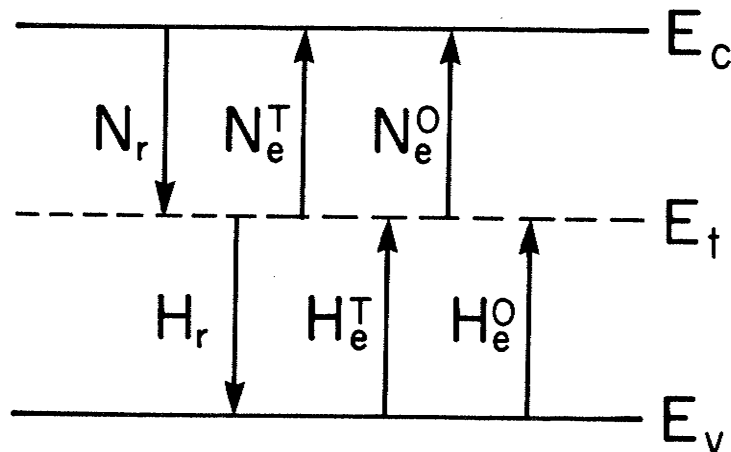

FIG. 5.1 Energy level diagram with defect center at E_t . Arrows show electron transitions.

For convenience, each symbol employed with its physical meaning is listed below:

N_r = Recombination rate for electrons, $cm^{-3}sec^{-1}$

H_r = Recombination rate for holes, $cm^{-3}sec^{-1}$

C_n = Recombination coefficient for electrons, $cm^{3}sec^{-1}$

C_p = Recombination coefficient for holes, $cm^{3}sec^{-1}$

N_e^T = Thermal emission rate for electrons, $cm^{-3}sec^{-1}$

H_e^T = Thermal emission rate for holes, $cm^{-3}sec^{-1}$

N_e^0 = Optical ionization rate for electrons, $cm^{-3}sec^{-1}$

H_e^0 = Optical ionization rate for holes, $cm^{-3}sec^{-1}$

ϕ_o = Photon flux density or intensity, no of photons $\cdot$ $cm^{-2}sec^{-1}$

σ_n^o = Optical cross section for electrons, cm^2

σ_p^o = Optical cross section for holes, cm^2

N_t = Trap concentration, cm^{-3}

n = Total concentration of electrons in conduction band when in non-equilibrium condition, cm^{-3}

P = Total concentration of holes in valence band when in non-equilibrium condition, cm^{-3}

n_1 = Concentration of electrons when the Fermi level coincides with the trap energy level, cm^{-3}

P_1 = Concentration of holes when the Fermi level coincides with the trap energy level, cm^{-3}

f_t^n = Occupation fraction for electrons in trap energy level when steady-state is reached

f_t^p = $1 - f_T^n$ = Occupation fraction for holes in trap energy level when steady-state is reached

n_o = Electron concentration in conduction band when in thermal equilibrium, cm^{-3}

P_o = Hole concentration in valence band when in thermal equilibrium, cm^{-3}

N_c = Effective density of states in conduction band, cm^{-3}

N_v = Effective density of states in valence band, cm^{-3}

Under steady-state (non-equilibrium) conditions, the following relationship should be satisfied:

$$N_r - (N_e^T + N_e^0) = H_r - (H_e^T + H_e^0) \tag{7}$$

Then, substituting Eqns. (1)-(6) into (7), we get the trap occupation probability

$$f_t^n = \frac{C_n n + C_p P_1 + \phi_o \sigma_p^o}{C_n(n+n_1) + \phi_o(\sigma_n^o + \sigma_p^o) + C_p(P+P_1)} \tag{8}$$

where

$$C_n = \sigma_n^T < V_{th} > \tag{9}$$

$$C_p = \sigma_p^T < V_{th} > \tag{10}$$

σ_n^T , σ_p^T are the thermal capture cross sections for electrons and holes respectively. $< V_{th} >$ is the average thermal velocity. Also,

$$n_1 = N_c \exp(- \frac{E_c - E_t}{kT}) \tag{11}$$

$$P_1 = N_v \exp(- \frac{E_t - E_v}{kT}) \quad (12)$$

Therefore, the net recombination rate R_n^* for electrons (or holes) will be given by

$$R_n^* = N_r - N_e^T - N_e^0 = H_r - H_e^T - H_e^0 = R_p^*$$

$$= C_n n N_t (1-f_t^n) - N_t \, f_t^n (C_n n_1 + \phi_o \sigma_n^o)$$

$$= C_p P N_t \, f_t^n - N_t (1-f_t^n)(C_p P_1 + \phi_o \sigma_p^o)$$

$$= \frac{N_t \lfloor C_n C_p (nP - n_1 P_1) - (\phi_o^2 \sigma_n^o + C_n n_1 \phi_o \sigma_p^o + C_p P_1 \phi_o \sigma_n^o) \rfloor}{C_n (n+n_1) + \phi_o (\sigma_n^o + \sigma_p^o) + C_p (P+P_1)} \quad (13)$$

With the definitions

$$\begin{aligned}
\tau_{no} &= (C_n N_t)^{-1}, \ \text{sec} \\
\tau_{po} &= (C_p N_t)^{-1}, \ \text{sec} \\
\alpha_n^o &= \sigma_n^o N_t, \ \text{cm}^{-1} \\
\alpha_p^o &= \sigma_p^o N_t, \ \text{cm}^{-1} \\
n^o &= \alpha_n^o \phi_o, \ \text{cm}^{-3}\text{sec}^{-1} \\
p^o &= \alpha_p^o \phi_o, \ \text{cm}^{-3}\text{sec}^{-1}
\end{aligned} \quad (14)$$

We have that

$$R_n^* = \frac{nP - (n_1+\tau_{no}n^o)(P_1+\tau_{po}P^o)}{\tau_{no}(P+P_1)+\tau_{po}(n+n_1)+\tau_{no}\tau_{po}(n^o+p^o)}$$

$$= \frac{nP - (n_1+\tau_{no}n^o)(P_1+\tau_{po}P^o)}{\tau_{no}(P+P_1+\tau_{po}P^o)+\tau_{po}(n+n_1+\tau_{no}n^o)} \qquad (15)$$

Again, let

$$n_1^* = n_1 + \tau_{no}n^o = n_1 + \tau_{no}\phi_o N_t \sigma_n^o$$

$$= n_1 + \frac{\phi_o \ \sigma_n^o}{\langle V_{th}\rangle \ \sigma_n^T} \qquad (16)$$

$$P_1^* = P_1 + \tau_{po}P^o = P_1 + \tau_{po}\phi_o N_t \sigma_p^o$$

$$= P_1 + \frac{\phi_o \ \sigma_p^o}{\langle V_{th}\rangle \ \sigma_p^T} \qquad (17)$$

so that

$$R_n^* = \frac{np - n_1^* P_1^*}{\tau_{no}\lfloor P+P_1^* \rfloor + \tau_{po}\lfloor n+n_1^* \rfloor} = R_p^* \qquad (18)^{(a)}$$

with n_1^* and P_1^* defined as above.

(a) Similarly, in the space-charge region when the reverse bias is applied, n and P are very small due to the depletion effect. In that case,

$$R_n^* \sim \frac{- n_1^* P_1^*}{\tau_{no}P_1^* + \tau_{po}n_1^*}$$

provided $\tau_{no}n^o \gg n_1$ or $\tau_{po}P^o \gg P_1$. Therefore, the photoionizatin of traps will make a substantial difference to the generation rate.

Also, the net recombination rate according to the simple SRH statistical theory is

$$R_n = \frac{nP - n_1 P_1}{\tau_{po}(n+n_1) + \tau_{no}(P+P_1)} \tag{19}$$

In A.Mircea, et al.[14], a similar expression to f_t^n (Eqn.(8)) has been given to discuss the Deep Level Transient Spectroscopy (DLTS) studies of depleted layers in semiconductor devices. Also, several authors[15-17] have developed well-known methods such as transient capacitance decay and thermally-stimulated relaxation to measure the photoionization cross section and emission rate for deep level defects and other physical parameters corresponding to those of DLTS. Therefore, Eqn. (18) can be converted to Eqn. (19) for certain conditions of temperature, reverse-bias voltage and optical illumination intensity. Usually the latter condition can be established seperately by the photon flux density or by the photon energy which in most cases is (i) larger than the band gap energy for diffusion-length or effective carrier lifetime measurements, and (ii) less than the band gap energy for impurity photoionizatin (sometimes called photo-thermal ionization) cross section measurements. In general, the excess carriers are created by an intrinsic optical absorption process for the former and extrinsic absorption process for the latter case (ii). The energy gap is a function of the temperature[18] ($Eg(T) = Eg(0) - \frac{\alpha_1 T^2}{T+B_1}$, where α_1, B_1 are constants independent of temperature) so that the interband optical absorption coefficient α is also temperature-dependent, and the trap concentration N_t is unknown in most cases. It is therefore not clear whether the secondary contributions from either the thermal

emission process or the trap photoemission process in general can be neglected in cases (i) or (ii). Therefore, the limitation on the minimum photon energy required to justify the neglect of direct photoionization of the traps will be estimated. Furthermore, this threshold energy is of interest in photovoltaic applications in order to achieve optimization of solar cell designs. The theoretical derivation may be developed as follows.

Based on the assumption that the electron recombination event in the center is simultaneous with the capture of a hole from the valence band, we can write the following expressions to describe the practical conditions with a transient incident light source,

$$|\Delta f_t^n| = |\Delta f_t^p| \qquad (20)$$

here,

$$\Delta f_t^n = f_t^n - f_o^n$$

$$\Delta f_t^p = f_t^p - f_o^p \qquad (21)$$

and

$$f_o^n = \frac{n_1}{n_o + n_1}$$

$$f_o^p = \frac{P_o}{P_o + P_1} \qquad (22)$$

f_o^n and f_o^p are the occupied and unoccupied fraction of the recombination centers respectively under thermal equilibrium conditions, and f_t^n and f_t^p are the corresponding quantities under steady-state (non-equilibrium) conditions. The f_t^n is given in Eqn. (8) and f_t^p will be

$$f_t^P = 1 - f_t^n = \frac{C_p P + C_n n_1 + \phi_o \sigma_n^o}{C_n(n+n_1)+\phi_o(\sigma_n^o+\sigma_p^o)+C_p(P+P_1)} \qquad (23)$$

Substituting Eqns. (8), (23), (21) and (22) into Eqn. (20), we obtain

$$n = \frac{\tau_{no}}{\tau_{po}} \left(\frac{n_o P}{n_1} - P_1^* \right) + n_1^* \frac{n_o}{n_1} \qquad (24)$$

where, τ_{no}, τ_{po}, P_1^* and n_1^* have been discussed earlier. Also, from Eqn. (18) we know that the recombination rate is equal to the generation rate $G^* = \phi_o \alpha$ and that α is the interband optical absorption coefficient, thus

$$\phi_o \alpha = \frac{nP - n_1^* P_1^*}{\tau_{no}\lfloor P+P_1^* \rfloor + \tau_{po}\lfloor n+n_1^* \rfloor} \qquad (25)$$

The simultaneous solution of Eqns. (24) and (25), leads to

$$\Delta n = n - n_o = \phi_o \alpha \lfloor \tau_{no}\left(1 + \frac{P_1}{P_o}\right) + \tau_{no}\left(\frac{P_1}{P_o}\right)\left(\frac{N_t \sigma_n^o}{\alpha}\right) \rfloor \qquad (26)$$

$$\Delta P = P - P_o = \phi_o \alpha \lfloor \tau_{po}\left(1 + \frac{n_1}{n_o}\right) + \tau_{po}\left(\frac{n_1}{n_o}\right)\left(\frac{N_t \sigma_p^o}{\alpha}\right) \rfloor \qquad (27)$$

If we assume that

$$\tau_{PSRH} \simeq \tau_{po}\left(1 + \frac{n_1}{n_o}\right) \quad \text{for N-type} \qquad (28)$$

$$\tau_{n\,SRH} \simeq \tau_{no}(1 + \frac{P_1}{P_o}) \quad \text{for P-type} \tag{29}$$

and that

$$\tau_n = \frac{\Delta n}{\phi_o \alpha} = \tau_{no}(1 + \frac{P_1}{P_o})\left[1 + (\frac{P_1}{P_1+P_0})\frac{N_t \sigma_n^o}{\alpha}\right]$$

$$= \tau_{nSRH}\left[1 + (\frac{P_1}{P_1+P_0})\frac{N_t \sigma_n^o}{\alpha}\right] \tag{30}$$

$$\tau_p = \frac{\Delta P}{\phi_o \alpha} = \tau_{po}(1 + \frac{n_1}{n_o})\left[1 + (\frac{n_1}{n_o+n_1})\frac{N_t \sigma_p^o}{\alpha}\right]$$

$$= \tau_{PSRH}\left[1 + (\frac{n_1}{n_o+n_1})\frac{N_t \sigma_p^o}{\alpha}\right] \tag{31}$$

It can be seen that the ratio of the true carrier lifetime to that predicted by the SHR model will be close to unity if the second terms inside the square brackets of Eqns. (30) and (31) are much less than 1. Obviously, this will depend on the temperature, on the energy level of the trapping centers, on the energy gap of the semiconductor and its doping concentration. For most semiconductors of interest for devices such as photoconductors (InSb, InAs, PbS, PbTe) and solar cells (Si, Se), we can assume that

$$P_1 \geqslant P_0 \qquad \text{and} \qquad n_1 \geqslant n_0 \tag{32}$$

Therefore, we conclude that the major consideration is the ratio of the

extrinsic absorption coefficient to the interband (intrinsic) absorption coefficient α. The former is given by $N_t \sigma^o_{n,p} = \alpha^o_{n,p}$ (defined by Eqn. (14)). In the following section, we discuss this ratio and give some numerical values in order to assess its importance under various conditions.

5.3 Discussion

As we have mentioned, the direct photoionization of the defect states is generally neglected in favour of the interband process in spite of the fact that excess carriers are generated by this process, we actually would expect the estimation of the carrier recombination rate to be larger than anticipated on the basis of SHR modelling. Unfortunately, it is difficult to determine experimentally how significant this discrepancy should be. Equation (18) has shown that the recombination rate would decrease if photoionization of the traps were included in the recombination statistics.

Comparing Eqn. (18) with Eqn. (19), the difference is between n_1^* and n_1 or p_1^* and p_1 which has been expressed in Eqns. (16) and (17). Since all the parameters involved are positive, the following inequality can be drawn.

$$n_1^* > n_1 \tag{33}$$

$$p_1^* > p_1 \tag{34}$$

The main point of concern is the ratio of the photoionization cross section to the thermal cross section, since the incident intensity and

average thermal velocity $\langle V_{th} \rangle$ can be determined precisely by the experimental apparatus. Although the theoretical development of the photoionization cross section and thermal cross sections of deep impurity levels have existed for a long time,(19-21) there remains a substantial lack of experimental cross sections to support this early work.

In 1965, Lucovsky(22) developed a theory of photoionization of deep impurity centers based on the assumption of a delta function potential well creating the ground states of the defect. These cross sections can be written as

$$\sigma(\hbar\omega) = \frac{1}{n}\left(\frac{E_{eff}}{E_o}\right)\frac{16\pi e^2\hbar}{3m^*c}\frac{(E_i)^{1/2}(\hbar\omega-E_i)^{3/2}}{(\hbar\omega)^3} \qquad (35)$$

where n is the index of refraction and E_{eff}/E_o is the effective field ratio(23) for the optical transition; m^* is the effective mass of the free carriers; c is the speed of light in vacuum; e is electronic charge; E_i is the ionization energy for impurity centers. A maximum in the photoionization cross section exists at $\hbar\omega = 2E_i$ in contrast with the hydrogenic (coulomb potential) model cross sections which have a maximum at $\hbar\omega = E_i$(24). Also, we observe that $\sigma(\hbar\omega)$ is independent of temperature (any possible dependence of E_i on temperature being neglected). The experimental photoionization cross-sections have been determined to be in the range between 10^{-16} - 10^{-24}cm^2 for common impurities found in Si and Ge.(19) On the other hand, the thermal cross sections have been found to vary between 10^{-12} - 10^{-15}cm^2 for attractive centers; 10^{-18} - 10^{-20}cm^2 for neutral centers, and less than 10^{-24}cm^2

for repulsive centers.[25] Therefore, it is obvious that the ratio discussed above could potentially vary between 10^{8} - 10^{-12} depending on the type of centers, the temperature, and the energy level.

In the following, we will give some numerical examples concerning the effects on minority carrier lifetime of including photoionization of the deep levels. First, we consider the N-type semiconductor (with energy gap ≃ 1 eV) having the energy level of trapping centers in the upper half of the energy gap. Under low-level excitation, we can make the following assumptions

$$n_1 > n_0 \gg P_0 > P_1 > \tau_{po}P^{o} > \tau_{no}n^{o} \quad (36)$$

Then, Eqn. (18) can be reduced to

$$\tau_{no}\left[P+P_1^*\right] + \tau_{po}\left[n+n_1^*\right] = \tau_{po}\left[n_1+n_0\right] + \tau_{no}\tau_{po}(n^{o}+P^{o})$$

$$\simeq \tau_{po}(n_1+n_0) \quad (37)$$

$$nP - n_1^*P_1^* = (n_0+\Delta n)(P_0+\Delta P) - (n_1+\tau_{no}n^{o})(P_1+\tau_{po}P^{o})$$

$$= \Delta nP_0 + n_0\Delta P + \Delta n\Delta P - \tau_{no}n^{o}P_1 - \tau_{po}n_1P^{o} - \tau_{no}\tau_{po}n^{o}P^{o}$$

$$\simeq n_0\Delta P - \tau_{po}n_1P^{o}$$

$$\simeq n_0\Delta P - \tau_{po}n_1\phi_o N_t\sigma_p^{o} \quad (38)$$

and

$$\tau_p = \frac{\Delta P}{R_p^*} = \frac{\Delta P}{\dfrac{n_0 \Delta P - \tau_{po} n_1 P^o}{\tau_{po}(n_1 + n_0)}}$$

$$= \frac{\Delta P}{\Delta P \left[n_0 - \dfrac{\tau_{po} n_1 P^o}{\Delta P} \right.} \quad \tau_{po}(n_0 + n_1)$$

$$= \frac{\tau_{po}(1 + \dfrac{n_1}{n_0})}{1 - \dfrac{\tau_{po} P^o}{\Delta P} (\dfrac{n_1}{n_0})} \qquad (39)$$

The numerator of Eqn. (39) gives the value predicted from the SRH model, and we observe that the denominator will give a value less than 1. As far as temperature variation is concerned, both terms will be affected. In Fig. 5.1, the dependence of the minority carrier lifetime τ_p upon inverse temperature is shown with the parameter $\gamma = \frac{\tau_{po} P^o}{\Delta P}$ from 10^{-1} to 10^{-3} under the assumption of $\tau_{po} = 1.0 \times 10^{-6}$ sec and $E_T = E_c - 0.25$ ev. The SRH model of minority carrier lifetime (γ=0) is very close to the solid line indicated in Fig. 5.2 with $\gamma \leqslant 10^{-3}$. This diagram implies that the direct photoionization of traps will not be important at low temperatures (for $1/T \geqslant 4$ in Fig. 5.2). Also in Fig. 5.3, we can see that the critical temperature above which photoionization is important depends upon the energy level of the defect. These calculations have been made for $\gamma = 10^{-4}$. This conclusion applies also the SRH model with γ=0.

In the case of high-level photo excitation, Eqn. (18) may be approximated by

$$\tau_{no}\lfloor P+P_1^* \rfloor + \tau_{po}\lfloor n+n_1^* \rfloor \simeq \tau_{no}\tau_{Po}(n^o+P^o)$$

$$\simeq \tau_{no}\tau_{po}\phi_o N_t(\sigma_n^o+\sigma_p^o) \qquad (40)$$

and

$$nP - n_1^* P_1^* \simeq \Delta n \Delta P \qquad (41)$$

Then

$$\tau_p = \frac{\Delta P}{R_p^*} = \frac{\Delta P}{\dfrac{\Delta n \Delta P}{\tau_{no}\tau_{po}\phi_o N_t(\sigma_n^o+\sigma_p^o)}} = \frac{\tau_{no}\tau_{po}\phi_o N_t(\sigma_n^o+\sigma_p^o)}{\Delta n}$$

$$= \frac{\tau_{po}\phi_o N_t \sigma_n (1 + \dfrac{\sigma_p^o}{\sigma_n^o})}{\dfrac{\Delta n}{\tau_{no}}} \qquad (42)$$

It can be seen that the minority carrier lifetime will not be a constant, as $\tau_p = \tau_{po} + \tau_{no}$,(6) predicted by the SRH model in high-level injection. On the other hand, the minority carrier lifetime depends on the incident photon energy, illumination intensity and the excess carrier concentration. Nevertheless, in some cases, if we can arrange that

$$N_t \sigma_n^o \phi_o = \frac{\Delta n}{\tau_{no}}$$

then, we shall obtain

$$\tau_p = \tau_{po}(1 + \frac{\sigma_p^o}{\sigma_n^o})$$

As we have already mentioned, a threshold photon energy is required in order to ensure that no significant contribution to the

recombination expression arises from photoionization of the defect centers. In Eqns. (30) and (31), we have shown that this criterion may be written as

$$\alpha = N_t \sigma_p^o \tag{43}$$

or

$$\alpha = N_t \sigma_n^o \tag{44}$$

In words, the interband absorption coefficient should at least be equal to the product of the volume concentration of defect centers and their photoionization cross-sections for either electrons or holes. The evaluation of this threshold energy can be derived as follows.

An indirect-energy gap semiconductor such as Si is assumed, and the defect considered is a deep impurity level such as gold, a recombination center which has a well-known defect level located at the middle of the energy gap.[26] The phonon-assisted interband absorption coefficient for example from Smith,[27] can be written as

$$\alpha = \frac{Me^2 m_h^{3/2} f_c E_p \Delta E_o (\hbar\omega + E_p - \Delta E)^2}{32\pi\varepsilon_o m^* m_d^{1/2} \hbar^2 Cn\omega(\ell_{co} kT_o)(\Delta E_i - \hbar\omega)^2 (e^{\frac{E_p}{kt}} - 1)} \tag{45}$$

here $E_p = \hbar\omega_m$ is the phonon energy, $\Delta E = E_c - E_v = E_g(K \neq 0)$ is the energy gap and $K = 2\pi/\lambda$ wave number, $\Delta E_o = E_c(K=0) - E_v(K=0)$ is the energy difference between the conduction and valence bands $K = 0$, c is the speed of light in vacuum = 3.0×10^{10} cm/sec, n is the refractive index, $\hbar\omega$ = photon quantum energy of incident rdiation, ℓ_{co} is the mean

free path for acoustic phonon scattering in the conduction band at temperature T_o , $f_c \sim 1$ is the oscillator strength, m_h is the effective mass for holes, where $m_h^{3/2} = m_{h1}^{3/2} + m_{h2}^{3/2}$ if the valence band is degenerate with two effective masses m_{h1} and m_{h2} , M is the atomic mass, ε_o is the permittivity of free space, e is the electronic charge and the density of states effective mass, $m_d = m_e$ neglects the "non-spherical" nature of the minima in the conduction band.

The implication of Eqns. (43) or (44) are more readily established if we simplify the Eqns. (35) and (45) by

$$A = \frac{M e^2 m_h^{3/2} f_c E_p \Delta E_o}{32\pi \varepsilon_o m^* m_e^{1/2} \hbar \, Cn(\ell_{co} kT_o)}$$

$$A' = \left(\frac{E_{eff}}{\varepsilon_o}\right)^2 \frac{16\pi e^2 \hbar}{3m^* n C}$$

$$A^* = \frac{A'}{A} = \left(\frac{E_{eff}}{\varepsilon_o}\right)^2 \frac{16\times 32\times\pi^2\times\hbar^2\times\varepsilon_o(\ell_{co} k T_o)}{3M m_h E_p \Delta E_o}$$

and employ the assumptions

$$m_e \simeq m_h$$

$$f_c \simeq 1$$

This leads, using Eqn. (43) or (44), to

$$A\left(\frac{(\hbar\omega - \Delta E + E_p)^2}{\hbar\omega(\Delta E_o - \hbar\omega)^2\left(\exp\left(\frac{E_p}{kT}\right)-1\right)}\right) = N_t A' \frac{E_i^{1/2}(\hbar\omega - E_i)^{3/2}}{(\hbar\omega)^3}$$

if we now let $\hbar\omega - \Delta E = \hbar\omega - E_g = \Delta$, then, after some manipulation and

approximation, we find that

$$\Delta + E_p = A^{*1/2}\left(\exp\left(\frac{E_p}{kT}\right)-1\right)^{1/2}(\Delta E_o - E_g)\left(\frac{E_i}{E_g}\right)^{1/4}\left(1-\frac{E_i}{E_g}\right)^{3/4}$$

$$= A^{**}\left(\frac{E_i}{E_g}\right)^{1/4}\left(1-\frac{E_i}{E_g}\right)^{3/4} \qquad (46)$$

here

$$A^{**} = A^{*1/2}\left(\exp\left(\frac{E_p}{kT}\right) - 1\right)^{1/2}(\Delta E_o - E_g)$$

A numerical example to calculate Δ is of interest. We assume an N-type silicon crystal with gold as the impurity,[26] our parameters become:

$E_p = 0.063\text{ev}$	$m_h = 0.337\ m_o = 0.337 \times 9.1 \times 10^{-28}\text{g}$
$\Delta E_o = 3.82\text{ ev}$	$\ell_{co} = 76\ \text{A} = 76 \times 10^{-8}\ \text{cm}$
$E_g = 1.12\text{ ev}$	$k_{To} = 8.62 \times 10^{-5} \times 300°\text{K} = 25.9\text{ mev}$
$E_i = 0.54\text{ ev}$	$\varepsilon_o = 8.85 \times 10^{-14}\ \text{F/cm}$
$N_t = 4.3\text{x}10^{15}\text{cm}^{-3}$	$\varepsilon_{eff}/\varepsilon_o = 3.3$ and $M = 28.09$

Substituting all these values into Eqn. (46), we obtain

$$\Delta \simeq 0.01\text{ ev}$$

The fact that Δ is small in relation to the energy gap implies that for monochromatic light with photon energy well in excess of the energy gap, the neglect of trap photoionization of the traps will provide little error in the determination of the recombination lifetime. On the other hand, a common practical situation involves illumination of the semiconductor material with broadband optical illu

mination. In these cases, as for example in the solar cell, the large portion of the optical spectrum below the band gap energy may in some cases have an appreciable effect on the recombination process.

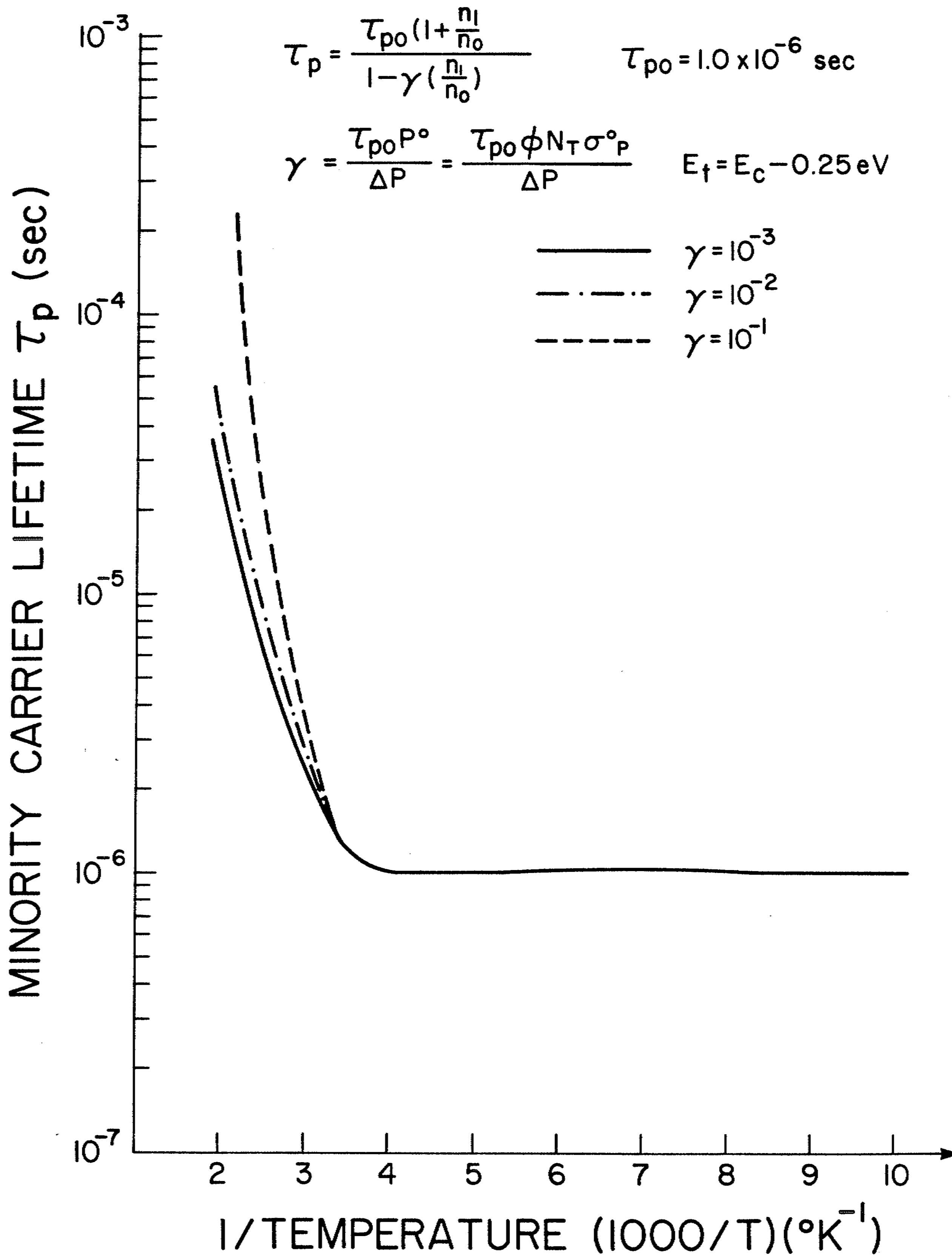

FIG. 5.2 Minority carrier lifetime vs. inverse temperature for different value of γ. The SRH model predicts a curve close to the solid line indicated by $\gamma \leq 10^{-3}$

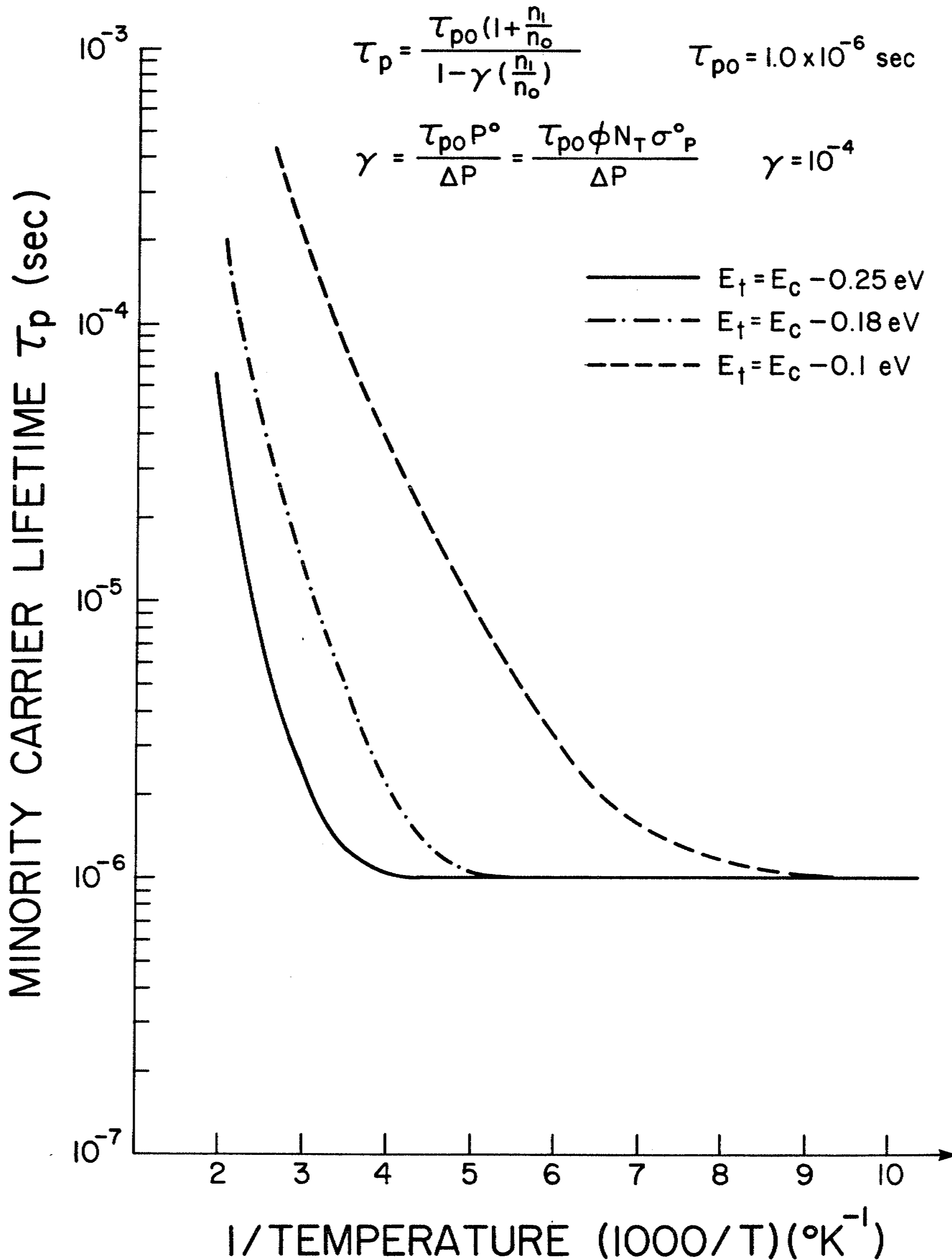

FIG. 5.3 Minority carrier lifetime vs. inverse temperature for different locations of trapping center. These curves indicated its consistence with SRH model when γ is much smaller.

References

1. W. Kohn, "Shallow Impurity States in Silicon and Germanium", Solid State Physics, Vol. 5, pp. 257-320, Academic Press, New York, 1957

2. D.V.Lang, "Deep-Level Transient Spectroscopy: A New Method to Characterize Traps in Semiconductors", J. of Apl. Phys., Vol. 45, No. 7, pp. 3023-3032, July 1974

3. H.G. Grimmeiss and L-A.Ledebo, "Spectral Distribution of Photo-ionization Cross Sections by Photoconductivity Measurements", J. of Appl. Phys., Vol.46, No. 5, pp. 2155-2162, May 1975

4. F.A. Lindholm, A. Neugroschel, C.T. Sah, M.P. Godlewski and H.W. Brandhorst, Jr., "A Methodology for Experimentally Based Determination of Gap Shrinkage and Effective Lifetimes in the Emitter and Base of p-n Junction Solar Cells and Other p-n Junction Devices", IEEE Trans. on Electron Devices, Vol. ED-24, No.4, pp. 402-410, April 1977

5. H.G. Grimmeiss, "Deep Level Imputries in Semiconductor", Ann. Rev. Mater. Sci.,Vol.7, pp. 341-376, 1977

6. W. Shockley and W.T. Read, Jr., "Statistics of the Recombinations of Holes and Electrons", Phys. Rev., Vol. 87, No. 5, pp. 835-842, September 1952

7. R.N. Hall, "Electron-Hole Recombination in Germanium", Phys. Rev., Vol. 87, p.387, 1952

8. Y.K. Hsieh and H.C. Card, "Recombination in Germanium: Voltage Decay Experiments on Induced-Junction Devices and Validity of SRH Model", Solid-State Electronics, in press 1984

9. S.R. Dhariwal, L.S. Kothari and S.C. Jain, "On the Recombination of Electrons and Holes at Traps with Finite Rexation Time", Solid-State Electronics, Vol. 24, No.8, pp. 749-752, August 1981

10. H.H. Poole, "On the Dielectric Constant and Electrical Conductivity of Mica in Intense Fields", Phil. Mag. (London), Vol.33, pp. 112-129, 1916

11. J. Frenkel, "On the Theory of Electric Breakdown of Dielectrics and Electronic Semiconductors", Phys. Rev., Vol. 54, p. 647, 1938

12. V.L. Bonch-Bruevich, "Concerning the Question of the Recombination of Hot Electrons", Soviet Phys.-Solid State, Vol. 6, No. 7, pp. 1615-1619, January 1965

13. D.D. Coon and R.P.G. Karunasiri, "Photoionization of Impurity Atoms in Semiconductors in the Presence of an Applied Electric Field", Solid-State Electronics, Vol. 26, No. 12, pp. 1151-1155, December 1983

14. A. Mircea, D. Pons and S. Makram-Ebeid, "Deep Layer Spectroscopy", Lecture Notes in Phys. 122, New Developments in Semiconductor Physics, edited by F. Belezany, G. Ferenczi and J. Giber, Springer-Verlag, pp. 69-96, 1975

15. C.T. Sah, L. Forbes, L.L. Rosier and A.F. Tasch, Jr., "Thermal and Optical Emission and Capture Rates and Cross Sections of Electrons and Holes at Imperfection Centers in Semiconductors from Photo and Dark Junction Current and Capacitance Experiments", Solid-State Electronics, Vol. 13, No. 91, pp. 759-788, September 1970

16. H.G. Grimmeiss and L-A Ledebo, "Photo-Ionization of Deep Impurity Levels in Semiconductors with non-parabolic bands", J. Phys. C: Solid State Phys., Vol. 8, pp. 2615-2626, 1975

17. M.D. Miller and D.R. Patterson, "Transient Capacitance Deep Level Spectrometry Instrumentation", Rev. Sci. Instrum., Vol. 48, No. 3, pp. 237-239, March 1977

18. J.I. Pankove, Optical Processes in Semiconductors Prentic-Hall, Inc., Englewood Cliffs, New Jersey, 1971, p.27

19. M. Lax, "Cascade Capture of Elecrons in Solids", Phys. Rev., Vol. 119, No. 5, pp. 1502-1523, September 1960

20. G. Ascarelli and S. Rodriquez, "Recombination of Electrons and Donors in n-type Germanium", Phys. Rev., Vol. 124, No. 5, pp. 1321-1328, December 1961

21. D.L. Bethe and P. Morrison, Elementary Nuclear Physics, 2nd Ed., John Wiley, New York (1956), Chap.4

22. G. Lucovsky, "On the Photoionization of Deep Impurity Centers in Semiconductors", Solid-State Communications, Vol. 3, pp. 299-302, 1965

23. D.L. Dexter, "Theory of the Optical Properties of Imperfections in Nonmetals", Solid State Phys., Vol. 6, pp. 353-411, Academic Press, New York, 1958

24. R. Newman and W.W. Tyler, "Photoconductivity in Germanium, Solid State Phys., Vol. 8, pp. 50-107, Academic Press, New York, 1959

25. A. Rose, Concepts in Photoconductivity and Allied Problems, Interscience Publishers, New York, 1963, Chap.7, pp. 118-128

26. A.F. Tasch, Jr. and C.T. Sah, "Recombination-General and Optical Properties of Gold Acceptor in Silicon", Phys. Rev. B, Vol. 1, No. 2, pp. 800-809, January 1970

27. R.A. Smith, Wave Mechanics of Crystalline Solid, Chapman and Hall Ltd., London, 1969, 2nd Edition, Chap. 13, p. 512

CHAPTER 6

CONCLUSIONS

The investigation of induced PN junctions in Germanium with its fundamental mechanisms and applications as long-wavelength photodetectors described in the previous chapters is concluded in this chapter. Further developments on this device or related problems are also suggested.

6.1 On Germanium Photodetectors with Induced PN Junctions

On the basis of experimentally-observed dependences of dark current and photocurrent upon bias voltage and temperature, we are able to unambiguously conclude that gold contacts to moderately doped N-type germanium behave as induced $P^{+}N$ junctions. The dark currents are due primarily to hole injection into the quasi-neutral region in forward bias, with a small additional component due to generation in the space-charge region in reverse bias. Thermionic emission of electrons over the Schottky barrrier contributes in a negligible way to the device current under both forward and reverse-biased conditions. These devices are therefore expected to perform as photodetectors for long wavelength fiberoptic communications at least as well as germanium PN junctions, and indeed may be superior as a result of the absence of heavily-doped diffused or ion-implanted surface regions.

6.2 On Influence of Minority Carrier Lifetime

The explicit and implicit effects of minority carrier lifetime τ_p on the performance of photodetectors have been presented. this includes the effects on quantum efficiency, speed of photoresponse and gain. These effects will be substantial if the appropriate conditions are not met concerning the multiplication of absorption coefficient and the width of the active region. Trade-offs exist between the depletion width and the transit time. τ_p does not directly affect the impact ionization coefficient of avalanche photodiodes and for appropriate PIN photodetector geometries, can be made to disappear from the expressions for gain or quantum efficiency and speed of response. In these cases, its primary effect is on shot noise through its connection with the reverse saturation current.

6.3 On Minority Carrier Recombination in Germanium

The SRH model has proven to be capable of accounting in an accurate manner for both the detailed temperature dependence and the dependence on injection level of recombination in germanium, over a wide range of these experimental variables. Isolated monoenergetic defects that lie above the equilibrium Fermi level at E_c = 0.128 eV explain the pronounced temperature dependence of the lifetime, and the trap parameters are also consistent with the injection-level dependence. The magnitude and temperature dependence of the capture cross-sections for electrons and holes are further in quantitative agreement with a theoretical treatment which identifies the acceptorlike nature of the centers. These observations help to justify

the use of the SRH treatment in the quantitative modelling of germanium induced-pn junction photodetectors.

The experimental results obtained for the variation of minority carirer lifetime with optical illumination intensity, wavelength and temperature have been qualitatively interpreted by means of the one-dimensional diffusion equation and the transient recombination equation. The latter departs substantially from steady-state recombination as described by the SRH model. The additional postulate of a shallow retrapping center found in POVD to explain the new features observed is not at variance with FCVD due to the different time-scales and excitation methods. Unlike the FCVD method, the POVD technique, while in principle capable of providing additional quantitative information concerning the recombination process, is plagued by practical limitations which we conclude will provide only qualitative information.

6.4 On Limitations to SRH Generation/Recombination Model

The direct photoionization of defect states has been included in the conventional recombination theory. This additional mechanism reduces the net recombination rate and enhances the effective minority carrier lifetime. Comparison with the standard SRH model shows that the optical emission rate from the defect states can only be neglected when the incident optical intensity is sufficiently weak, the value depending upon the relative magnitudes of the photoionization cross-section and the thermal cross-sections. Significant modifications to the minority carrier lifetime occur at high temperature. A principal conclusion is that, for photon energies even slightly in excess of the

energy gap ($\hbar\omega \geq E_g + 0.01$ ev) photogeneration via defect states may normally be neglected in comparison with interband photogeneration, even in indirect semiconductors. For photon energies below E_g , the recombination expressions of SRH are found to be simply replaced by similar expressions with effective values n_1^* and p_1^* which incorporate the photoionization of the trapping centers.

6.5 Suggestions for Further Research

Our investigation on gold-contacted N-type Germanium photodetectors with induced PN junctions has provided its scientific significance and engineering applications in fiber optical communications. Nevertheless, the present results still initiate a wide variety of interesting practical and theoretical problems which are worthy of further study.

First, most metal-semiconductor devices are associated with the problems of degradation due to oxidatation in the exposed environment. With our experience on the fabrication of Schottky barrier devices, we found that the degradation can be reduced by immersing the etched wafers into the Methonal for several days before it is deposited with metal in the high vacuum chamber. We suggest that the microscopic analysis of the chemical-reacted surface will be the key to understanding this important factor which will play a vital role in the design of highly reliable photodetectors.

Second, as we have discussed in Chapter 3, the minority carrier lifetime was indicated to be of no impact on the multiplication noise factor under the assumption of excluding the recombination effect from the transport mechanisms in both space charge and bulk regions.

In spite of the complication in the mathematical integration, it is expected that the numerical method can be used to develop this theoretical model.

Third, the difference of measuring the minority carrier lifetime between FCVD and POVD methods has been discussed in Chapter 4. The discrepency in the characterization has been considered to be caused by the instantaneous optical source and the complicated decay mechanisms. The solution to this problem can be achieved by the following investigation; (1) Theoretical Model development. A two-dimensional recombination equation with comparable and different (nonlinear) surface recombination velocity can be solved exactly by using quadratic, isoparametric finite-element modelling techniques.* (2) Experimental consideration. A design of electrical pulse with a similar time varied shape as in the optical case will be further applied to this device in order to confirm the inconsistency between the two methods.

Fourth, other than we have mentioned on the limitations to the SRH statistic model (discussed in the introduction of Chapter 5), there are a variety of related problems which are inherent to one fundamental assumption: the equivalent relationship between the capture and emission rates was made under thermal equilibrium conditions. It is believed that this is derived from the principle of detailed balance. In fact, it may not continue to hold under non-equilibrium

---

*See J.G. Shaw and A. Wexler, Report TR79-4; and A. Wexler Report TR80-4, Department of Electrical Engineering, University of Manitoba, Winnipeg, Canada (unpublished).

conditions but it is nevertheless applied there since all device phenomena occur under these conditions. An approach with quantum mechanic technique (Time-dependent perturbation method) applied to the transition probabilities between two energy levels may be pursued for further study.